TÉCNICO LISBOA

Air-water Flow on a Stepped Chute downstream of a Piano Key Weir over Gravity Dams: An Experimental Study

Nismah Rizwan

Thesis to obtain the Master of Science Degree in

Energy Engineering and Management

Supervisors: Prof. Jorge de Saldanha Gonçalves Matos

Dr. Maria Teresa Fontanelas Viseu

Examination Committee

Chairperson: Prof. Duarte de Mesquita e Sousa

Supervisor: Prof. Jorge de Saldanha Gonçalves Matos

Member of the Committee: Prof. João Pedro Gomes Moreira Pêgo

December 2019

Acknowledgements

First and foremost, I would like to acknowledge the invaluable knowledge, guidance, and support provided by my supervisor, Prof. Dr. Jorge Matos. I am grateful for the encouragement he gave me and the effort and time he put in throughout the course of this dissertation.

I would like to thank my co-supervisor, Dr. Maria Teresa Viseu, for providing me with access to the experimental facilities at LNEC and ensuring that my experience there was as comfortable and productive as possible.

I would also like to thank Dr. Stefan Felder from UNSW Australia, for sharing his data acquisition equipment and processing software, which made this dissertation possible. I am also grateful for the time and effort he dedicated to explaining the technicalities of the system and his willingness to help whenever needed.

I gratefully acknowledge the support of Prof. João Teixeira Borges, from the Department of Mechanical Engineering at IST, for allowing the use of the National Instruments data acquisition board in the present work.

I would like to express my profound gratitude to Rogério Castilho Gomes, a former Masters student at IST, for his help and guidance, especially during the experimentation phase. His unparalleled support made it possible to complete this dissertation on time.

I would also like to thank EIT InnoEnergy for providing me the opportunity to pursue this Masters degree at IST, Lisbon, and its staff for their assistance during all phases of the programme.

Last but not the least, I am grateful to my loving family for all their kindness, motivation and support, especially my brothers for providing assistance whenever I sought it.

Abstract

Gravity dams have been used for centuries as reservoirs for both, water and energy. To ensure that the structure has the desired output and cost-efficiency, the design of the crest, spillway, and stilling basin should be optimized. This dissertation combines the use of a Piano Key Weir (PKW) and stepped spillway to analyze the skimming flow over it. All experiments were conducted, for a 4 cm step height, at an experimental facility built in LNEC in Lisbon, Portugal. Air entrainment and interfacial velocity were measured using a dual-tip phase intrusive probe developed at WRL, UNSW Australia. Data recorded by the probe was used to characterize the flow and its energy dissipation, by calculating parameters including: air concentration and velocity distributions, mean air concentration, representative flow depths, and specific energy. The cross-section was analyzed for four different discharges, and nine steps along the chute. The analysis revealed the occurrence of a skimming flow regime for all the tested discharges however, its initiation moved downstream with the increase in flow rate. The mean air concentration, as the flow moved closer to the toe of the chute, decreased with increasing discharge, while the mean water velocity, flow depths, and specific energy increased. Additionally, the inlet and outlet keys of the PKW had a significant impact on the flow properties, particularly in the vicinity of the weir.

.

Key Words: Air Entrainment, Dual-tip Phase Intrusive Probe, Energy Dissipation, Piano Key Weir (PKW), Skimming Flow, Stepped Spillway.

Resumo

As barragens são usadas há séculos como reservatórios de água e de energia. Para garantir que a estrutura tenha uma forma e relação custo-benefício desejadas, o projeto da soleira descarregadora, do canal e da bacia de dissipação de energia deve ser otimizado. Nesta dissertação, faz-se uso de uma soleira descarregadora em teclado de piano (PKW) com um descarregador em degraus, sendo analisado o escoamento deslizante sobre turbilhões ao longo do descarregador. Os ensaios experimentais foram realizados com degraus de 4 cm de altura, numa instalação construída no LNEC, em Lisboa, Portugal. A concentração de ar e a velocidade interfacial ar-água foram medidas usando uma sonda de condutância de ponta dupla desenvolvida pelo WRL, UNSW, Austrália. Os dados adquiridos permitiram o cálculo de perfis de concentração de ar e de velocidade, concentração média de ar, velocidade média da água, alturas representativas do escoamento e energia específica. A seção transversal do escoamento foi analisada para quatro caudais distintos e para nove verticais ao longo do descarregador. Verificou-se a ocorrência do escoamento deslizante sobre turbilhões para os caudais analisados, com início a deslocar-se para jusante com o aumento da vazão. A concentração média de ar, na extremidade de jusante do descarregador, diminuiu com o aumento do caudal, enquanto que a velocidade média da água, as alturas representativas do escoamento e a energia específica aumentaram. Acresce que a tecla interior e tecla exterior da soleira PKW tiveram um impacto significativo nas grandezas representativas do escoamento, em particular na vizinhança da soleira descarregadora.

Palavras Chave: Emulsionamento de ar, Sonda de condutância de ponta dupla, Dissipação de energia, Soleira descarregadora em teclado de piano (PKW), Escoamento deslizante sobre turbilhões, Descarregador de cheias em degraus.

Table of Contents

List of Figures

List of Tables

List of Acronyms

EDF	Électricité de France
LNEC	Laboratório Nacional de Engenharia Civil (National Laboratory of Civil Engineering)
NI	National Instruments
NRE	Núcleo de Recursos Hídricos e Estruturas Hidráulicas (Water Resources and Hydraulic Structures Unit)
PKW	Piano Key Weir
UNSW	University of New South Wales
USBR	Unites States Bureau of Reclamation
WES	Waterways Experiment Station
WRL	Water Research Laboratory

List of Symbols

α	Kinetic energy coefficient
B_i	Length of downstream (inlet key) overhang of the PKW
B_o	Length of upstream (outlet key) overhang of the PKW
C	Local air concentration
C_{mean}	Mean air concentration
ΔE	Head loss between PKW crest and each step
Δx	Difference in length between the leading and trailing tips of the dual-tip probe
E	Specific energy at each step
E_{max}	Maximum specific energy (potential energy Head) relative to the elevation of each step
g	Acceleration due to gravity
h_{PKW}	Height of water above the PKW in the upstream reservoir
H_u	Total upstream head developed over the Crest
h_w	Equivalent clear-water depth
N	Parameter (exponent) of the Power law equation
P_i	Height of the inlet key of the PKW
P_o	Height of the outlet key of the PKW
Q	Flow rate/Discharge
q	Specific discharge
S_i	Slope of the inlet key of the PKW
S_o	Slope of the outlet key of the PKW
θ	Slope of the flow channel (angle of stepped chute from the ground surface)
t	Interfacial travel time for which the cross-correlation function is maximum
T_s	Thickness of the sidewalls of the PKW
$U_{reservoir}$	Velocity of water in the upstream reservoir
U_w	Mean water velocity
v	Interfacial velocity

v_{90}	Velocity at the flow depth corresponding with a void fraction of 90%
w	Width of the channel
W	Total width of the PKW
w_i	Width of the inlet key of the PKW
w_o	Width of the outlet key of the PKW
W_u	Width of a single unit of the PKW
y	Distance, normal to the pseudo-bottom, from the step edge
y_{90}	Distance, normal to the pseudo-bottom, from the step edge at a void fraction of 90%
Z_{crest}	Elevation of the spillway crest measured from the ground surface
Z_{step}	Elevation of the step edge measured from the ground surface

Chapter 1: Introduction

1.1. Background

For centuries, dams have been considered one of the most versatile civil engineering structures. They act as both, reservoirs and outlets for energy using water as the medium. With regard to this, an important component of the dam's structure is its spillway. Its design has the most significant impact on the flow of water as it moves from the upstream reservoir to the downstream basin.

Of the many types of spillway structures that exist today, the stepped spillway is one of the rapidly growing options. Although stepped spillways have been around for centuries, their use decreased very significantly after the introduction of hydraulic jump stilling basins for energy dissipation [1]. However, a realization of the additional benefits stepped spillways offer, has led to a renewal of interest in their application in recent years.

The unique structure of a stepped spillway provides a number of advantages, two of which are analyzed in detail in this dissertation. The first is the pattern of energy dissipation over the length of the spillway, which differs considerably from conventional spillways due to the presence of steps rather than a smooth surface. The second advantage is connected with the aeration of flow as water moves down the spillway. This phenomenon may be of relevance for the protection of the structure against cavitation damage, the sustainment of aquatic life, and the maintenance of natural conditions within the water body upon which the dam is built.

In addition to the spillway itself, the crest is also vital in defining the flow path and energy dissipation characteristics. Traditionally, a smooth Ogee crest or Creager weir is most commonly used for all types of spillways. However, the need for a more efficient and cost-effective design has led to the development of a labyrinth-type crest known as the Piano Key Weir (PKW). This type of weir allows the improvement of a dam's flood release capacity, without the need to increase the space occupied by the crest. The most appealing aspect of the PKW is, perhaps, the fact that it increases the overall discharge capacity of the dam by at least three times in comparison with the conventional options [2].

An effective method to increase the overall efficiency of a dam is to combine the advantages associated with the two structures defined above. This has been the focus of quite a few studies, including this one. Generally, numerical models are used to simulate the flow over such structures however, the complexity of a PKW reduces the accuracy of this approach. Therefore, it is always more useful to test the geometry of a PKW, along with the energy dissipation structure of the dam, on a physical model [3]. Keeping this in view, all the experiments in this study were conducted on a physical model located at Laboratório Nacional de Engenharia Civil (LNEC), Portugal. The model comprised of a PKW crest attached at the head of a stepped spillway with a step height of 4 cm.

A factor of great interest in the analysis of any structure is the equipment used to gather the relevant data. The most common instrument used in the analysis of air entrainment over a spillway is the phase detection intrusive probe. Traditionally, a single-tip probe was used in such studies, including multiple experiments conducted on the model described above. However, the use of dual-tip probes is an interesting alternative, as it allows the collection of more information on flow properties, such as the interfacial velocity.

1.2. Aim

The major objective of this dissertation is to characterize the flow and analyze the energy dissipation over a stepped spillway fitted with a PKW, with the help of a dual-tip phase detection intrusive probe developed at the Water Research Laboratory (WRL) of the University of New South Wales (UNSW), Australia [4]. The analysis was conducted on a test assembly set up at LNEC, located in Lisbon, Portugal.

1.3. Scope

The analysis involved in this study focused primarily on the collection and analysis of data, using the dual-tip phase detection intrusive probe, in order to determine important flow parameters including air concentration and interfacial velocity profiles, mean air concentration, characteristic flow depth, and equivalent clear-water depth. These parameters were recorded at nine different steps, along the stepped chute, and for four different values of flow rate: 60, 80, 140, and 180 L/s. For each step, six positions were chosen, along the width of the channel, keeping in view the structure of the weir and ensuring that all its focal points were examined. All the analyses was conducted only for a step height of 4 cm.

Additionally, the specific energy and head loss at the bottom of the spillway were also determined by collecting data in a similar way. However, measurements were made for only two steps close to the foot of the spillway and for 10 different positions along its width, to evaluate the uniformity and occurrence of two-dimensional flow. Here, the energy parameters were calculated using a set of equations for open channel flow rather than piezometric measurements in the stilling basin.

During the initial stages of data acquisition, a comparison was also drawn between the results obtained in the current study and those obtained in a previous study conducted on the same assembly under similar conditions but with a single-tip probe. This was deemed necessary to catch any errors that may have occurred during the data acquisition process. The dual-tip probe allows the collection of a larger set of data and a greater number of parameters, which include air concentration and interfacial velocity profiles. Since the single-tip probe does not have a mechanism to determine the interfacial velocity, a comparison could not be made for this parameter. Additionally, data from the previous study was available only for two positions (C and E; defined in Chapter 4) and at discharges of 80 L/s and 140 L/s.

Chapter 2: Literature Review

This chapter provides a brief overview of the theoretical background of the multiple components involved in the present study. Sections 2.1 and 2.2 highlight the major features and benefits of the structural components, i.e. the weir and spillway, while Section 2.3 includes examples of studies conducted on the same experimental facility. Section 2.4 describes the instrumentation used to measure and analyze flow over the structure.

2.1. Piano Key Weirs

Piano Key Weirs (PKW) are a special type of Labyrinth Weirs, which were introduced with the aim of providing a cost-effective way to increase the discharge capacity of already built dams [5]. Their concept was first introduced in the 1990's by Lempérière and Ouamane, supplemented by pilot studies in multiple countries to determine the ideal crest shape. Ultimately, the first PKW crest was built at the Goulours dam in France by Électricité de France (EDF) in 2006. Since then, PKWs have been incorporated in nearly 25 dams worldwide [3].

PKWs have very simple geometrical features, with the overall structure resembling that of a series of piano keys. The basic structure is comprised of a narrow rectangular labyrinth with an inclined base on both, the upstream and downstream sides, commonly known as the inlet and outlet keys, respectively. A single unit of the PKW comprises one complete inlet key with two half outlet keys on either side [3]. The basic structure of a PKW is highlighted in Figure 2.1.

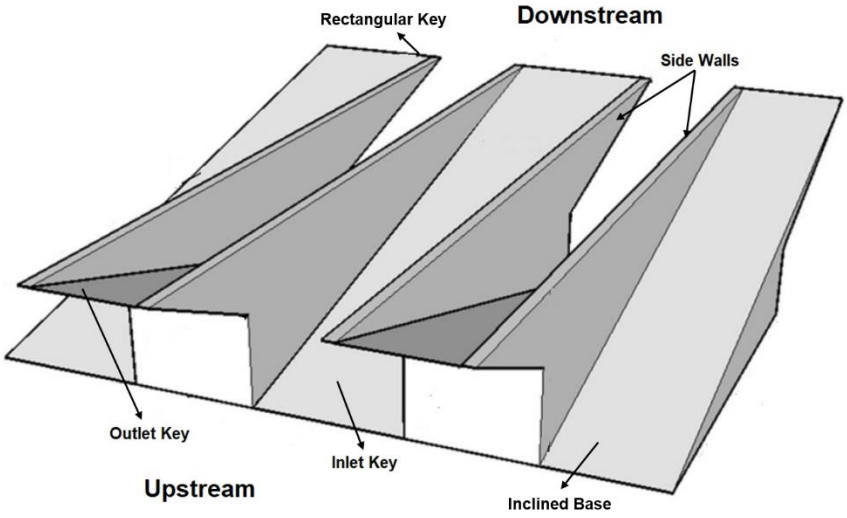

Figure 2.1: Three-dimensional view of a typical PKW structure [6]

The concept behind the labyrinth-type structure of a PKW is to allow water to flow through a longer length while crossing the weir. This increases the overall discharge capacity without the need to widen the area required by the weir or enlarge the overall volume of the dam [2]. This is particularly important for low head dams and during the refurbishment of old dams [3].

The efficiency and effectiveness of a PKW depend largely on the geometry of the structure and the ratio between its various dimensions. The key dimensions include: width of the inlet (w_i) and outlet (w_o) keys, height of the inlet (P_i) and outlet (P_o) keys, slope of the inlet (S_i) and outlet (S_o) keys, thickness of the sidewalls (T_s), length of the upstream (B_o) and downstream (B_i) overhangs, width of one PKW unit (W_u), and overall width of the PKW (W). Figure 2.2 illustrates the parameters discussed above.

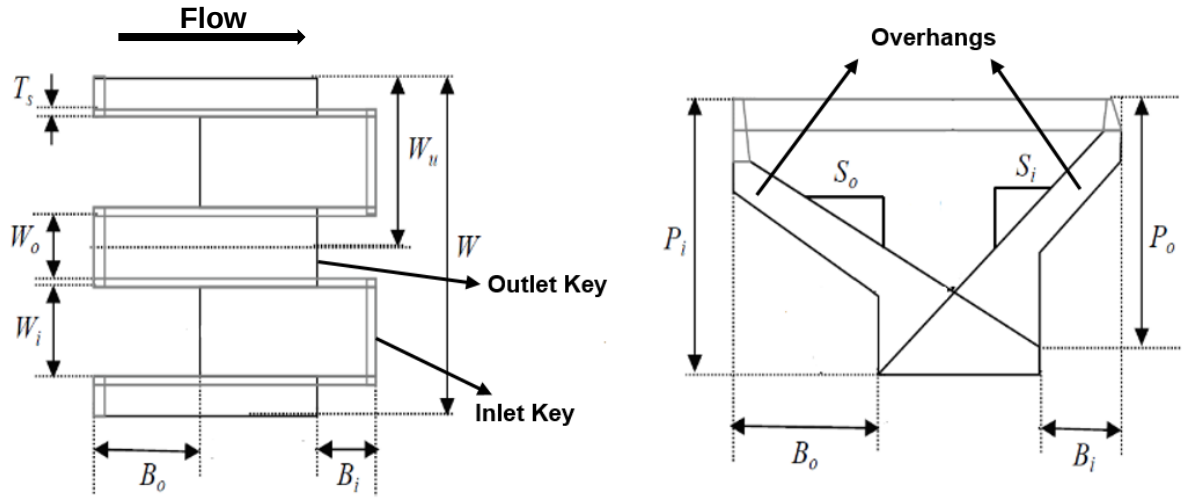

Figure 2.2: Key dimensional parameters of a PKW: Plan view (Left); Side/Cross-sectional view (Right) [7]

The stability of a PKW depends largely on the balance between the upstream and downstream overhangs [8]. Therefore, the slope, i.e. the ratio between the length and height, of the keys is of great importance. It also reduces the required height of the vertical walls [9]. Additionally, a longer overall height is preferred for the PKW, since it results in a more even distribution of flow in the inlet keys and lower chances of submergence in the outlet keys [3].

The effectiveness of the PKW is defined by its 'crest length magnification ratio', which refers to the ratio between the overall developed length and width of the weir [3]. It should ideally be between 4 and 7 to ensure that discharge over the weir is maximized [2]. The width of both keys is also important in determining the overall efficiency since it has a significant effect on the specific discharge and subsequently, the discharge capacity [3]. Optimizing the sidewall thickness may also increase overall capacity of the weir [10].

Based on the design and position of the overhangs, four different types of PKWs exist today [3]. As depicted in Figure 2.3, Type A has overhangs on both, the upstream and downstream sides. Type B has a single overhang on the upstream side (inlet key), while Type C has a single overhang on the downstream side

(outlet key). Type D has no overhangs all together. The type of PKW is important in determining the stability of the crest and the effective length achieved. As a result of numerous experiments, Type A has been found to be the most efficient and is therefore, most commonly used in real-world applications.

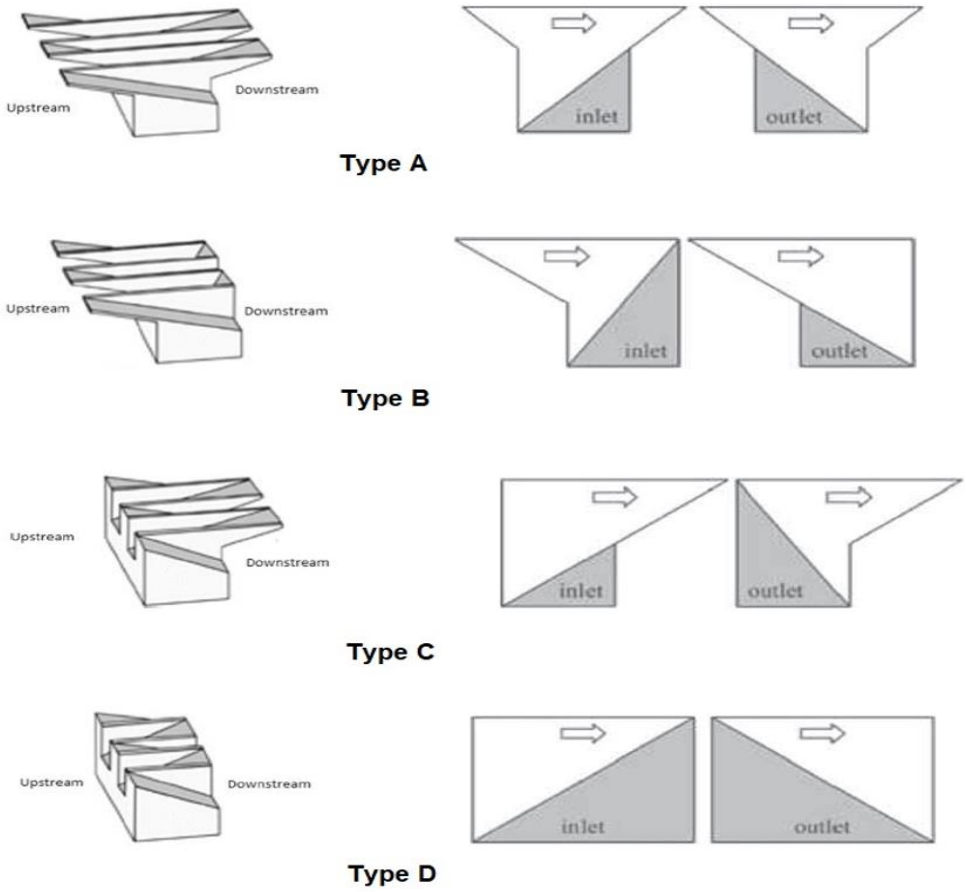

Figure 2.3: Types of PKW: Three-dimensional view (Left) [11]; Side/Cross-sectional view (Right) [12] with arrows indicating the flow direction

Regardless of the design and geometry of the PKW, it is still around three times more efficient than a conventional weir of similar width. It increases the overall spillway discharge capacity with a minimal increase in the overflow depth (maximum water level). Additionally, these weirs are easy to construct and require minimal maintenance [2].

PKWs are often treated as a safer alternative to controlled spillways, such as gates since they encourage the free flow of water while fulfilling the same purpose. The absence of electro-mechanical components reduces the need for constant supervision and the chances of operational failure. This, combined with the geometrical features of the PKW, reduces the amount of material required for its construction. As a result, the overall cost of the structure is much lower in comparison with conventional weirs [8].

Generally, the design of a PKW is a compromise between hydraulic efficiency, structural complexity, environmental/local constraints, and cost. They are usually built with a small number of units, such that the crest width is not too large [8]. Most of the projects under operation or construction, till date, are retrofit or dam refurbishment projects.

2.2. Stepped Spillways

Stepped spillways have been in use for centuries as a method of energy dissipation, with the first structures emerging in Greece over 3500 years ago [13]. This phenomenon was particularly common in breaking the flow of water as it moved down a mountain, as can be seen in Figure 2.4. However, their use significantly diminished during the first half of the 20th century owing to the introduction of hydraulic jump stilling basins. Nevertheless, their adaptation on a large scale in dam structures has re-emerged during the past two centuries, an example of which can be seen in Figure 2.5. Today, stepped spillways are seen as an effective and low-cost option for flood control [14].

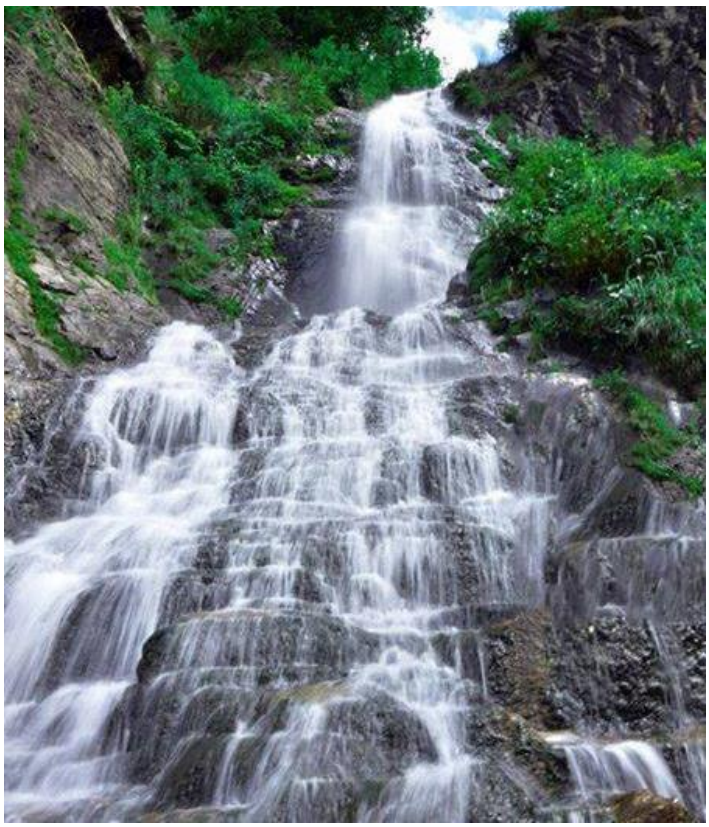

Figure 2.4: Natural stepped spillway: Machal waterfall in Neelum Valley, Pakistan [15]

Figure 2.5: Stepped spillway in Stone Mountain dam, Georgia, USA [16]

The concept behind stepped spillways is that when water moves through an inclined flow channel in a series of drops, prompted by the steps, it dissipates energy along the route. This prevents the rapid increase in flow velocity and specific energy associated with the conversion of potential energy into kinetic energy. This, in turn, reduces, or eliminates, the need for an energy dissipation structure at the base of the spillway thus increasing the overall stability of the dam structure [14].

Flow over a stepped spillway is defined mainly by the unit discharge, step height, and spillway slope. Depending on these parameters, the flow may be characterized as nappe, transitional, or skimming flow. Theoretically, for a constant geometry of the spillway, the flow evolves from nappe to transitional to skimming flow regimes with an increase in discharge [14]. Each of these flow regimes is described briefly in the following subsections.

2.2.1. Nappe Flow Regime

Nappe flow occurs at relatively small values of discharge and spillway slope. The flow is characterized by a series of individual falls, followed by air jet fragmentation and, possibly, the creation of small hydraulic jumps, between each step of the channel. As a result, a large portion of the energy may be dissipated at each step [17]. In order to achieve nappe flow, the step length should always be greater than the critical flow depth. Figure 2.6 illustrates a schematic of the nappe flow regime.

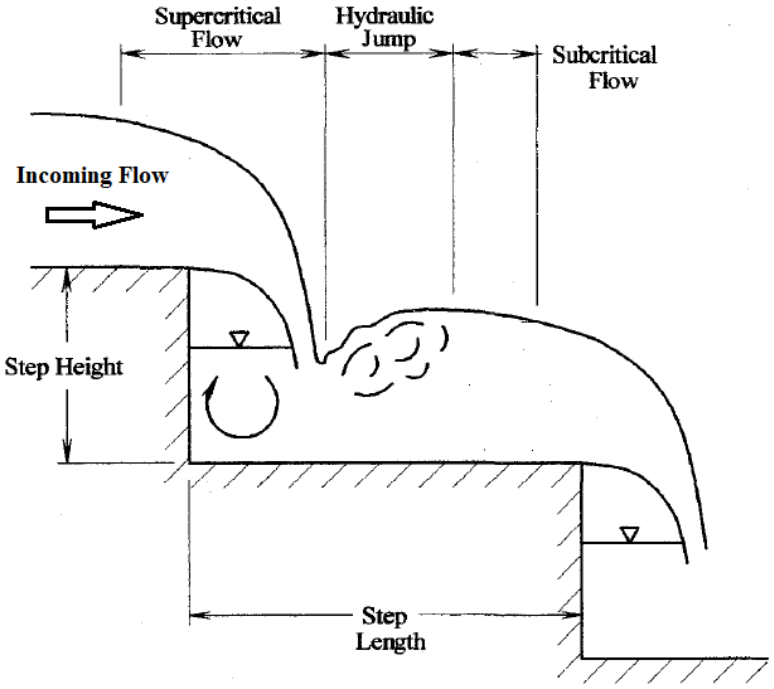

Figure 2.6: Schematic of the nappe flow regime [18]

2.2.2. Transitional Flow Regime

Transitional flow occurs in between nappe and skimming flow (described in subsection 2.2.3), such that both the flow regimes co-exist at a single discharge. This flow regime may be observed at moderately high values of discharge and a wide range of spillway slopes [14].

2.2.3. Skimming Flow Regime

Skimming flow occurs at high values of flow rate and spillway slopes, ranging from 3˚ to 60˚ from the ground surface [19]. Multiple studies have shown that distinct values of discharge exist at which flow over a stepped spillway of defined geometry, moves from nappe to transitional, and eventually to the skimming flow regime [14].

The skimming flow regime is characterized by water moving down the channel slope as a coherent stream, such that the spillway steps are fully submerged and do not interfere directly with the surface flow [18]. In this manner, the flow surface resembles that of an open channel. Beneath the surface, the flow occupies cavities formed by the steps, where it dissipates its energy. Theoretically, the bottom of flow, known as the 'pseudo-bottom', is formed by an imaginary line connecting the step edges [20].

Flow beneath the surface is typically in the form of vortices, and is governed by the flow rate and spillway geometry. It has a significant impact on air entrainment and energy dissipation along the structure. Based on this, the flow pattern varies along the length of the spillway, and may be categorized as one of the flow regions [14], depicted in Figure 2.7 and described below:

- Clear-water flow region – This region, marked as 1 in Figure 2.7, occurs closest to the crest of the spillway. The boundary layer gradually starts growing from the spillway floor to form an undisturbed and glassy flow surface. This region has a nearly negligible air concentration and generally has a smaller flow depth than the regions downstream of it [21].
- Air-water flow region – This region occurs beyond the point of inception, which is the point where the boundary layer reaches the free surface. This region is characterized by an initial partially aerated region (marked 2 in Figure 2.7), which usually spans over a very short portion of the spillway length. In a stepped spillway, this region is characterized by considerable flow bulking and a rapid increase in air concentration and velocity along the length. It is followed by a fully aerated region (marked 3 in Figure 2.7), with rapidly varying flow and hence, a wavy surface layer. The flow then transforms into a uniform region (marked 4 in Figure 2.7) with a relatively flat surface layer, near the bottom of the spillway. This region has an established two-dimensional flow owing to nearly constant flow characteristics including, air concentration, velocity, characteristic depth, and equivalent clear-water depth. All three of these regions may be observed for high flow rates however, the relative depth of the partially aerated flow region decreases with increasing discharge [21].

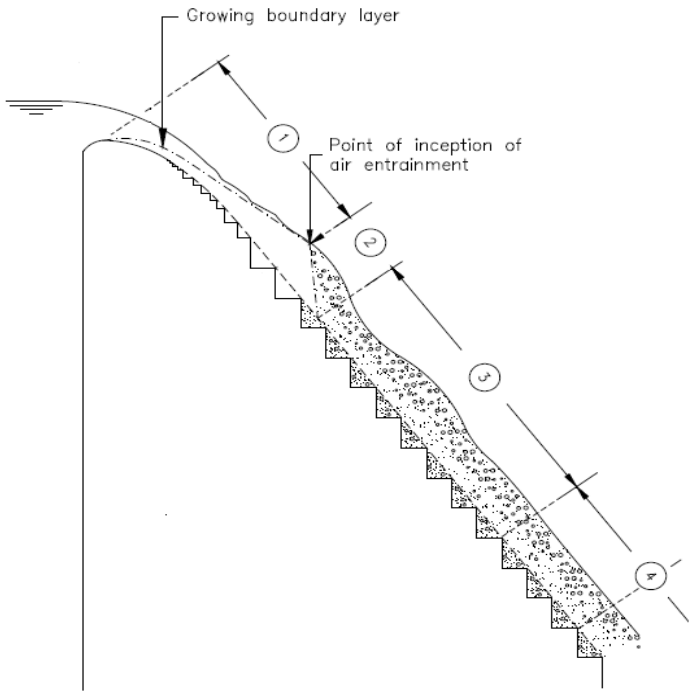

Figure 2.7: Skimming flow regimes: (1) Clear-water flow region; (2) Partially aerated flow region; (3) Fully aerated flow region; (4) Uniform flow region [14]

2.3. Related Work

The experimental facility used in this dissertation has been the subject of numerous studies over the past two decades. While most of these explored the various aspects of an Ogee crest, only the most recent ones have incorporated the use of a PKW with a stepped spillway, to characterize the flow over it. A few of these are discussed below.

The study by Reis [22] sought to estimate the rating curve of a PKW, which describes the relationship between specific discharge (q) and total upstream head developed over a weir (H_u). These curves were then compared with those obtained for an Ogee crest in several other studies [23] [24]. The results showed that a PKW has a linear and more efficient rating curve, while the discharge over it is 2 – 3 times higher than a conventional weir. Perhaps, the most important observation made in this study was the occurrence of three distinct flow zones along the stepped chute. The initial flow was divided between free jets from the inlet keys and a slowly evolving air-water skimming flow from the outlet keys. The second zone displayed a fully evolved three-dimensional skimming flow throughout the channel's cross-section. Whereas the third, and final, zone illustrated a shift from three-dimensional to two-dimensional flow. This study also highlighted key facts such as the creation of cross-waves that results in an intersection of air concentration profiles corresponding with the inlet and outlet keys, and a decrease in the influence of weir type on the flow as it moves away from the crest. It also indicated that the mean air concentration across the chute was affected by the PKW's keys, but not by the incoming flow rate of water. Also, the concentrations near the bottom of the chute were generally similar to those observed in smooth spillways.

Another study, by Pinto [25], investigated the development of a hydraulic jump in the stilling basin, which helped explore the energy dissipation behaviour, following the flow of water over the PKW and stepped spillway. This was achieved by the analysis of flow depth near the bottom of the chute and piezometric heads measured in the stilling basin. The results showed that the energy dissipation was lower when using a PKW and therefore the residual specific energy at the bottom of the stepped chute was relatively higher than an Ogee crest.

A more recent study, conducted by Gomes [26], examined both, the flow over a PKW and stepped spillway, and the development of a hydraulic jump and subsequent energy dissipation in the stilling basin. Moreover, this was done for two different step heights: 4 cm and 8 cm. In addition to confirming the energy dissipation behaviour observed by Pinto [25], the results of this study indicated that the mean air concentration and residual specific energy increased with an increase in the step height. A detailed analysis, and comparison, of the results obtained in this study is presented later on in this dissertation (Section 5.1).

2.4. Phase Detection Intrusive Probe

Air-water flows, similar to the ones in this study, are often characterized by strong interactions between the particles of air and water. This is particularly common in high velocity flows where the surface is exposed to air (free surface). Flow analysis in such conditions may become quite complex. Conventional instrumentation, such as traditional Pitot tubes and velocimeters, may result in highly unreliable measurements, as they are negatively affected by the presence of air bubbles [19]. In such cases, 'Phase Detection Intrusive Probes' provide a suitable alternative and are now widely used for the analysis of flow.

The Phase detection intrusive probe works on the principle of a conductivity probe, which generates voltage signals based on the difference in electrical resistivity between different particles (or phases) present in the flow [27]. Such probes have been in use for the past 50 years and today many versions exist, differing in the number of tips, tip diameters, data acquisition systems, data analysis methods, etc. However, they are mostly based on the needle-like probe tip design introduced by Neal and Bankoff [28].

A conductivity probe makes measurements based on the amount of air bubbles pierced by the probe tip within a given amount of time. The probe is usually connected with a data acquisition system, which transforms the detected information into voltage signals. The voltage signal is affected by the medium surrounding the probe. It generates a constant signal when it is exposed to water however, every time it interacts with an air bubble, the voltage drops. This is attributed to the larger resistivity of air relative to water. The result is a series of nearly rectangular fluctuations, describing the amount of time the probe comes in contact with air, and hence the air entrained in the flow [29].

Traditionally, conductivity probes have a single tip, however in the recent years multiple designs have emerged with an additional 'trailing' tip. This additional tip allows the verification of data gathered by the main 'leading' tip and also the direct determination of interfacial velocity and several other parameters. One such probe was developed and experimented with at WRL, UNSW Australia [19]. This probe was tested for accuracy against several other dual-tip probes, working on different principles, such as fibre optics [4]. It was also benchmarked against another well-established conductivity probe used for similar studies [30].

All the research conducted on this probe also highlighted a few important operational requirements to ensure precision and accuracy of measurement. For a dual-tip probe, the tips should be as small as possible. They must be positioned adjacent to each other and be surrounded fully by water or air to detect the particles. Additionally, they should be placed parallel to the flow direction, in order to allow the water to flow naturally without any interference [4].

Studies also indicate a number of factors that may affect the voltage signal created by the data acquisition software and hence, the results of the flow analysis. Sampling duration, frequency, and threshold are the most important parameters for the determination of void fractions [19]. Often, the same probe tip may be covered by both, air and water particles, at the same time. This often results in inaccuracies in the voltage signal involved, such that it may not touch the defined threshold limits [4].

Chapter 3: Experimental Setup

This chapter describes, in detail, the assembly used to model flow in a steep chute and the equipment used to gather the required data. The test assembly used in this study is located in the National Laboratory of Civil Engineering (LNEC) in Lisbon, Portugal. It is a fairly large scale model of a stepped spillway with a PKW. The weir, spillway, and stilling basin (only the initial half), illustrated in Appendix A and described in detail in Sections 3.2 – 3.4, are all made of clear acrylic glass, with a thickness of 12 mm. The transparency of the structural components allows an easy visualization of the flow.

All the measurements were made using a dual-tip phase detection intrusive probe connected to a data acquisition board. The acquired data was displayed on a programme designed in LabVIEW and analyzed with the help of a FORTRAN code developed by Felder [31]. This system is described in detail in Sections 3.5 – 3.6.

3.1. Upstream Reservoir

Water passing through the test assembly follows a closed circuit. It is supplied from an underground, constant feed reservoir, built solely for the Water Resources and Hydraulic Structures Unit (NRE) at LNEC. Water is transferred from the main pump to the internal reservoir of the assembly with the help of two suction pumps. Once there, the water can be withdrawn from the internal reservoir via another pair of pumps. This water is collected in a chamber at the top of the assembly that simulates an upstream reservoir.

The upstream reservoir, depicted in Figure 3.1, can cater to a flow as high as 200 L/s, which is regulated by a valve connected at the inlet. The flow is monitored with the help of a hydrometer. The reservoir is divided into two parts, separated by an un-cemented single brick wall (to allow water to pass through), shown in Figure 3.2. The brick wall ensures that all unnecessary turbulence is eliminated from the flow before it reaches the weir.

Figure 3.1: Upstream reservoir of the test assembly

Figure 3.2: Brick wall in upstream reservoir

3.2. Piano Key Weir

Water flows from the upstream reservoir to the stepped spillway via a Type A Piano Key Weir, whose structure is highlighted in Figure 3.3. The rectangular shaped, zig-zag structure of the weir keys, combined with their sloping bases, contributes to the relatively higher discharge capacity associated with these weirs. It also facilitates the movement of water over and away from the crest, resulting in a complex, three-dimensional flow.

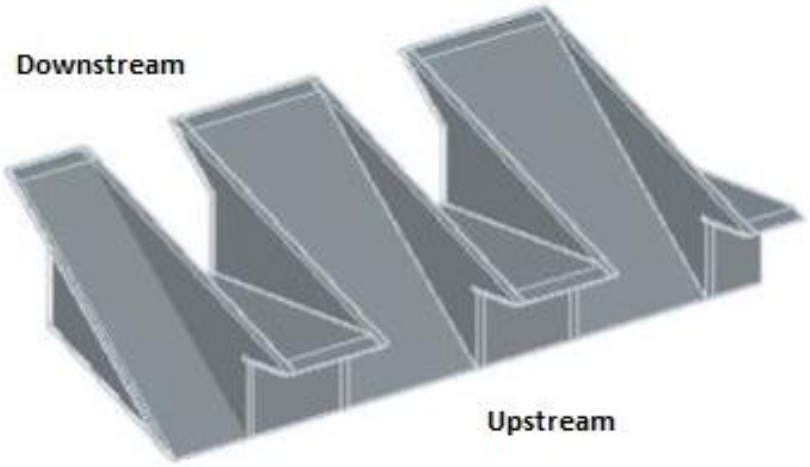

Figure 3.3: Three-dimensional view of the PKW in the test assembly

The weir is composed of two complete and one half PKW units, i.e. there are two inlet keys (Width = 22.1 cm each), 2 outlet keys (Width = 14.7 cm each), and one-half of each adjacent to the walls of the channel, as illustrated in Figure 3.4. This design ensures that flow through the inlet key is not restricted over the developed crest, while no submergence occurs at the outlet key (Figure 3.5). Therefore, water passing over the weir flows through a longer length in comparison with a linear weir, such as a Creager weir. This results in a higher discharge, which may prove beneficial for a dam's structure and operation.

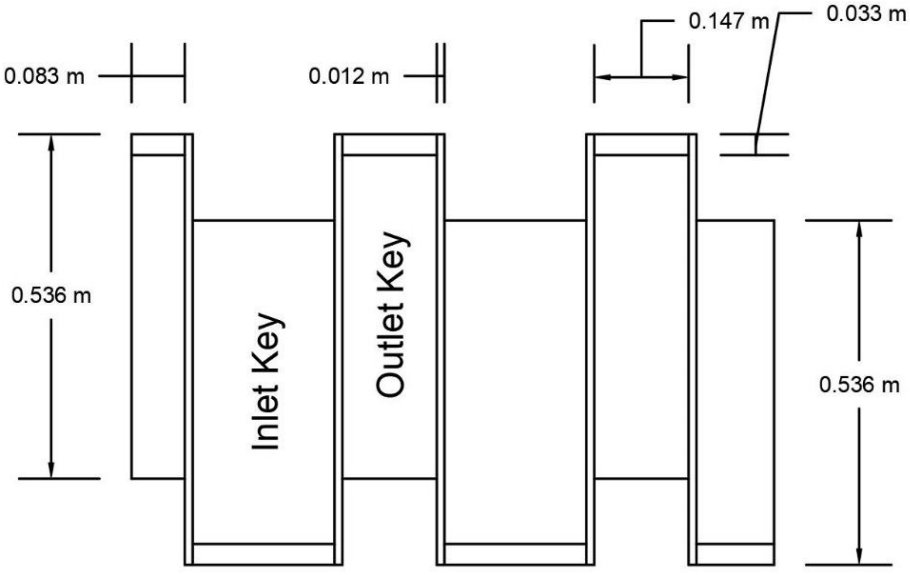

Figure 3.4: Plan view of the PKW in the test assembly with dimensions (Flow direction: top to bottom)

Figure 3.5: Flow of water over the PKW

3.3. Flow Channel

The major flow channel, as illustrated in Figure 3.6, has a width of 1 m and a crest height of 3.36 m. It is comprised of a spillway lined with a series of steps, each with a height of 4 cm. The channel has a uniform slope of 1:0.75, i.e. it has a 53˚ angle with the horizontal. The side walls of the channel help contain flows up to 200 L/s. Owing to the stepped spillway, the channel acts as a major energy dissipation structure along the path of the water [21].

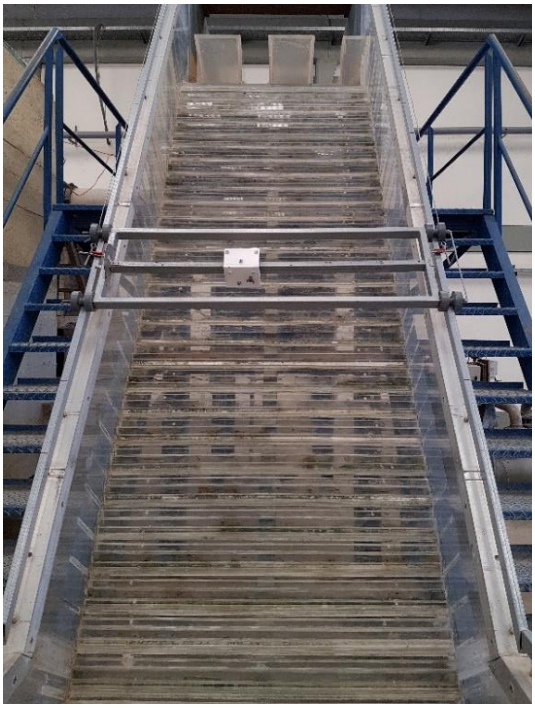

Figure 3.6: Stepped spillway with a 4 cm step height

A major auxiliary component of the flow channel is a rectangular iron frame, made mobile with the aid of PVC wheels attached at all four corners (also shown in Figure 3.6). These wheels allow the frame to move along the complete length of the flow channel, which is lined with rectangular iron rods at the top of the side walls. The frame also has a sliding cube attached to its central structure, which acts as a support to hold the test probe (described in Section 3.5) in position, while making it mobile to gather data across the cross-section (width of the channel).

3.4. Stilling Basin

Water flowing over the stepped spillway flows into a stilling basin, where it dissipates a portion of its energy in the form of a hydraulic jump. The basin is a narrow, 5 m long, channel with a width of 1 m, and a sluice gate located at the end to control the stability of flow. The initial 0.34 m of the basin are a continuity of the flow channel and are made entirely of acrylic glass. The remaining 4.66 m have a base made of concrete slabs, whereas the first half of the walls is made of acrylic glass, as can be seen in Figure 3.7, and the second half is made of concrete slabs. The initial clear walls allow a more explicit visualization of the hydraulic jump, an example of which is shown in Figure 3.8.

Figure 3.7: First half of the stilling basin made of acrylic glass

Figure 3.8: Visualization of a hydraulic jump through the clear acrylic walls of the stilling basin

Water passing through the basin exits it via a sluice gate, following which it flows into a 0.8 m wide channel. This channel allows the flow to stabilize before flowing back to the internal reservoir of the test assembly. It uses a floating wooden frame, to break the force of surface waves, and three adjacent rows of single brick walls to reduce turbulence and smoothen the flow. These structures are displayed in Figure 3.9.

Figure 3.9: Flow control structures: Sluice gate (Left); Brick walls and wooden frame (Right)

A hydrometer, shown in Figure 3.10, is located near the end of the stabilization channel. It helps monitor the flow depth and hence, estimate the discharge through the system based on the Bazin weir rating curve. Similar hydrometers may be found next to the upstream reservoir and stilling basin.

Figure 3.10: Hydrometer to measure depth and estimate discharge from the Bazin weir rating curve

3.5. Data Acquisition Probe

A dual-tip phase detection intrusive probe, developed at the Water Research Laboratory (WRL) of University of New South Wales (UNSW), Australia, was used to gather data related to the desired flow parameters. The probe allows direct measurement of air concentration (C) and interfacial velocity (v), whereas other parameters such as mean air concentration (C_{mean}), mean water velocity (U_w), equivalent clear-water depth (h_w), and residual energy may be derived from this data.

As the name suggests, the dual-tip probe is comprised of two identical sensor tips, made of hypodermic needles. They have an outer diameter of 0.5 mm, which helps optimize the piercing of flow particles. The two tips, placed in parallel as shown in Figure 3.11, are referred to as the leading and trailing tips, where the leading tip is 4.82 mm longer than the trailing tip. Usually measurements made by the leading tip are of greater importance, while those made by the trailing tip are considered only for more detailed analysis and calculations [4].

Figure 3.11: Dual-tip phase detection intrusive probe

The probe works with the help of conductivity sensors, which identify particles present in a solution by detecting their resistivity and converting it into an electric signal. The sensor electrodes are separated by an epoxy and are housed within the probe tips. They are made of platinum wires and have a diameter of 0.125 mm. The circuitry of the probe is housed within a thin, hollow, steel rod (Figure 3.11), which allows it to be maneuvered more easily [4].

The probe gathers and displays information in the form of voltage signals, which vary based on the electrical resistivity of the particles that hit the tips. Similar to other high velocity flows, the major particles involved in this study are air and water. A constant signal of 4.3 – 4.5 V is generated as long as the probe tips remain in contact with water. Since air has a different resistivity than water, the voltage signal is disrupted every time an air bubble is pierced by the probe. In such cases, the voltage drops to a value around 0.9 V or lower, owing to the significantly higher resistivity of air. Consequently, the overall output signal is composed of constant fluctuations, which are then translated into numerical data [19].

While recording data, the probe should be placed parallel to the flow direction so that it is as minimally intrusive to the flow as possible. The basic information it provides is the air concentration, bubble frequency, and interfacial velocity, measured across both, the leading and trailing tips. It has been reported to have a measurement accuracy of 4% for air concentration and 5-10% for interfacial flow velocity [4]. Post-processing of the data is required to determine other parameters, which is achieved with the help of a FORTRAN code.

3.6. Data Processing Software

The data acquisition system connected with the probe is designed with LabVIEW (Version 2009), based on a National Instruments (NI) acquisition board. Data analysis and post-processing, of the raw voltage signals, is carried out using a FORTRAN 95/2003 code developed by Felder [31], at UNSW Australia.

The programme allows the selection of multiple probes (which represent the number of tips here) at the same time, up to a total of eight (corresponding with the number of digital channels of the acquisition board). Additionally, it allows the adjustment of parameters that have a direct effect on the output voltage signal and the subsequent calculations. These include: sampling frequency (rate), sampling time, the number of samples to be taken within the sampling time, and the threshold for the air-water interface. All the recorded data may be saved as a binary or text file depending on the storage space available.

The programme has two modes of data acquisition; one to record data over a fixed amount of time and the other to display the voltage signal in real time. Whenever an air bubble is pierced by either of the probe tips, the voltage signal drops, resulting in a series of nearly rectangular waves, an example of which is shown in Figure 3.12. The shape depends on a number of factors including the size of the probe tips, their wetting and drying time, and the response time of the data acquisition and processing systems [29].

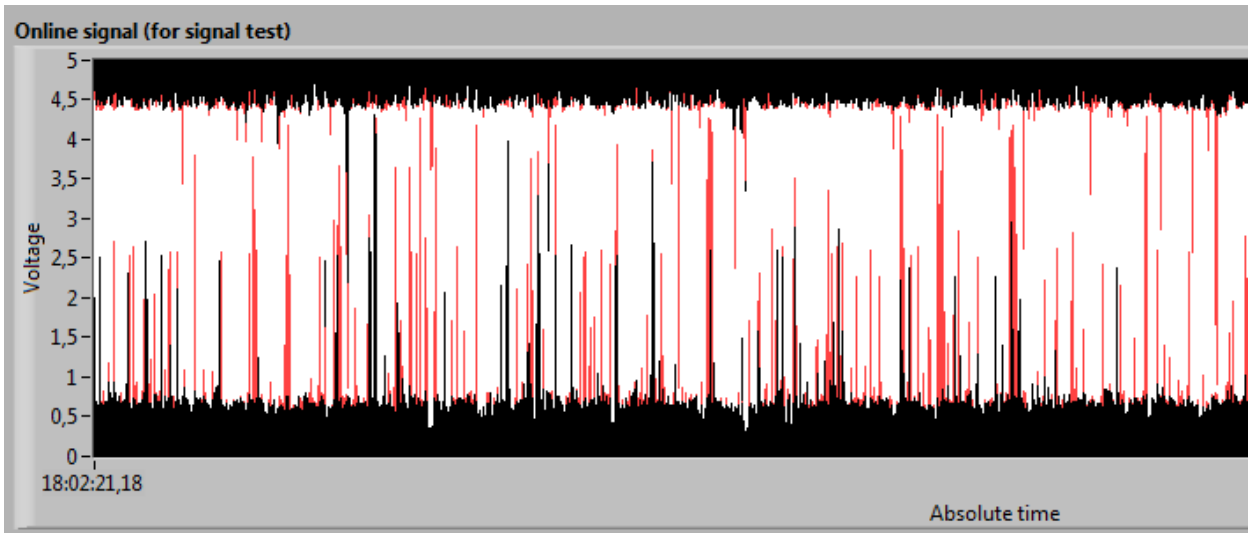

Figure 3.12: Typical voltage signal detected by the dual-tip probe when in water

Chapter 4: Experimental Methodology

In order to fulfill the objectives of this study, a large amount of data was gathered with the help of the dual-tip probe described in Chapter 3. The collected data was then analyzed to determine a set of parameters to describe the flow through the PKW and stepped spillway. The analysis was focused mainly on determining flow properties (Section 4.1) and energy dissipation (Section 4.2). The methodology used to collect data and the formulae involved in its analysis are highlighted in this chapter.

4.1. Flow Characteristics

Measurements were made for four different flow rates, which include: 60, 80, 140, and 180 L/s. These flow rates represent low, medium, and high flows relative to the potential range of the spillway model. The model's spillway has over 40 steps, each with a height of 4 cm. For flow rates of 60, 80, and 140 L/s, measurements were made at 9 different steps[1], which include steps 15, 17, 19, 21, 24, 27, 30, 32, and 37. Whereas for a flow rate of 180 L/s, the same set of steps was used with the exception of step 15. This step was excluded because it was too close to the crest and therefore the flow intensity was very high, which could result in considerable shaking (due to vibrations) of the probe and data prone to errors. Also, the flow consisted almost entirely of water and so, was of little importance with regards to the current analysis, which focuses on air entrainment in skimming flows.

In order to analyze the flow, measurements were made at six positions in the transverse direction, referred to as 'verticals' here. Each vertical corresponds with a key element of the PKW, as shown in Figure 4.1. Positions B and E correspond with the centre of the inlet keys, and are expected to depict similar behaviour. Positions C and D correspond with the centre and edge of the outlet key, respectively, and Positions A and F correspond with points closest to the side walls on either side of the channel.

To record the desired data, the dual-tip probe was placed perpendicular to the fictitious bottom of the flow, viz. the pseudo-bottom, ensuring that the probe tips were in-line with the step and parallel to the flow direction. At each vertical, numerous measurements were made across the flow depth to study the flow properties, such as air concentration and velocity distributions.

In order to achieve this, the first measurement was made as close to the bottom as possible, following which the probe was gradually raised (moved away from the step), recording data at constant intervals of 5 mm till a height of 53 mm from the pseudo-bottom. After this point, the interval was increased to 1 cm, since the probe was now not fully submerged in water and the changes in void fraction and flow velocity were less relevant. Measurements were made up to a point where the void fractions recorded by both, the

[1] It is important to note that the step numbers indicated here are based on a spillway with a WES Ogee crest and a step height of 8 cm rather than 4 cm. However, for the sake of maintaining an easy comparison with previous studies on the topic, the same labels were adopted here.

leading and the trailing, tips reached 99%. Figure 4.2 illustrates the typical placement of the probe (herein the single-tip probe) and the direction of movement for data acquisition.

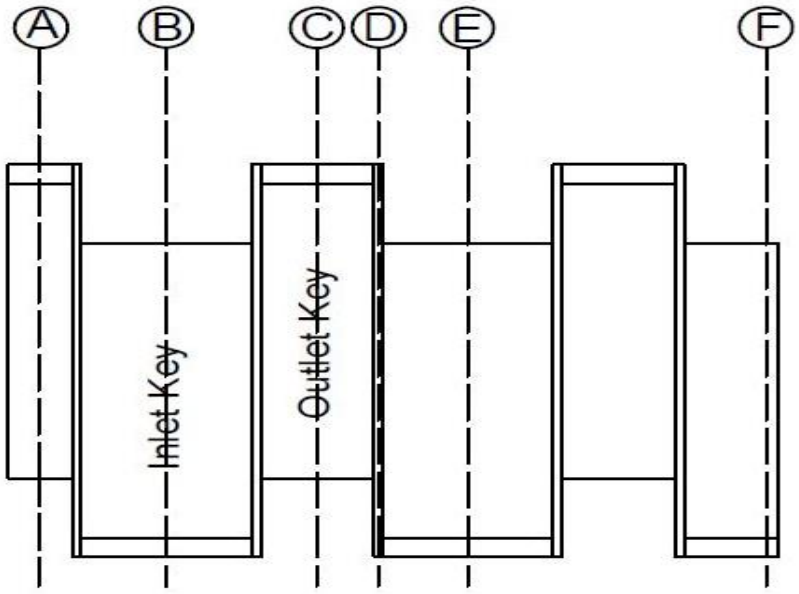

Figure 4.1: PKW with verticals highlighted for flow measurement

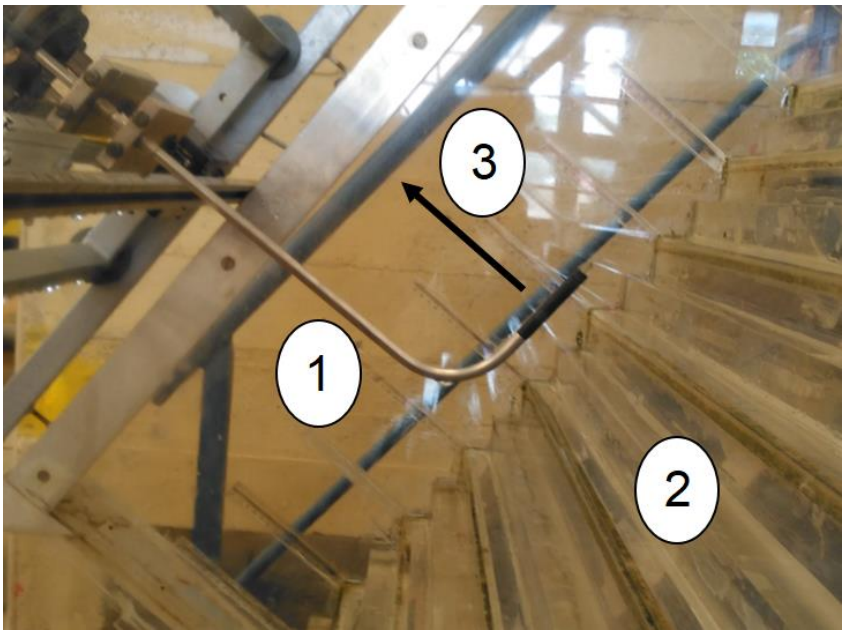

Figure 4.2: (1) Placement of the single-tip phase detection probe along the (2) pseudo-bottom and (3) direction of movement to record data

While recording data, settings on the data acquisition software were kept constant for all the measurements. A sampling frequency of 20 kHz was used, while each measurement lasted for 45 seconds. These were chosen based on a previous study, which indicates that lower values for these parameters result in low precision of the overall results [19]. Higher values could have been chosen as well however, they present limitations in terms of storage space on the computer.

A key parameter during the analysis of data was the threshold of air-water interface. It is defined within the programme and is crucial in reducing background noise in voltage signals formed when the flow interacts with the probe tips. In previous studies using the dual-tip probe developed at WRL, UNSW Australia, a threshold of 50% was usually adopted [4] [19]. However, when gathering data at the facility in LNEC, and comparing it with the study by Gomes [26], a difference was observed between air concentration profiles measured with the single and dual tip probes. Upon investigating further, this difference was linked to the threshold, as both the probes have different sensitivities and therefore, react differently to it. An extensive analysis was made to review and determine an adequate threshold for the dual-tip probe [33]. Values of 50%, 80%, 85%, and 90% were tested and comparisons were made between data gathered with the two probes, under similar conditions. The results showed that the effect of varying threshold on the acquired data became less prominent at higher values. So, a threshold of 80% was chosen [33], as it was high enough to not have a negative impact on the data while still being comparable with measurements made using the single-tip probe [26].

Once all the data was acquired, a number of parameters was determined in order to analyze the flow. These parameters, along with their formulae, are described in Subsections 4.1.1 to 4.1.6.

4.1.1. Air Concentration (C)

Air concentration, or void fraction, refers to the local amount of air, present in the flow of water, at a given point. Here, it was measured and calculated as the average volume of air, detected individually by each tip, per unit volume of flow (air + water) during the 45 second time interval for which each measurement was made. The air concentration for each tip of the phase detection intrusive probe was measured and displayed directly on the software.

4.1.2. Interfacial Velocity (v)

In theory, due to the presence of two tips, the same air bubble or water droplet may be pierced by both of them. When the distance between both tips is known, the interfacial velocity may be determined as the time a bubble would take to travel this distance. However, in reality it is very difficult to know if the same bubble is pierced twice. To account for this, usually a detailed cross-correlation analysis is made between the

voltage signals obtained for both probe tips, which suggests that the interfacial velocity at a given point may be determined using Equation 1 [19]. This relation was used by the post-processing software here, as well.

$$\boldsymbol{v} = \frac{\Delta \boldsymbol{x}}{\boldsymbol{t}} \quad \textbf{(1)}$$

Where,

v = Interfacial velocity [m/s]

Δx = Stream-wise distance between probe tips [m]

t = Interfacial travel time for which the cross-correlation function is maximum [s]

4.1.3. Characteristic Depth (y_{90})

This parameter is the distance, measured vertically from the pseudo-bottom of the flow depth, at which the air concentration is 90%. Considering the extremely complex nature of flows consisting of both, air and water, points connecting the characteristic depth are chosen as the free surface. Therefore parameters calculated for this depth are used in determining the associated flow properties. Here, the value for y_{90} was determined through linear interpolation between two values of depth, between which an air concentration of 90% was likely to lie.

4.1.4. Normalized flow parameters

In order to minimize the effect of errors that may arise during the data acquisition process, normalized values of flow depth (y/y_{90}) and velocity (v/v_{90}) were calculated. This set of values was then fitted as a curve observing the power law to determine the relationship between velocity and depth of flow. Using the power law for such purposes is quite common in the analysis of open channel flows, such as this stepped spillway module, especially when measurements are made at multiple points along the cross-section [32]. Here, the power law, as expressed in Equation 2, was chosen particularly because it is simple to use and can be applied to the entire flow region [32].

$$\frac{\boldsymbol{v}}{\boldsymbol{v_{90}}} = \left(\frac{\boldsymbol{y}}{\boldsymbol{y_{90}}}\right)^{1/N} \quad \textbf{(2)}$$

Where,

y = Distance, normal to the pseudo-bottom, from the step edge [m]

y_{90} = Distance, normal to the pseudo-bottom, from the step edge at a void fraction of 90% [m]

v_{90} = Velocity corresponding with y_{90} [m/s]

N = Parameter (exponent) of the Power law

The exponent, N, is a property of the channel bed and may be determined by plotting the results of each measurement and fitting the curve to the power law equation. The coefficient provides an indication of the resistance the channel bed imparts on the flow over it and therefore has a direct effect on the vertical velocity distribution [32]. Typically, the value of this coefficient is less than 5 for skimming flows over stepped spillways of identical slope and step height, in the gradually varied flow region. Within this range, it lies close to 4, near the end of the spillway [24]. Also, the value may vary from one step edge to the next so, a distinct value was calculated for all the tested steps and verticals.

4.1.5. Mean Air Concentration (C_{mean})

In order to visualize more clearly the change in air concentration across the cross-section and the length of the spillway, a mean value was calculated for each vertical. For this, Equation 3, valid for a single vertical along the cross-section, was used.

$$C_{mean} = \frac{\int_0^{y_{90}} C\, dy}{y_{90}} \quad (3)$$

Where,

C_{mean} = Mean air concentration

C = Local air concentration

4.1.6. Equivalent Clear water depth (h_w)

The equivalent clear-water depth refers to the hypothetical flow depth that would occur if all the air was removed from it, i.e. if the flow constituted entirely of water. This parameter was calculated using Equation 4, which is valid for a single vertical along the cross-section.

$$h_w = \int_0^{y_{90}} (1 - C)\, dy = (1 - C_{mean}) * y_{90} \quad (4)$$

4.2. Energy Dissipation

In order to study the energy dissipation of the flow, four additional verticals were examined. These are highlighted in grey in Figure 4.3. They enable a more detailed analysis as they cover a greater number of

points along the cross-section. They also provide a means for verifying the data previously gathered in similar locations across the PKW. These measurements were made only at steps 32 and 37, which were the last steps the probe could reach, given the limitations of the metal frame and support structure, to acquire data at the bottom of the spillway and beginning of the stilling basin, respectively.

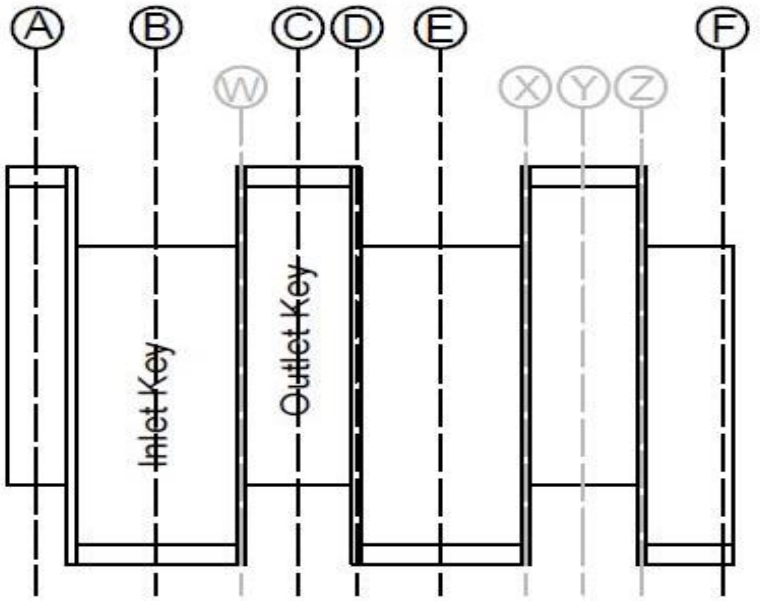

Figure 4.3: PKW with verticals highlighted for specific energy analysis

The specific energy available at the bottom, or residual energy, of a spillway is simply the difference between the maximum energy, per unit weight of fluid, which a body of water possesses at the top and the amount it loses along the path it takes to the bottom, viz. the head loss. As stated in Equation 5, the head loss is defined by two components, which are described in detail in the following subsections.

$$\Delta \boldsymbol{E} = \boldsymbol{E_{max}} - \boldsymbol{E} \qquad \textbf{(5)}$$

Where,

ΔE = Head loss [m]

E_{max} = Specific energy of the potential flow (maximum specific energy) relative to the elevation of each step [m]

E = Specific energy at each step [m]

4.2.1. Maximum Specific Energy (E_{max})

The maximum specific energy, or specific energy of the potential flow, possessed by a body of water associated with a dam is the energy, per unit weight of fluid, it possesses at the top, i.e. when it resides in the upstream reservoir. The major components of this energy are expressed in Equation 6. The kinetic head (the last component of the equation) is dependent on the velocity with which water flows into the reservoir, which is a function of the incoming discharge.

$$\boldsymbol{E_{max} = \left(Z_{crest} - Z_{step}\right) + h_{PKW} + \frac{U^2_{reservoir}}{2g}} \quad \textbf{(6)}$$

Where,

Z_{crest} = Elevation of the spillway crest measured from the ground [m]

Z_{step} = Elevation of the step edge measured from the ground [m]

h_{PKW} = Height of water above the PKW in the upstream reservoir [m]

$U_{reservoir}$ = Mean water velocity in the upstream reservoir [m/s]

g = Acceleration due to gravity [m/s^2]

4.2.2. Specific Energy (E)

Specific Energy, defined by Bernoulli's equation, refers to the energy head relative to the bottom of an open channel. The major components include kinetic, potential, and pressure heads. In this study, Equation 7 was used to calculate the specific energy at each step, of the chute. Here, the equivalent clear-water depth is used in order to avoid the over estimation of specific energy that may result from the use of the bulked flow depth [21].

$$\boldsymbol{E = h_w \cos\theta + \alpha \frac{U_w^2}{2g}} \quad \textbf{(7)}$$

Where,

Θ = Slope of the Spillway [˚]

α = Kinetic energy coefficient

U_w = Mean water velocity [m/s]

In the kinetic energy head in Equation 7, the mean water velocity (U_w) is simply the discharge of water per unit area of the flow channel, as expressed by Equation 8.

$$U_w = \frac{Q}{w * h_w(avg)} \quad \textbf{(8)}$$

Where,

Q = Flow rate of water [m^3/s]

w = Width of the channel [m]

h_w (avg) = Cross-sectional average clear-water depth at each step [m]

In a three-dimensional flow, the kinetic energy coefficient is calculated using Equation 9, which has been adapted from Matos [23].

$$\alpha = \frac{1}{U_w^2} * \frac{\int_0^1 \int_0^{y_{90}} (1 - C) v^3 dy\, dw}{\int_0^1 \int_0^{y_{90}} (1 - C) v\, dy\, dw} \quad \textbf{(9)}$$

Chapter 5: Results and Discussion

This chapter discusses the results of the extensive analysis carried out to determine the flow properties and the energy dissipation over a stepped chute fitted with a PKW crest. Section 5.1 makes a comparison of the results of this study with those of a previous study that used a single-tip probe to analyze flow under similar conditions. Sections 5.2 and 5.3 deal with the analysis of flow and energy dissipation, respectively, made in this study using the dual-tip probe developed at the WRL, UNSW Australia.

5.1. Comparison of the Single-tip and Dual-tip Probes

The test assembly at LNEC, used in this study, has been the focus of multiple experiments related to flow analysis [22] [23] [25] [26] [34]. However, a single-tip conductivity probe, developed and calibrated by the United States Bureau of Reclamation (USBR), has been used each time. In this study, a dual-tip probe was used instead to allow the collection of a broader set of data. In the initial stages of the current analysis, a comparison was drawn between the air concentration profiles, determined, under similar conditions, using the single-tip [26] and dual-tip probes.

The air concentration plots at discharges of 80 L/s and 140 L/s, are presented in Figures 5.1 and 5.2, respectively. The graphs include lines for verticals C and E only, since the other positions were not analyzed in the previous study. For the same reason steps 15, 17, and 37 were excluded from the comparative analysis. The graphs also serve as an opportunity to analyze the difference in trend between the inlet and outlet keys, with greater clarity. The graphs indicate a fairly close comparison between the air concentration profiles obtained using the single and dual tip probes, for both flow rates. In general, air concentrations recorded by the dual-tip probe are slightly different than those recorded by the single-tip probe for all the analyzed steps. After careful analysis, the reason for this was found to be an error in the adjustment of the voltage threshold while making measurements with the dual-tip probe. More often than not, the threshold was set slightly higher or lower than the chosen value, which could not be observed precisely due to the limited voltage scale of the data acquisition system. However, since the difference in results was generally very low (within 10%), this effect was ignored for the data that had been obtained already, and changes were made only for measurements at steps 32 and 37 for the increased number of verticals used in the energy dissipation analysis (discussed in Sections 4.2 and 5.3).

This analysis also provides information on the relation between the flow through the inlet and outlet keys of the PKW. For steps close to the spillway crest, air concentration in the outlet key, i.e. Position C, is higher than in the inlet key, i.e. Position E. As the flow moves downstream, the trend switches resulting in a higher

concentration at the inlet key than at the outlet key. This change occurs around step 21 for 80 L/s and step 24 for 140 L/s.

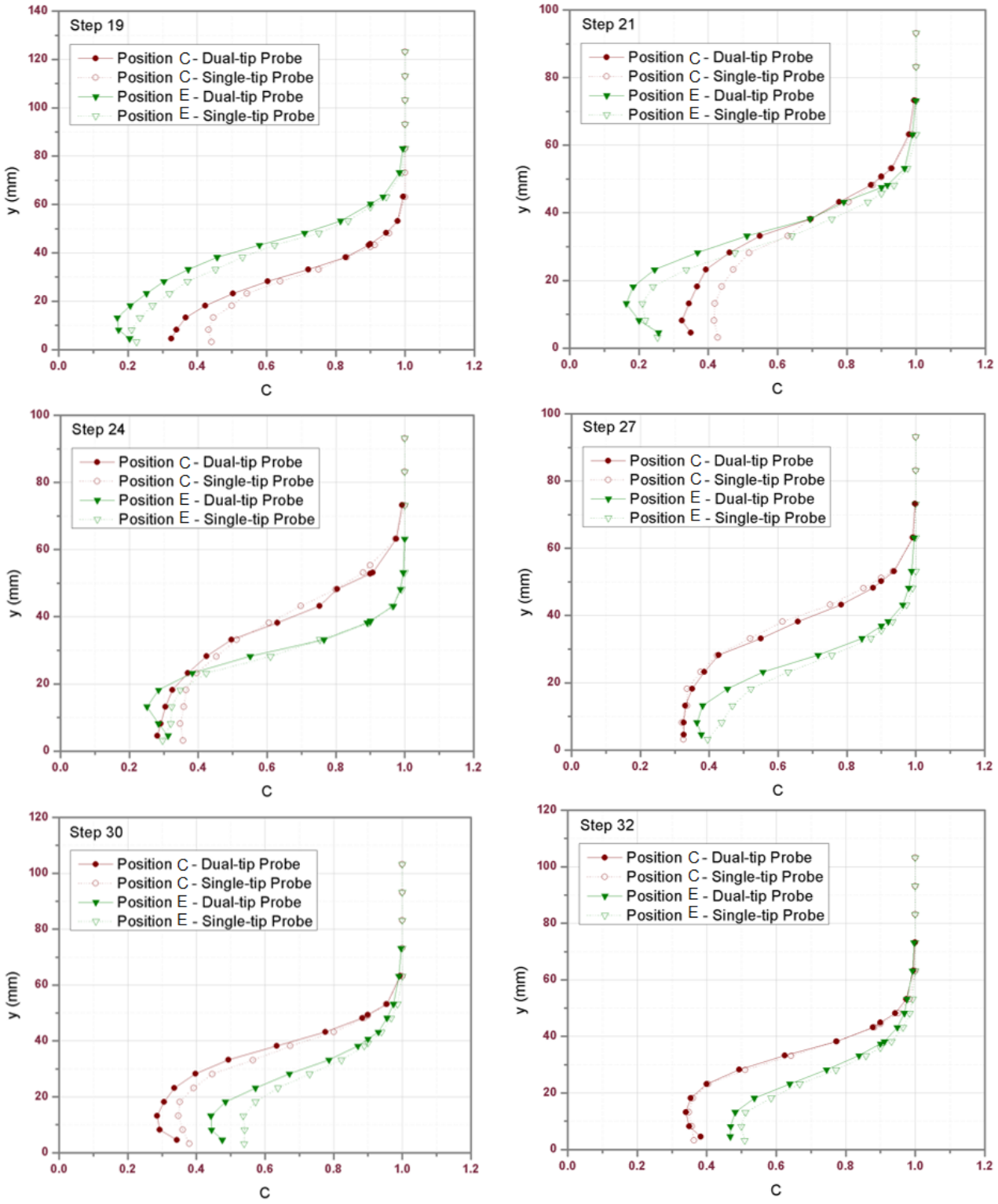

Figure 5.1: Comparison of air concentration profiles obtained with the dual-tip and single-tip [26] probes at Q = 80 L/s

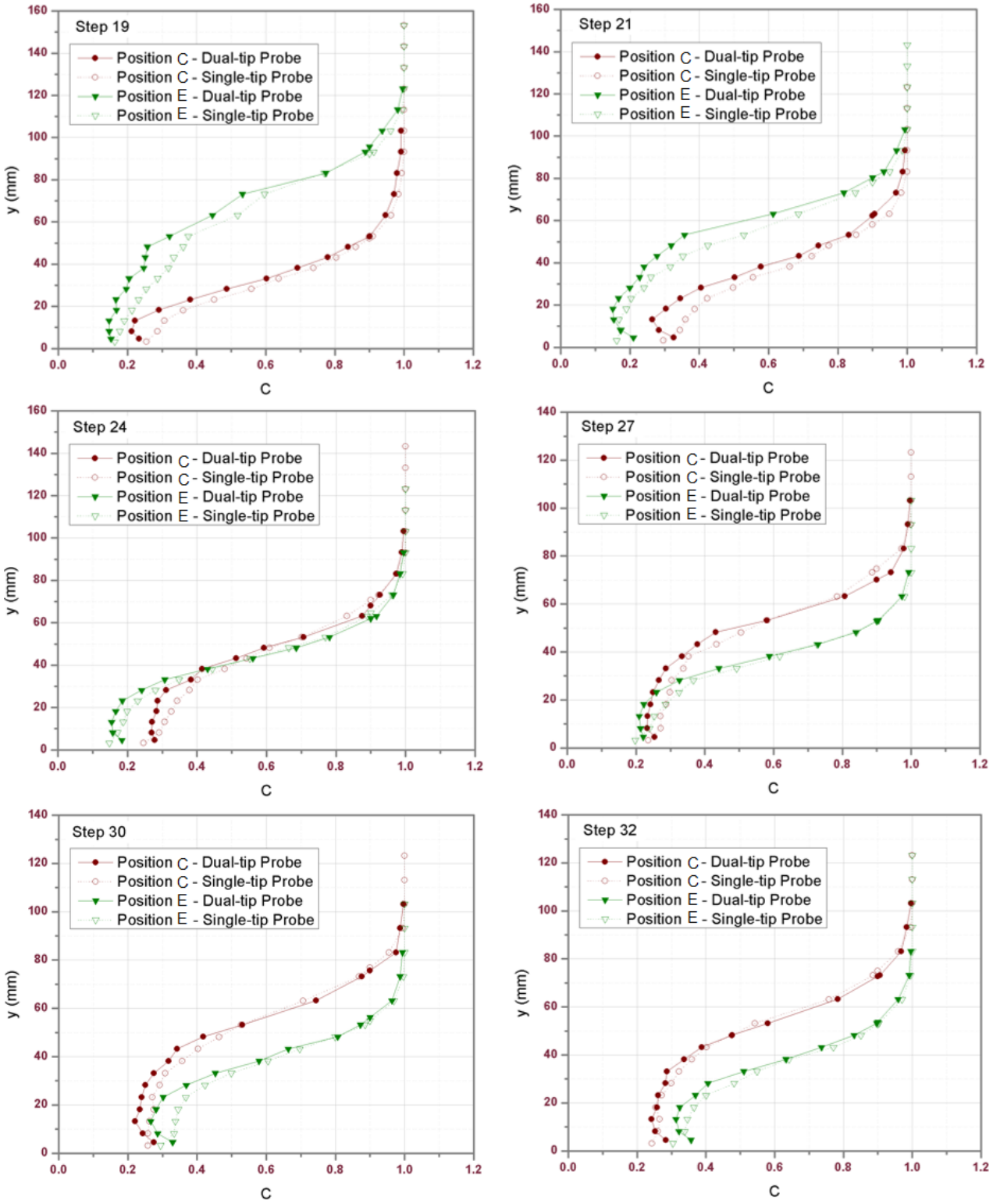

Figure 5.2: Comparison of air concentration profiles obtained with the dual-tip and single-tip [26] probes at Q = 140 L/s

The variation in mean air concentration, characteristic depth, and equivalent clear-water depth at verticals C and E was also compared for the two discharges. Figure 5.3 shows the comparison between mean air concentrations calculated using data recorded by the two probes at the two flow rates. The graphs show that the mean air concentrations resulting from the dual-tip probe are lower than the ones from the single-tip probe for all the analyzed steps. This may again be attributed to the imprecise allocation of the voltage threshold. The difference between the two probes remains relatively constant across the chute length.

The graphs also show that the mean air concentration near the upstream end of the stepped chute is higher at the outlet key. The difference between the inlet and outlet keys gradually decreases till a point close to step 27. Downstream of this, the mean air concentrations corresponding with the inlet key become higher than the outlet key, indicating the formation of cross-waves within the flow. However, at both flow rates, the values lie within the same narrow range of 0.38 – 0.6.

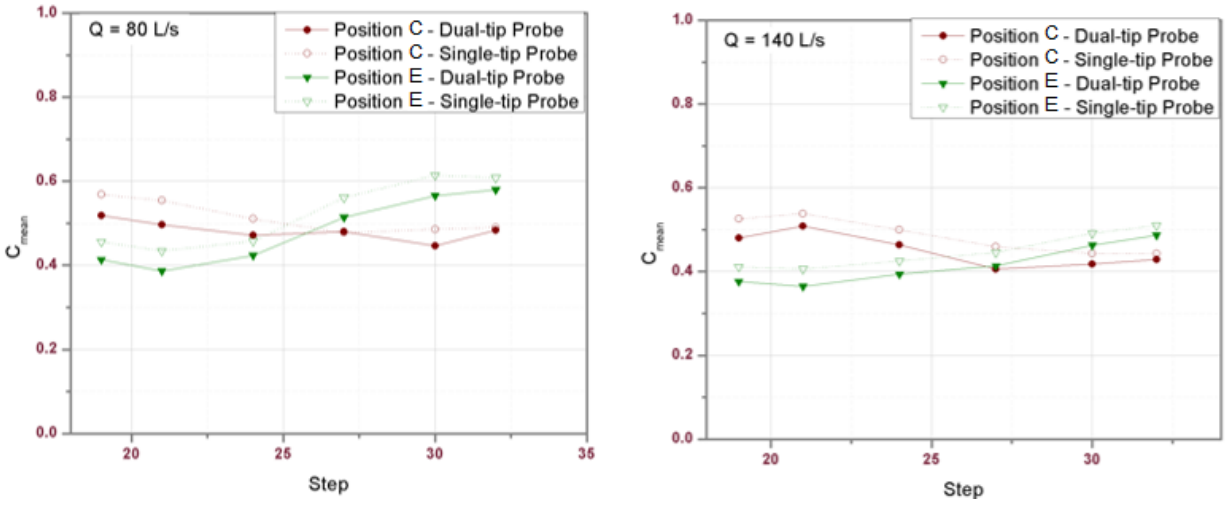

Figure 5.3: Comparison of mean air concentrations obtained with the dual-tip and single-tip [26] probes at Q = 80 L/s (Left) and Q =140 L/s (Right)

Figure 5.4 shows a comparison between the characteristic depths recorded using the single-tip and dual-tip probes. The resulting graphs show a very close comparison between the depths. In the cases where a difference does exist, the trend is similar to the parameters discussed above, i.e. the values determined from the dual-tip probe are lower than the single-tip probe.

The graphs also show that the characteristic depth corresponding with the inlet key decreases along the channel length for both flow rates. Whereas, the depth corresponding with the outlet key increases till a position close to Step 24, after which it starts to decrease gradually. For both keys, the depths become relatively constant close to the bottom of the spillway.

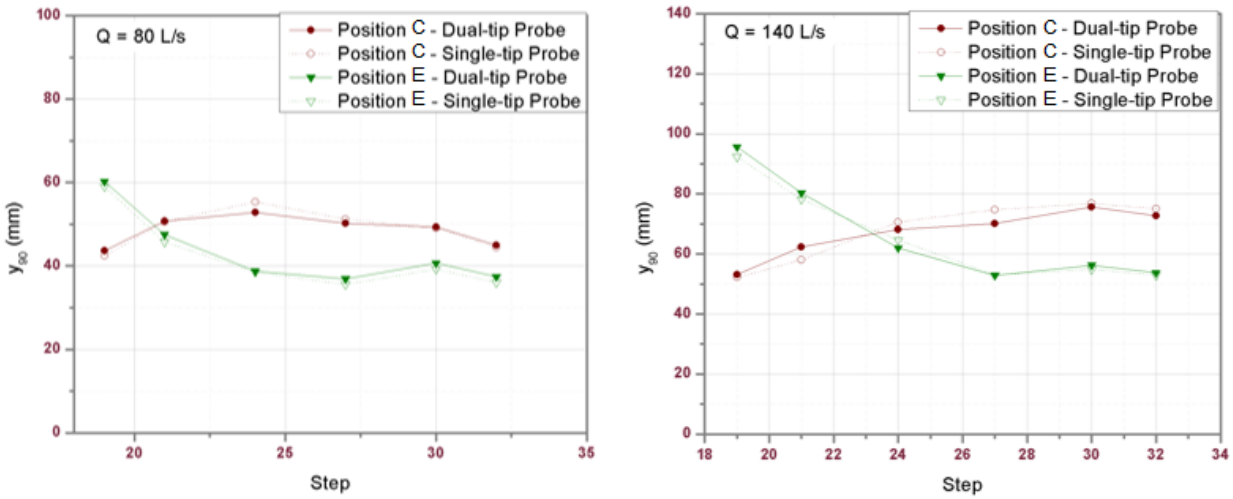

Figure 5.4: Comparison of characteristic depths obtained with the dual-tip and single-tip [26] probes at Q = 80 L/s (Left) and Q = 140 L/s (Right)

Figure 5.5 shows a comparison of the equivalent clear-water depth calculated using the data obtained from both probes. The graphs show that the difference between the two probes is more pronounced in the depths corresponding with the inlet key, i.e. the vertical E. This difference may be attributed to the slightly bigger gap in values of mean air concentration, as can be seen in Figure 5.3, because the equivalent clear-water depth depends significantly on it.

The graphs also show that the equivalent clear-water depth corresponding with the outlet key tends to increase over the channel's length. The opposite can be seen for the inlet key. As expected, the clear-water depths observed at Q = 80 L/s are lower than at Q = 140 L/s, while they are always lower than the characteristic depths presented in Figure 5.4.

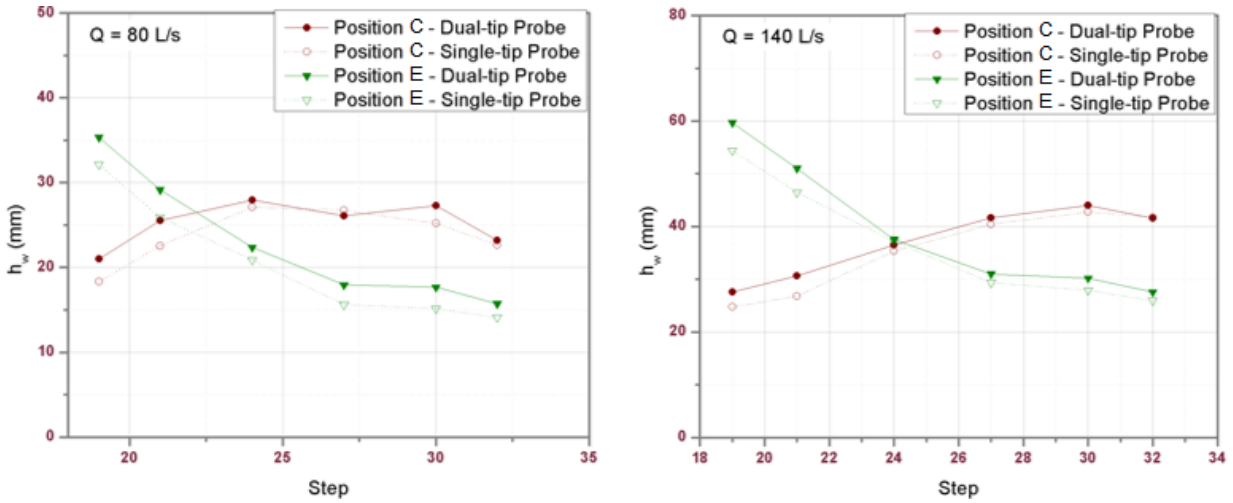

Figure 5.5: Comparison of equivalent clear-water depths obtained with the dual-tip and single-tip [26] probes at Q = 80 L/s (Left) and Q = 140 L/s (Right)

5.2. Analysis and Characterization of the Flow

A number of measurements, as described in Chapter 4, were made using the dual-tip probe. The results were used to characterize flow over a PKW and stepped spillway with a step height of 4 cm. The analyzed parameters are presented and discussed in detail in the proceeding subsections.

5.2.1. Air Concentration Profiles

Air concentration profiles along the cross-section tend to vary with both, the flow rate and the distance from the spillway crest. Figures 5.6 to 5.14 illustrate the profiles resulting from the measurements made at various steps with the dual-tip phase detection intrusive probe. Based on the trends depicted in the graphs, the following general observations can be made:

- At each step and discharge, beyond a distance of 10 – 20 mm from the pseudo-bottom, the air concentration increases continuously, and eventually becomes constant as the probe reaches the surface layer and moves out of the water.
- For all discharges, the air concentration profiles vary across the channel's cross-section, depending on the vertical, or key, they correspond with. This changing behaviour is observed till a certain step, after which the profiles become relatively constant. This indicates a shift from three-dimensional to two-dimensional flow.
- For all four discharges, the tendency of the flow to become two-dimensional increases as water moves down the stepped chute. This is due to decreasing influence of the high intensity jets formed over the PKW, as the water moves away from the crest and the flow moves towards stability.
- For the two higher discharges, the air concentrations initially decrease with an increase in the distance from the pseudo-bottom. This may be due to the probe being positioned slightly within the step cavity near the pseudo-bottom.

In addition to the general observations mentioned above, and supplemented by the normalized air concentration profiles presented in Appendix B, a more detailed analysis of each flow rate is presented below:

<u>At Q = 60 L/s</u>

- The flow is relatively smooth and the overall flow depth decreases as water moves down the stepped chute. This pattern is in accordance with the skimming flow regime, which is established very early on, around step 17.
- At steps 15, 17, and 19, the air concentrations corresponding with the inlet keys are lower than the outlet keys. Beyond this point, they start moving to the higher side, and eventually become greater than the air concentrations corresponding with the outlet keys, until two-dimensional flow is achieved. This is usually an indicator of the formation of cross-waves within the flow channel, which is characteristic of flow over a PKW.

- At steps 15, 17, 19, and 37, positions corresponding with verticals A and C depict nearly identical air concentration profiles across the flow depth. The profiles are quite similar for steps 21, 24, and 27 as well. This may be due to the fact that both verticals lie at positions corresponding with the outlet key and should therefore have similar flow patterns. However, the vertical C acts as an outlier at steps 27, 30, and 32. This may be a consequence of the cross-waves that develop in the vicinity of vertical C.
- The air concentration profiles at verticals B and E are nearly identical across the channel's length, which is a consequence of both being at the centre of the inlet keys.
- The air concentration at vertical A is the highest on steps 15 – 21, while it is the lowest at vertical F on steps 17 – 24. These verticals correspond with the two points closest to the edges of the channel on either side. As a result, the flow may have been influenced by the side walls depending on the distance from the edges.
- The water appears to start moving from three-dimensional to two-dimensional flow at step 24, since beyond this point the variation in air concentration profiles across the cross-section appears to become insignificant.

<u>At Q = 80 L/s</u>

- The flow is relatively irregular at the head of the spillway but tends to become smooth as water moves downstream. This occurs around step 19, which is where the water appears to enter the skimming flow regime, as it exits the influence of the jets coming from the PKW. The overall flow depth follows a similar trend, i.e. it is high near the crest, gradually decreases downstream and eventually becomes constant.
- For steps 15 and 17, the increase in air concentration is quite rapid owing to the high intensity of the incoming jets of water, particularly at the outlet keys. Downstream of this, the change is relatively slower and consistent across the channel's cross-section.
- At steps 15, 17, 19, and 21, air concentrations corresponding with the inlet keys are lower than those at the outlet keys however, the difference is not as pronounced as that seen at Q = 60 L/s. At step 24, the profiles for both keys begin to overlap after which air concentrations in the inlet keys become higher than the outlet keys, before becoming relatively similar around step 37. This indicates that the development of cross-waves occurs a little later in comparison with Q = 60 L/s.
- At steps 27, 30, 32, and 37, air concentration profiles corresponding with verticals A and D are nearly identical. This is a divergence from the behaviour observed at Q = 60 L/s. On the other hand, vertical C acts as an outlier the same way it did at the lower discharge. This behaviour occurs between steps 24 and 37, which is concurrent with the potential development of cross-waves at this discharge.

- The profiles corresponding with verticals B and E are also quite similar for all the steps except 15. This acts as added verification for the recorded data as, theoretically, both verticals at the centre of the inlet keys should show similar behaviour.
- The air concentration profiles for verticals A and F indicate an influence of the side walls here as well. Air concentrations are the highest for vertical A between steps 15 and 24, while they are the lowest for vertical E for steps 15 and 17 and for vertical F till step 24.
- The water appears to achieve two-dimensional flow somewhere between steps 24 and 27, which is downstream of the point observed at Q = 60 L/s. This can be observed more clearly in the figures presented in Appendix B.

At Q = 140 L/s

- The air concentration profiles at step 15 show significant fluctuations around the middle of the flow depth. This may be attributed to the high speed and intensity at which water enters the stepped chute. The overall flow depth is considerably higher than the lower flow rates but follows the same pattern of variation across the flow length. The development of skimming flow also occurs further downstream in comparison with the lower flow rates.
- Upstream of step 24, the change in air concentration profiles is rather uneven, with large differences observed between the verticals. Beyond this point, the increase in air concentration is quite steady and identical across the cross-section. The initial irregularity is again due to the different paths the flow takes over the inlet and outlet keys, combined with the high volume of water that passes through them.
- At steps 15, 17, 19, and 21, there is a significant difference between air concentrations at the inlet and outlet keys, with the inlet concentrations always being lower than the outlet. Downstream of this, air concentrations corresponding with the inlet become higher than the outlet however, the profiles for both keys are quite similar.
- For steps 15 and 17, the outlet keys have a higher air concentration than the inlet keys. Following this, the air concentration profiles for verticals A and C still remain significantly higher than the other verticals at steps 19 and 21. However, the profile corresponding with vertical D begins to merge with the inlet keys. Around step 30, vertical C begins to acts as an outlier similar to the previous two cases of flow rate, indicating the formation of cross-waves, further downstream in comparison with Q = 80 L/s.
- At all steps, except 15, the air concentration profiles corresponding with the inlet keys at verticals B and E are nearly identical. Here, Vertical F depicts a slightly irregular trend, which may be warranted by the increased influence of the side wall at a relatively higher discharge.
- The water starts to shift from three-dimensional to two-dimensional flow between steps 27 and 30, which is again downstream of the lower discharges.

At Q = 180 L/s

- Air concentration profiles at step 15 were not obtained for this flow rate since it was out of range of the incoming jets of water before they hit the spillway's surface.
- The profiles are quite erratic at step 17 but tend to gradually smoothen beyond this point. The fluctuations at step 17 are more prominent near the centre of the flow depth, similar to those observed for step 15 at Q = 140 L/s.
- The overall flow depth is higher than the previously discussed cases and tends to follow a pattern consistent with the skimming flow regime, which occurs beyond step 21, as it moves across the stepped chute.
- The differences observed between the air concentration profiles at the inlet and outlet keys are similar to those seen at Q = 140 L/s. On the other hand, the anomaly observed in the profile for vertical C in the earlier cases is not seen here, which may suggest that the development of cross-waves is not significant, for the analyzed steps, in its vicinity at higher discharges.
- At steps 17, 19, and 21, the profiles corresponding with verticals B and F (rather than E) are quite similar, which is a diversion from the trend observed for the lower flow rates. However, downstream of this point, the profiles exhibit patterns similar to the earlier cases, i.e. they are nearly identical for verticals B and E.
- The air concentration profiles obtained for vertical F, here, are slightly different than the earlier cases, with the concentrations being close to the lower end at all steps. This may be due to the insufficiency of the side wall's height to sustain the entire flow depth at all times. Also, a high discharge results in a stronger impact on the walls, and therefore on the pattern of circulation of air in the flow.
- The water appears to move towards two-dimensional flow between steps 27 and 30, since the variation in air concentration along the channel's cross-section and length becomes negligible.

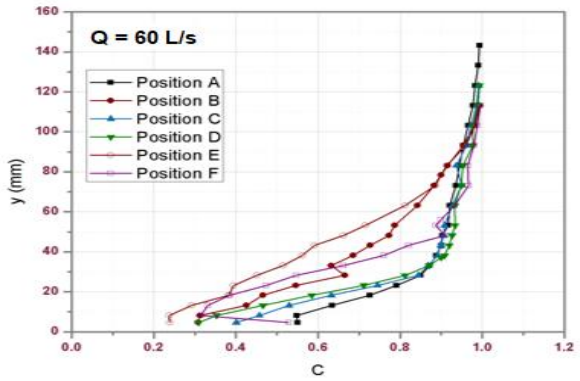

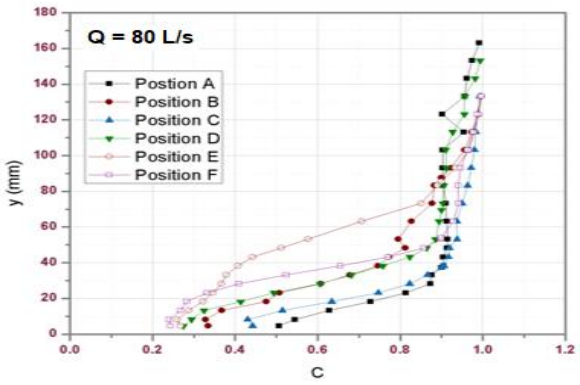

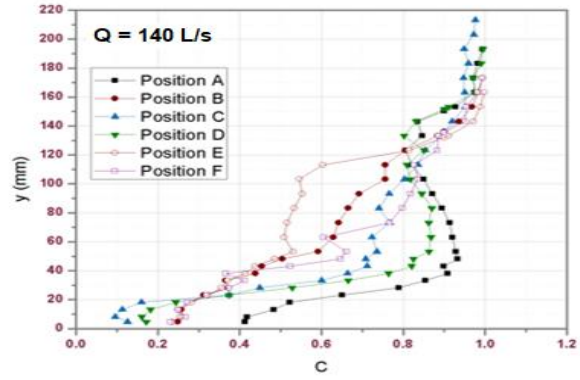

Figure 5.6: Air concentration profiles at step 15 for discharges of 60, 80, and 140 L/s (from top to bottom, respectively)

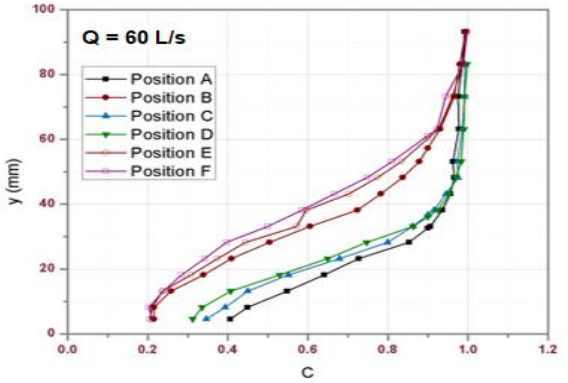

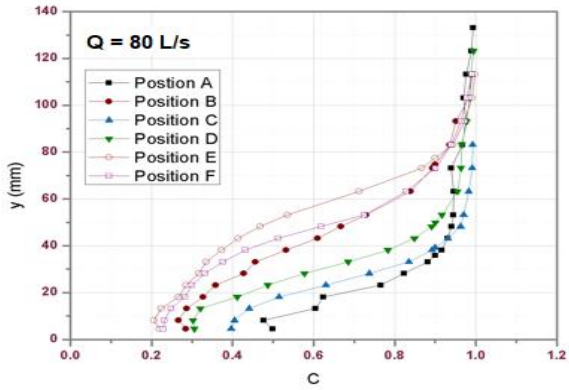

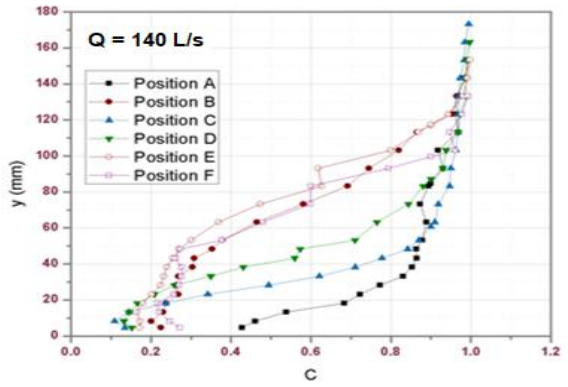

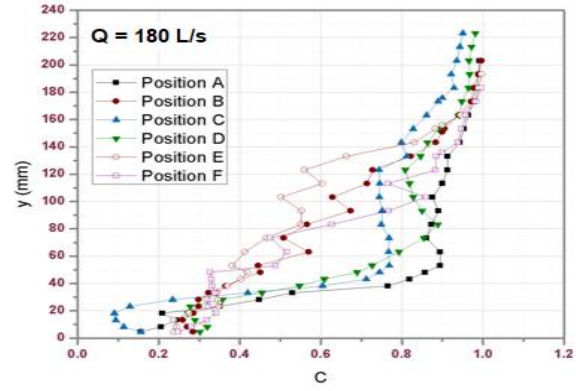

Figure 5.7: Air concentration profiles at step 17 for discharges of 60, 80, 140, and 180 L/s (from top to bottom, respectively)

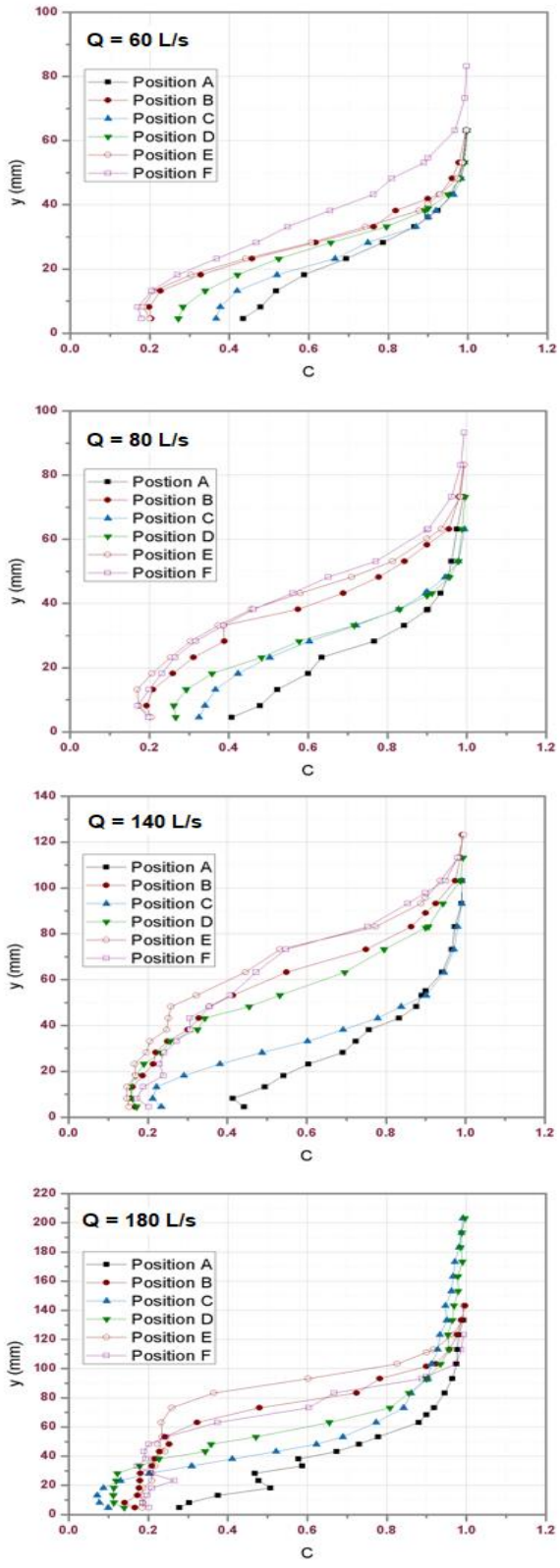

Figure 5.8: Air concentration profiles at step 19 for discharges of 60, 80, 140, and 180 L/s (from top to bottom, respectively)

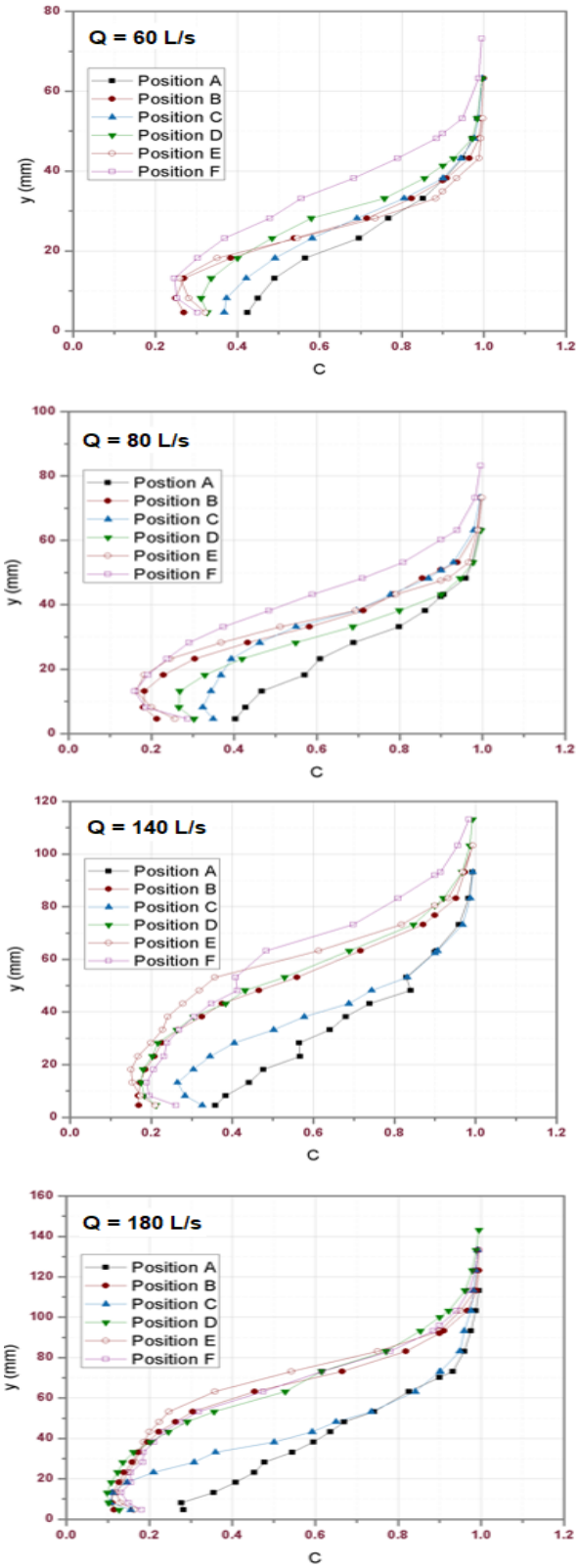

Figure 5.9: Air concentration profiles at step 21 for discharges of 60, 80, 140, and 180 L/s (from top to bottom, respectively)

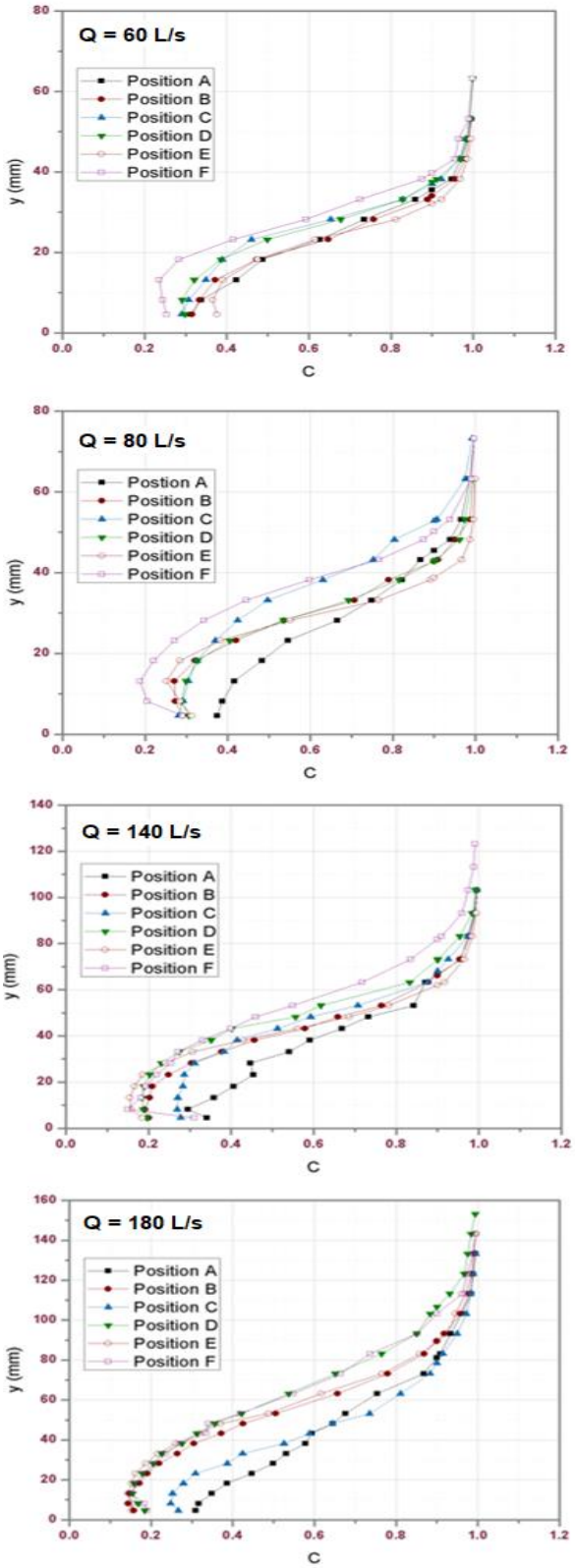

Figure 5.10: Air concentration profiles at step 24 for discharges of 60, 80, 140, and 180 L/s (from top to bottom, respectively)

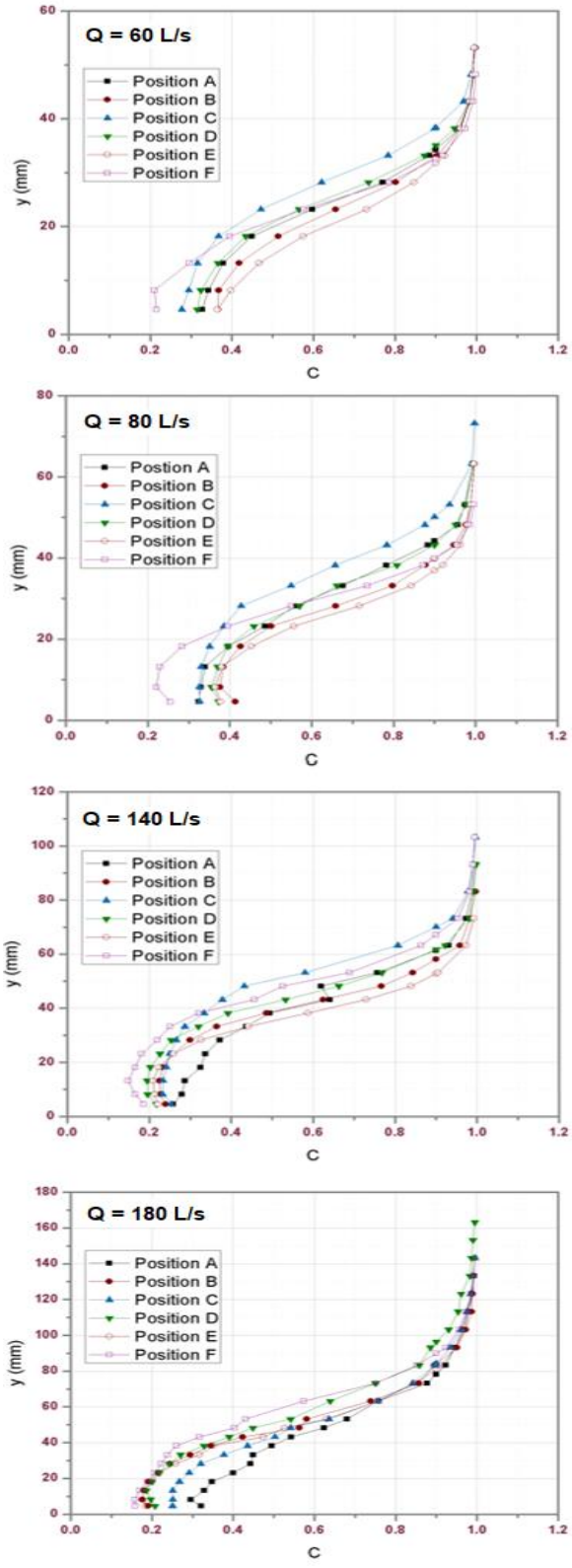

Figure 5.11: Air concentration profiles at step 27 for discharges of 60, 80, 140, and 180 L/s (from top to bottom, respectively)

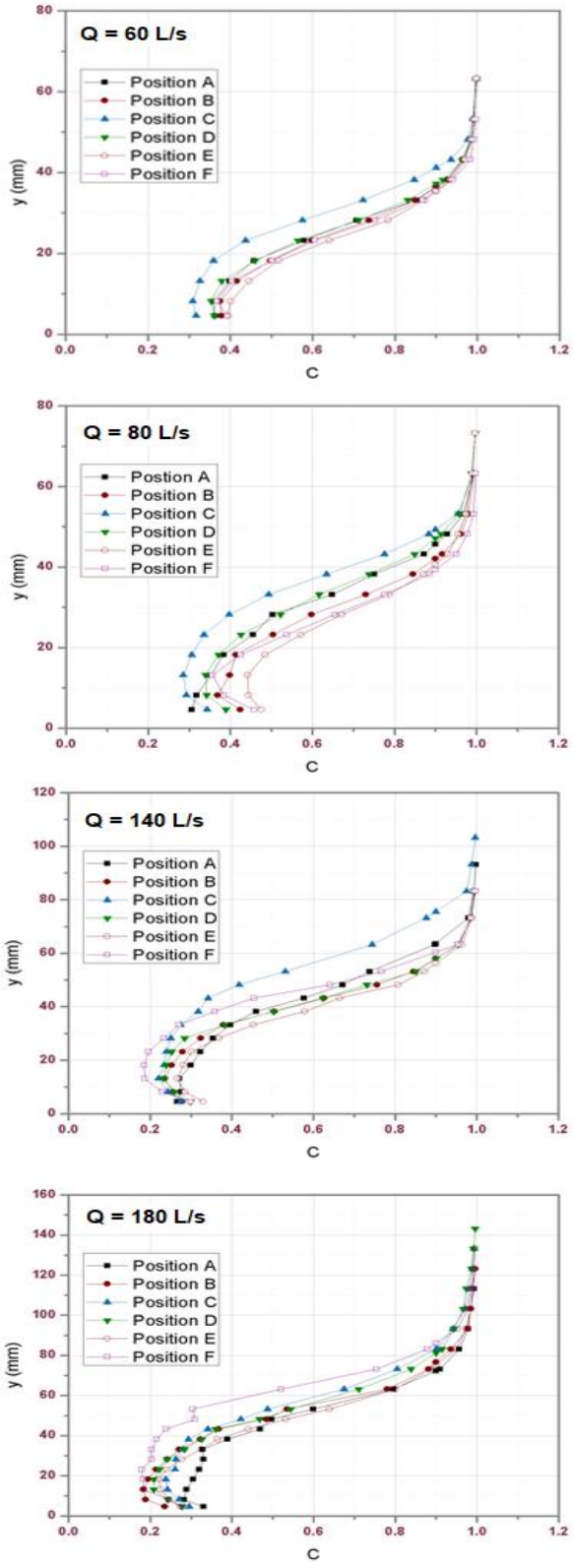

Figure 5.12: Air concentration profiles at step 30 for discharges of 60, 80, 140, and 180 L/s (from top to bottom, respectively)

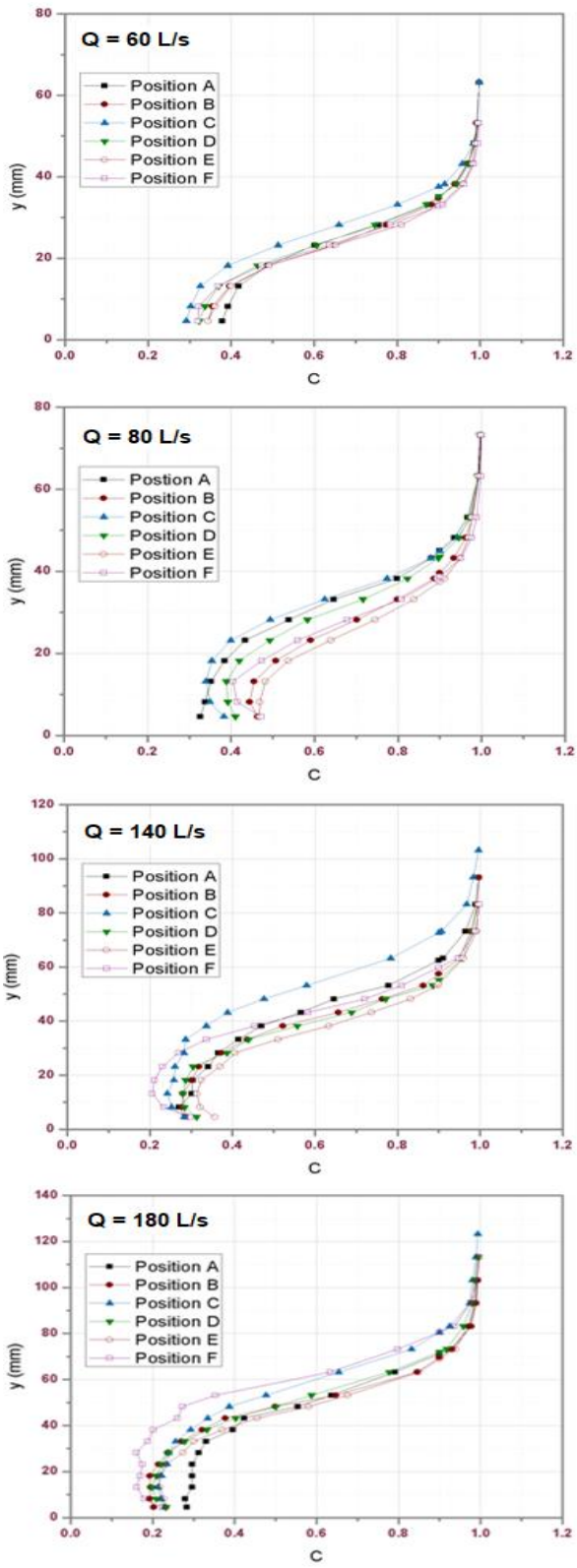

Figure 5.13: Air concentration profiles at step 32 for discharges of 60, 80, 140, and 180 L/s (from top to bottom, respectively)

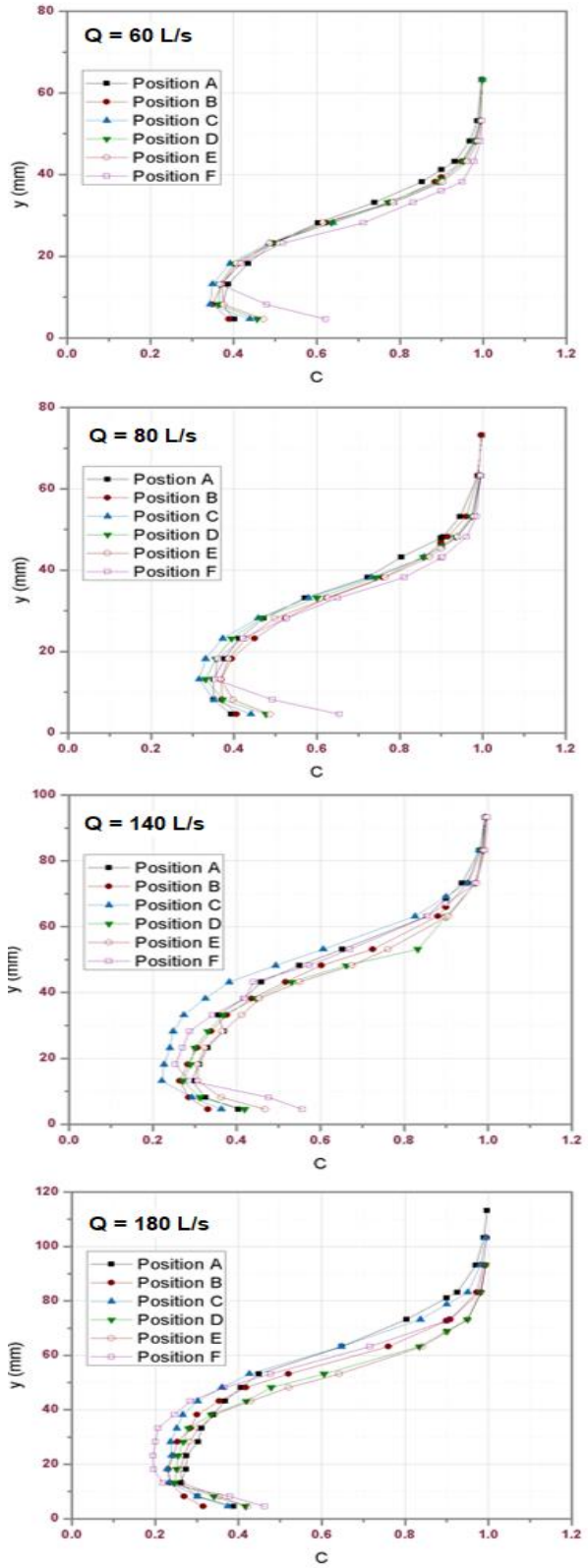

Figure 5.14: Air concentration profiles at step 37 for discharges of 60, 80, 140, and 180 L/s (from top to bottom, respectively

5.2.2. Velocity Profiles

The velocity tends to vary with the incoming discharge and the distance travelled by water from the crest. The velocity profiles illustrated in Figures 5.15 to 5.23 correspond with the interfacial velocities determined with the help of the dual-tip probe. Based on these graphs, a few general trends may be observed:

- The velocity at each step generally increases with an increase in discharge. This is justified considering that the two parameters are directly proportional for open channel flows.
- The velocity at a given flow depth also increases as water flows down the stepped chute. This is as expected, and is a result of the influence of gravity being greater than the energy losses in a gradually varied flow.
- In all the cases, the velocity shows a rapid increase up to a flow depth of 20 – 40 mm, after which it becomes constant till the surface layer is reached. There are occasional fluctuations close to the surface layer, which may be due to the impact of the incoming jets as water flows over the PKW.

A detailed analysis of the velocity profiles at each discharge was also made, which is presented and discussed below:

<u>At Q = 60 L/s</u>

- The velocity profiles are generally smooth, except for a few erratic changes at step 15 for vertical F, which may be due to an influence of the side walls on the flow.
- For all the steps, the increase in velocity is quite rapid, i.e. it changes from minimum to maximum at a small increase in the flow depth. There are no significant differences between the various verticals examined.
- Initially, there is no clear difference between the velocity profiles at the inlet and outlet. However, at step 17 it can be observed that the velocities corresponding with the outlet keys are lower than the inlet keys, with the difference becoming more pronounced as the flow moves downstream, till step 24. Beyond this point, the outlet profiles begin to merge with the inlet profiles as water moves towards the uniform flow regime.
- The velocity profiles corresponding with verticals B and E are nearly identical, which is justified since both points are located at similar positions on the inlet keys.
- From steps 27 to 37, the velocity profiles corresponding with the verticals A and F lie at extreme ends of the cluster of lines. A similar trend may be observed at step 15. This is synonymous with their relative positions along the channel's cross-section. For the steps in between this range, this trend is not very clear due to the effect of cross-waves that may alter the flow properties.

<u>At Q = 80 L/s</u>

- The overall velocity profiles are quite similar to the ones observed at Q = 60 L/s, only slightly higher at each step as the flow moves down the chute. This may be justified by the fact that the

difference in discharges is quite small so, under similar conditions the flow is not very distinct for the same structural geometry.

- Initially, the increase in velocity with the flow depth is fairly quick up to step 21, after which this change becomes relatively gradual. This trend is somewhat different from that seen at Q = 60 L/s, and may be due to the stronger force of the incoming jets of water closer to the crest at the higher discharge.
- The difference between the velocity profiles corresponding with the inlet and outlet keys is similar to the trend observed at the lower flow rate. However, the complete pattern moves a few steps downstream, i.e. the profiles begin to separate at step 19 rather than step 17. This trend continues till step 30 after which the profiles merge again.
- The profiles corresponding with the inlet keys at verticals B and E, again, depict nearly identical patterns and values for all the steps.
- The profiles for verticals A and F lie near, or at, the two edges of the cluster at all steps except 19 and 21. This may again be attributed to the effect of cross-waves on the flow. The trend is consistent for each analyzed step until the velocities become nearly identical at step 37, where the flow clearly exists as two-dimensional.

At Q = 140 L/s

- The velocity profiles are considerably irregular for steps 15 and 17, which may be due to a vibration of the probe caused by the strong force of water close to the PKW crest. However, beyond this point, the profiles begin to smoothen and the maximum velocity achieved at each step is, more often than not, similar to that at the lower discharges. Even in the cases where it differs, the velocities are only slightly greater.
- No clear trend may be observed for the rate of increase of the velocities at each step. The trend also differs between the inlet and outlet keys, with the change in the outlet keys being more rapid than the inlet keys till step 21. Downstream of this point, the increase with flow depth becomes steadier however, the range between minimum and maximum velocity becomes wider. This uneven trend may be a result of the increased intensity and intermittency of water jets, close to the spillway crest, associated with the high discharge.
- The difference between the velocity profiles corresponding with the inlet and outlet keys is very prominent at steps 15 and 17, with the outlet velocities being higher than the inlet velocities. Beyond this point, the difference begins to decrease with the profiles completely merging around step 21. The initial difference may be attributed to the varying path the water jets take while flowing over the PKW's keys. Flow over the inlet key is smoother than the outlet key therefore, the variation and increase in velocity is also steadier.
- The velocity profiles at verticals B and E are nearly identical at steps 19, 21, 24, 30, 32, and 37. Nonetheless, they are quite similar for the remaining steps as well.

- There is no clear indication of the velocity profiles for positions A and F, to occur near the edges of the cluster, upstream of step 30. This lack of clarity may be ascribed with the increased influence of both, the side walls and the formation of cross-waves at a higher discharge.

At Q = 180 L/s

- Similarly to the air concentration profiles, interfacial velocity profiles were not obtained for step 15 at this flow rate, due to the high intensity of the incoming jets and the point occurring upstream of the beginning of the boundary layer.
- The overall velocity profiles are considerably smooth, with the exception of step 17, where minor irregularities exist. Nevertheless, the general trend depicted by the velocity profiles is somewhat similar to that seen at Q = 140 L/s. This is similar to the situation observed between Q = 60 L/s and Q = 80 L/s and therefore, may have occurred due to similar reasons.
- The rate at which the velocities move from their minimum to maximum values is considerably high in comparison with the simultaneous increase in flow depth. This is again a property of the high flow rate analyzed here.
- The velocity profiles corresponding with the inlet and outlet keys are fairly intertwined, such that no clear differences may be observed here as they could be for the lower discharges.
- A few minor differences may be observed in the velocity profiles corresponding with verticals B and E till step 21, downstream of which the profiles are identical.
- As was seen for the lower discharges, velocity profiles for verticals A and F lie close to the extreme ends of the cluster of lines. However, here, the difference between these and the remaining verticals is not very prominent.

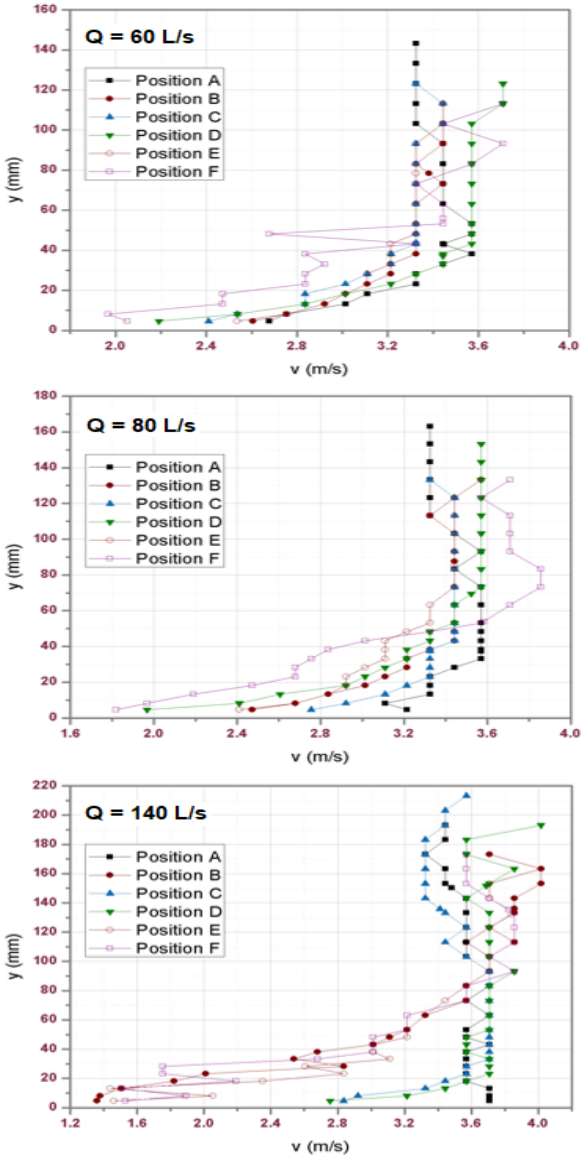

Figure 5.15: Velocity profiles at step 15 for discharges of 60, 80, and 140 L/s (from top to bottom, respectively)

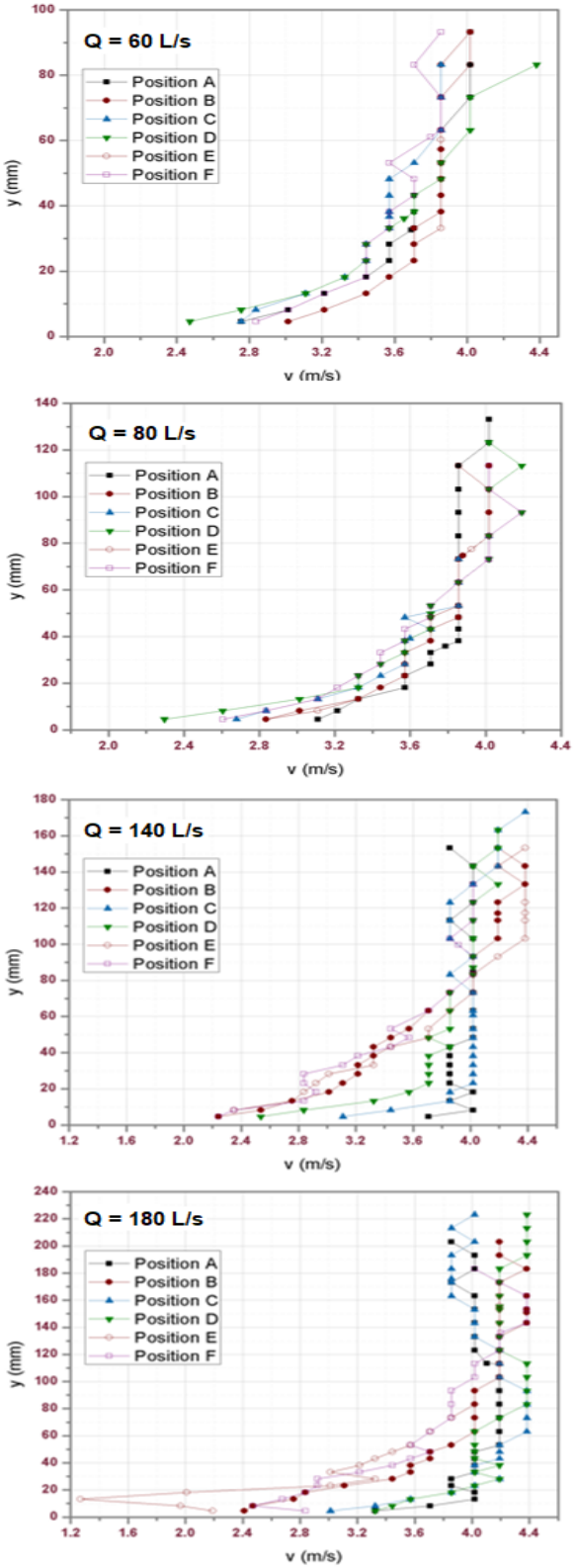

Figure 5.16: Velocity profiles at step 17 for discharges of 60, 80, 140, and 180 L/s (from top to bottom, respectively)

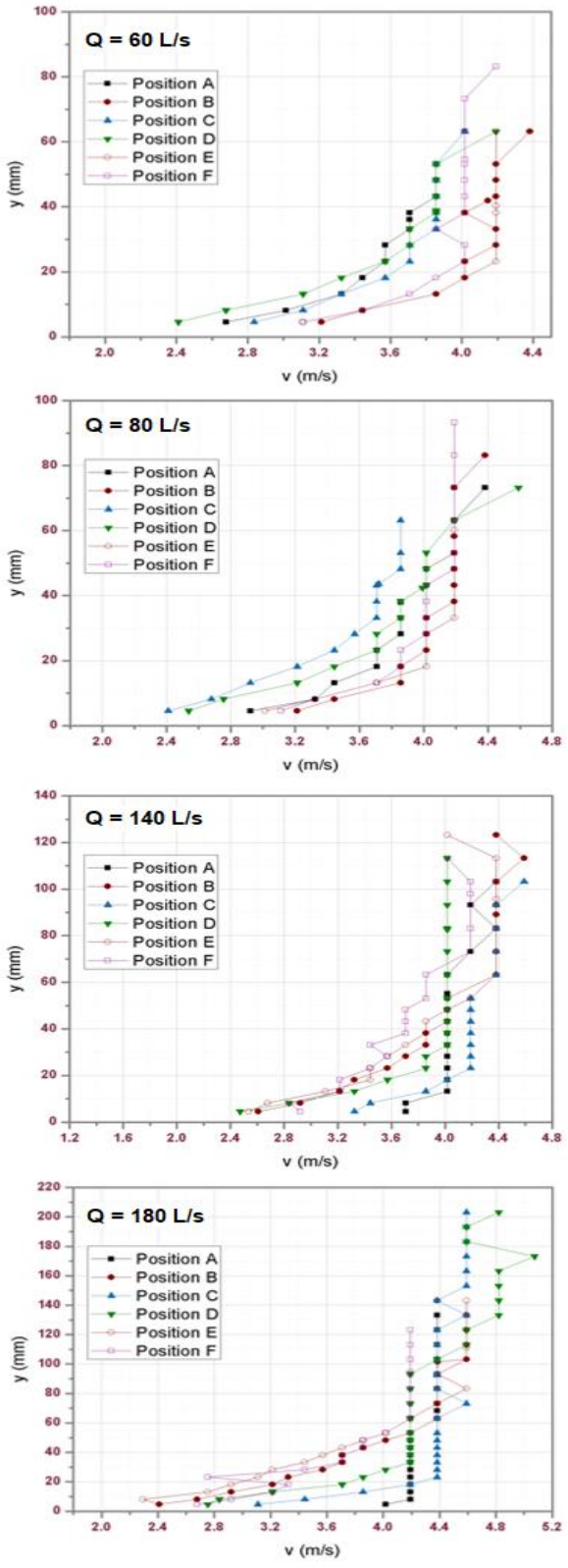

Figure 5.17: Velocity profiles at step 19 for discharges of 60, 80, 140, and 180 L/s (from top to bottom, respectively)

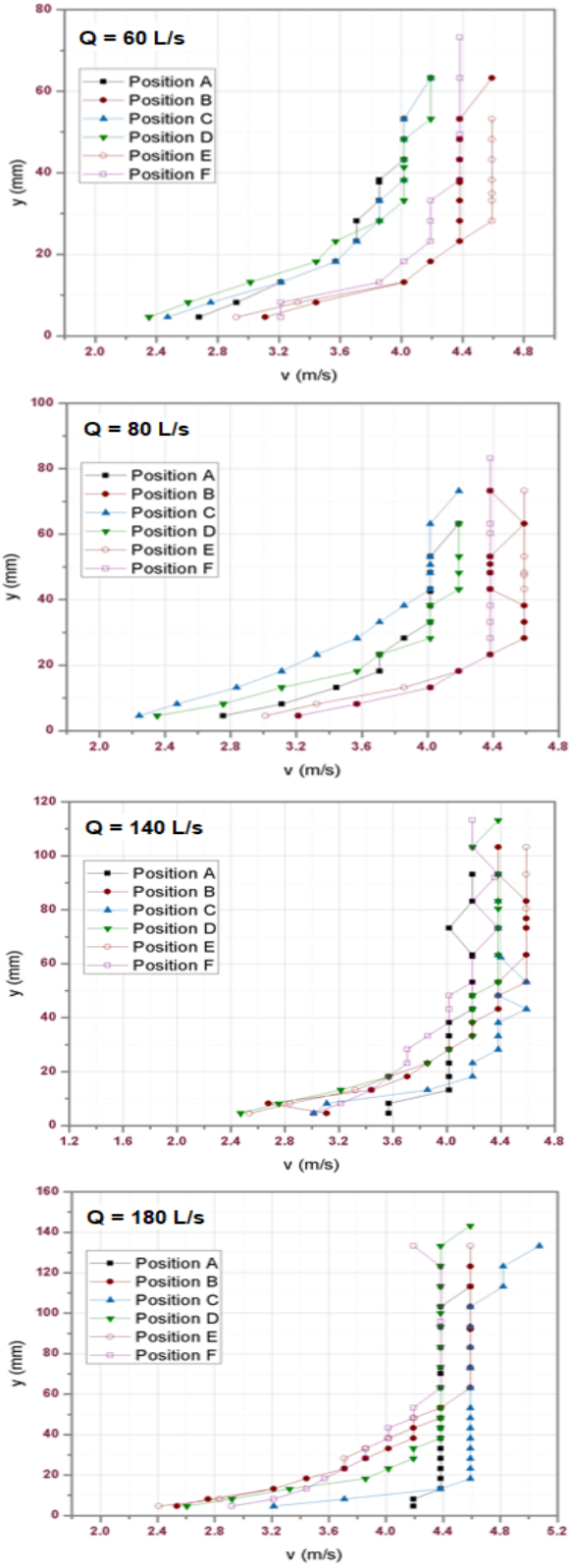

Figure 5.18: Velocity profiles at step 21 for discharges of 60, 80, 140, and 180 L/s (from top to bottom, respectively)

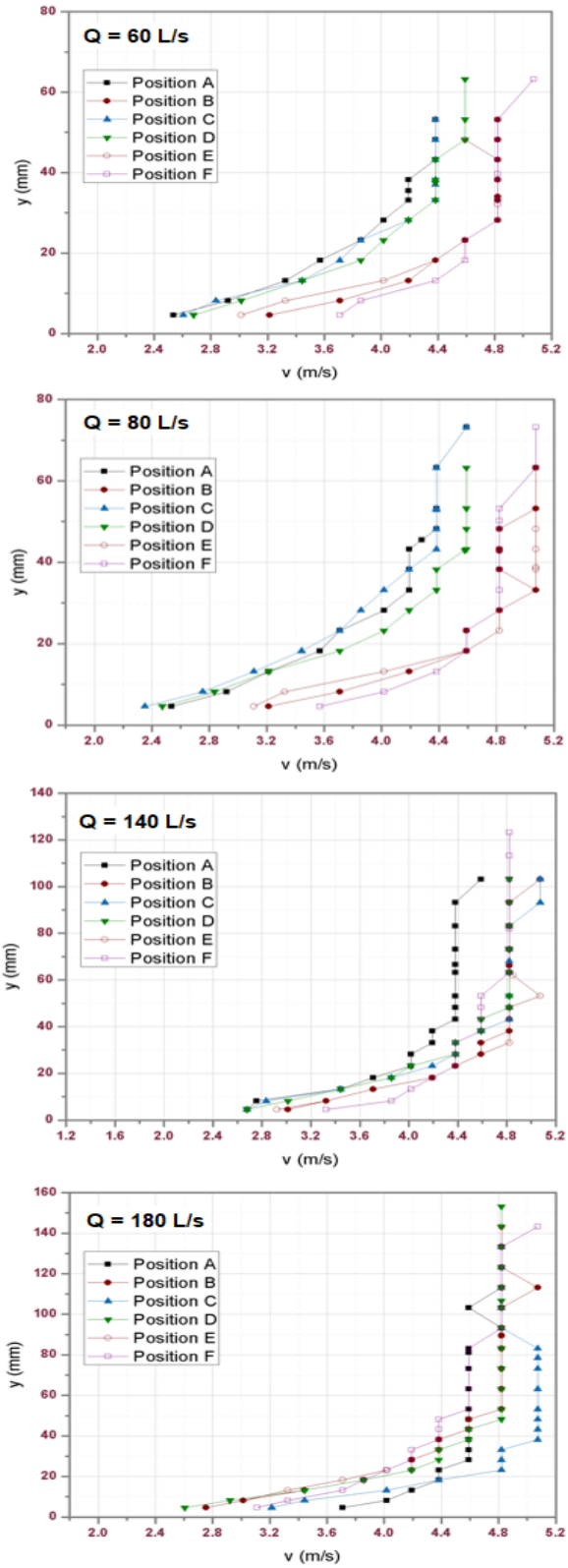

Figure 5.19: Velocity profiles at step 24 for discharges of 60, 80, 140, and 180 L/s (from top to bottom, respectively)

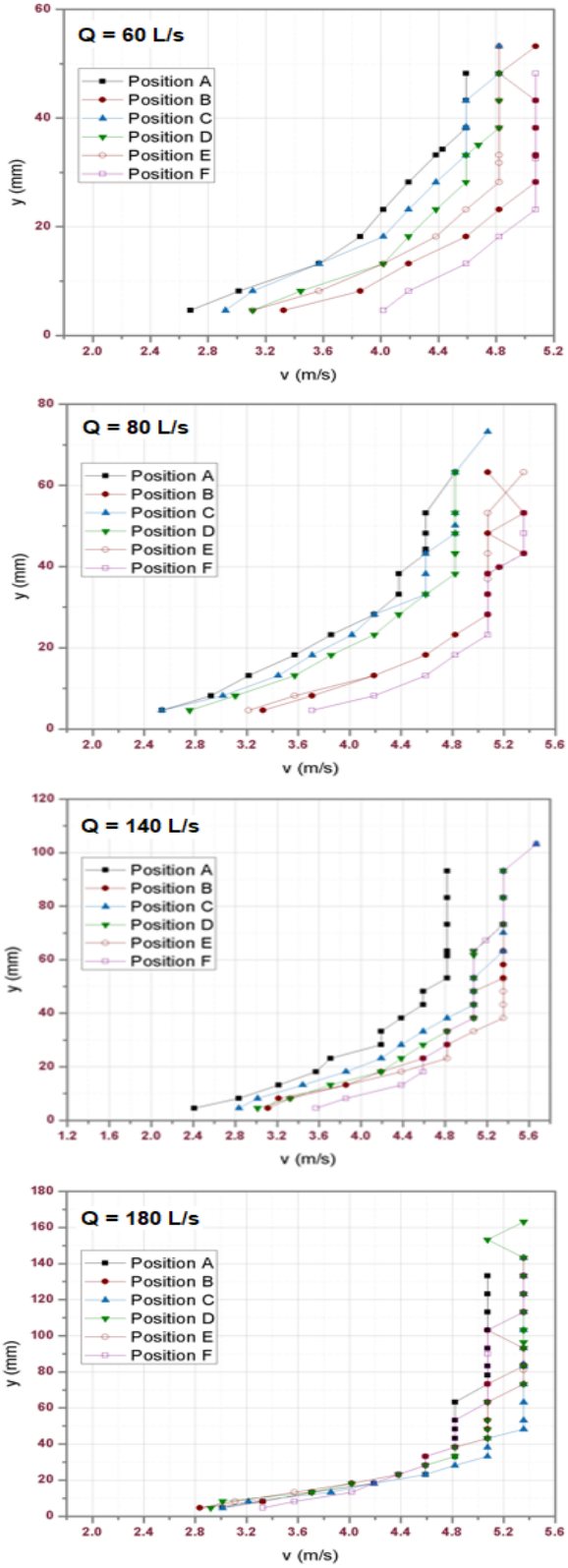

Figure 5.20: Velocity profiles at step 27 for discharges of 60, 80, 140, and 180 L/s (from top to bottom, respectively)

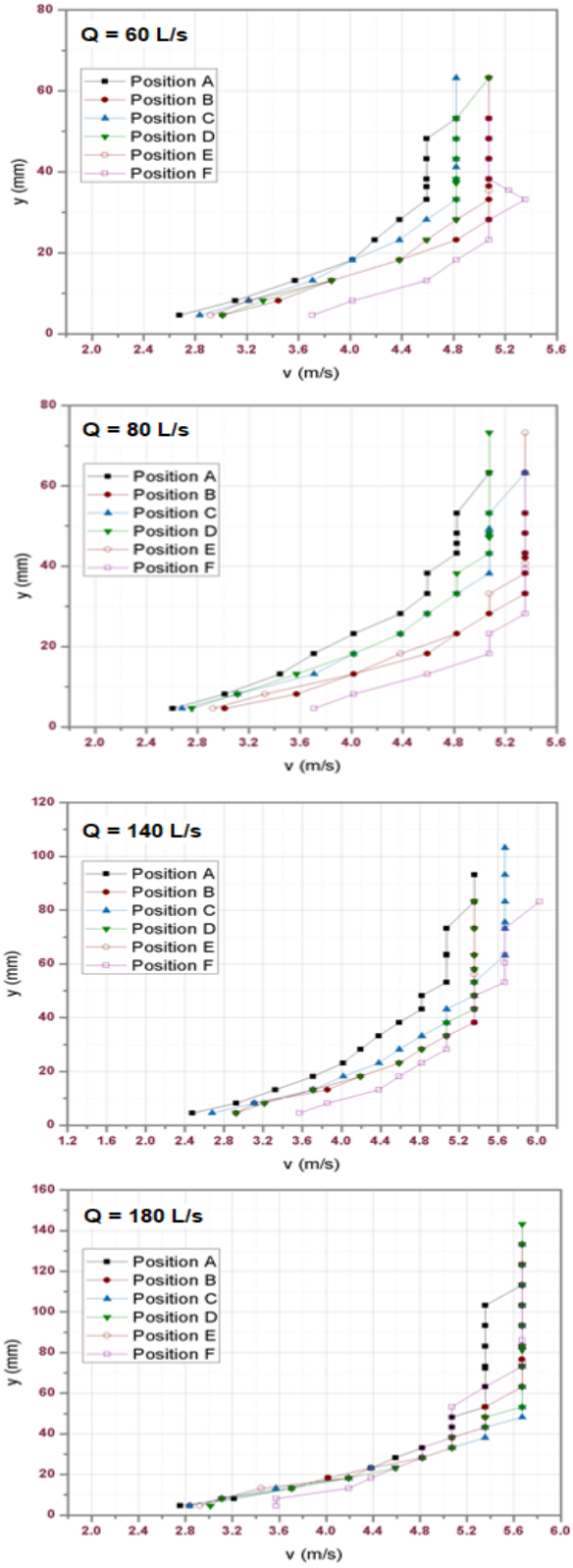

Figure 5.21: Velocity profiles at step 30 for discharges of 60, 80, 140, and 180 L/s (from top to bottom, respectively)

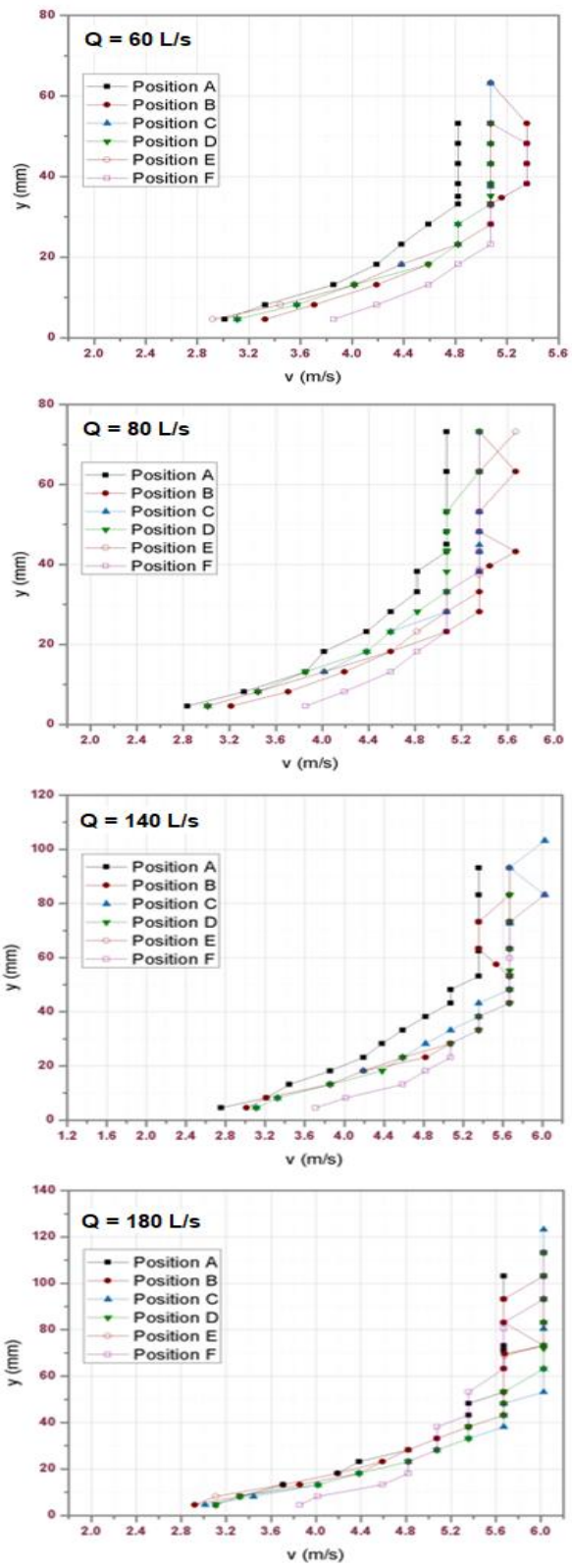

Figure 5.22: Velocity profiles at step 32 for discharges of 60, 80, 140, and 180 L/s (from top to bottom, respectively)

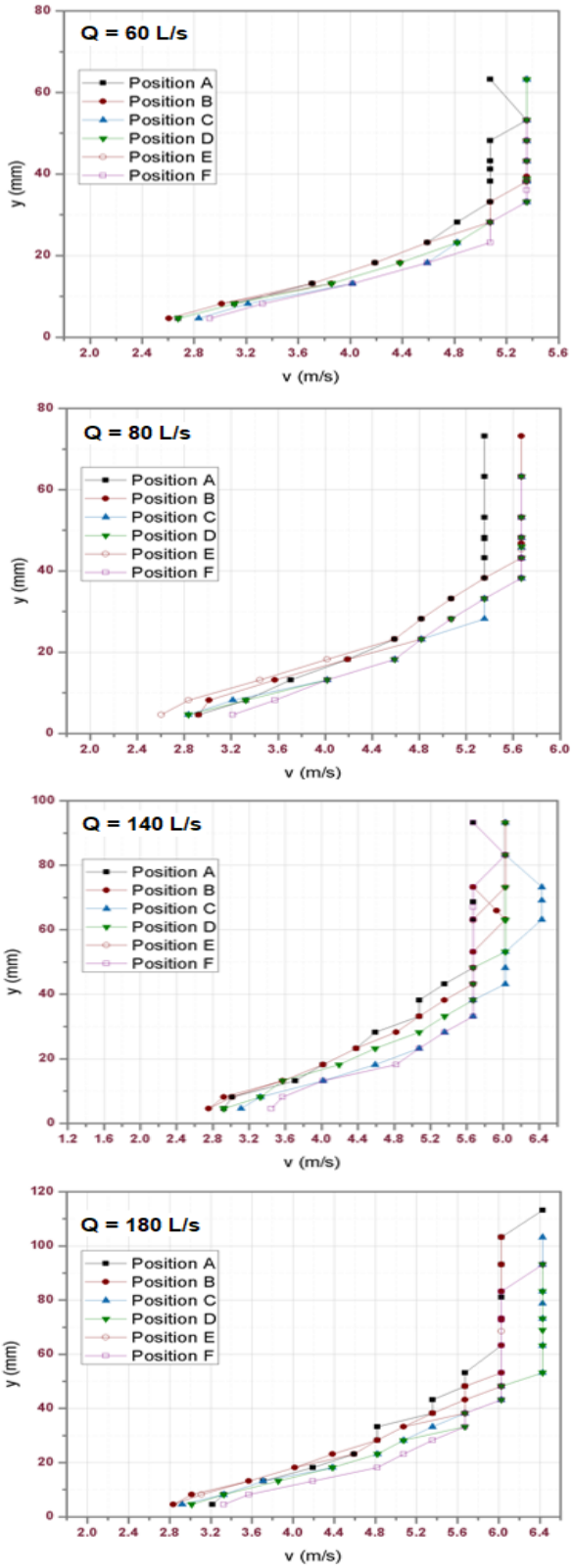

Figure 5.23: Velocity profiles at step 37 for discharges of 60, 80, 140, and 180 L/s (from top to bottom, respectively)

In addition to the interfacial velocity, the normalized velocity profiles, included in Appendix C, were also analyzed at each flow rate. The obtained graphs further validate the observations made and discussed above for the velocity profiles, particularly regarding the transformation of flow and its dimensionality along the stepped chute in accordance with the skimming flow regime.

The most important information the normalized velocity profiles provide is regarding the Power law exponent 'N'. As can be seen in the resulting curves, in Appendix C, the normalized velocity profiles generally fit well as a function of the Power law equation. However, this observation does not hold in all the cases, as can be seen in the few erroneous values of 'N', particularly at the higher flow rates. The individual values for each vertical, at all the tested discharges are presented in Appendix D.

Figure 5.24 illustrates the variation in the adjustment coefficient at each tested step, as the flow moves down the chute. In the graphs for the two higher discharges, the scale of the y-axis has been limited from 0 to 20 to obtain a clearer picture of the trend, since beyond this they are affected by the anomalous values. The values obtained for 'N', at each step, increase with an increase in the incoming discharge. In all the cases, the values obtained at the inlet and outlet keys are somewhat similar to each other. Additionally, the curves obtained for the outlet keys depict atypical behaviour at the two higher discharges, whereas the opposite can be seen for the lower discharges.

All the graphs depict a similar pattern, with the values converging as water moves from the crest to the bottom of the stepped chute. The trend at the first few steps is rather erratic, with the irregularity increasing with increasing discharge. This may be justified by the fact that the flow is influenced by the incoming jets from the PKW and is yet to achieve skimming flow. As a result, it does not fit well as a power law curve and the values of 'N' lie well out of the typical desired range. Once skimming flow is established, the curves also begin to smoothen and eventually become parallel, as the flow becomes two-dimensional. This phenomenon is also reflected in the absolute numerical values of 'N' as the flow moves over the stepped chute. They are high at the steps close to the crest, decrease along the chute and are fairly close to 4 near the downstream end of the spillway.

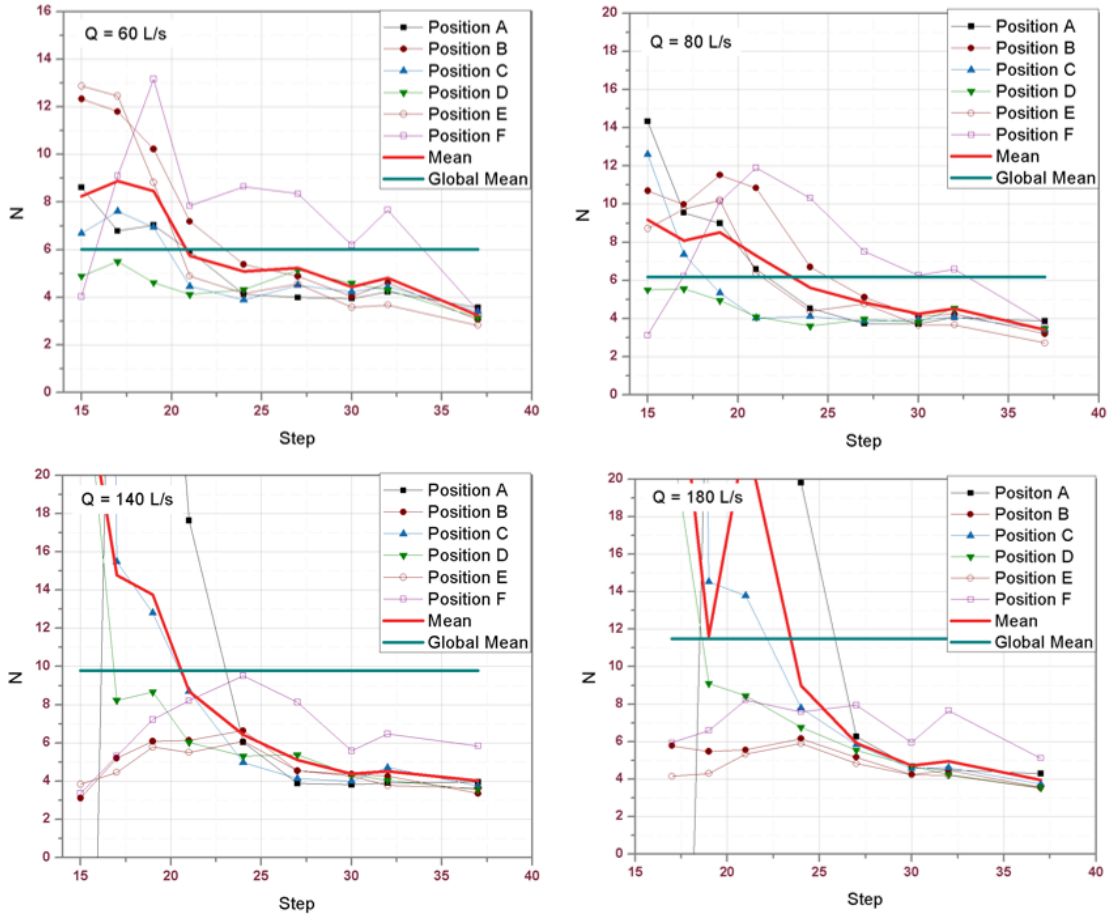

Figure 5.24: Variation in the exponent of the Power law 'N' along the stepped chute at 60 (Top left), 80 (Top right), 140 (Bottom left), and 180 L/s (Bottom right)

5.2.3. Characteristic Depth

The characteristic depth along the stepped chute is an indicator of the overall flow depth achieved. Since this parameter is likely to vary in a skimming flow regime, the characteristic depth at various steps is plotted and presented in Figure 5.25 at each of the four discharges. The maximum depth achieved by the flow increases with an increase in discharge. This is justified by the higher volume of water flowing over the chute at higher flow rates. The overall mean characteristic depth achieved also exhibits a similar increasing trend across the four flow rates.

All the graphs show a greater variation in the characteristic depth near the crest and a smoother profile a few steps downstream of it. At all the analyzed flow rates, the characteristic depth is initially high, then varies through the channel as a series of weak waves, exhibiting short-lasting fluctuations, until it eventually becomes constant near the base of the chute. This pattern is in accordance with the skimming flow regime, particularly in stepped spillways. The initial irregularity may be a consequence of the high intensity of the jets of water coming from the PKW, before skimming flow is achieved.

Generally, the variation in characteristic depth along the channel's cross-section is not very great. Minor differences can be observed at the initial steps, which may be attributed to the different flow paths taken by the water moving through the inlet and outlet keys (as discussed in Section 3.2).

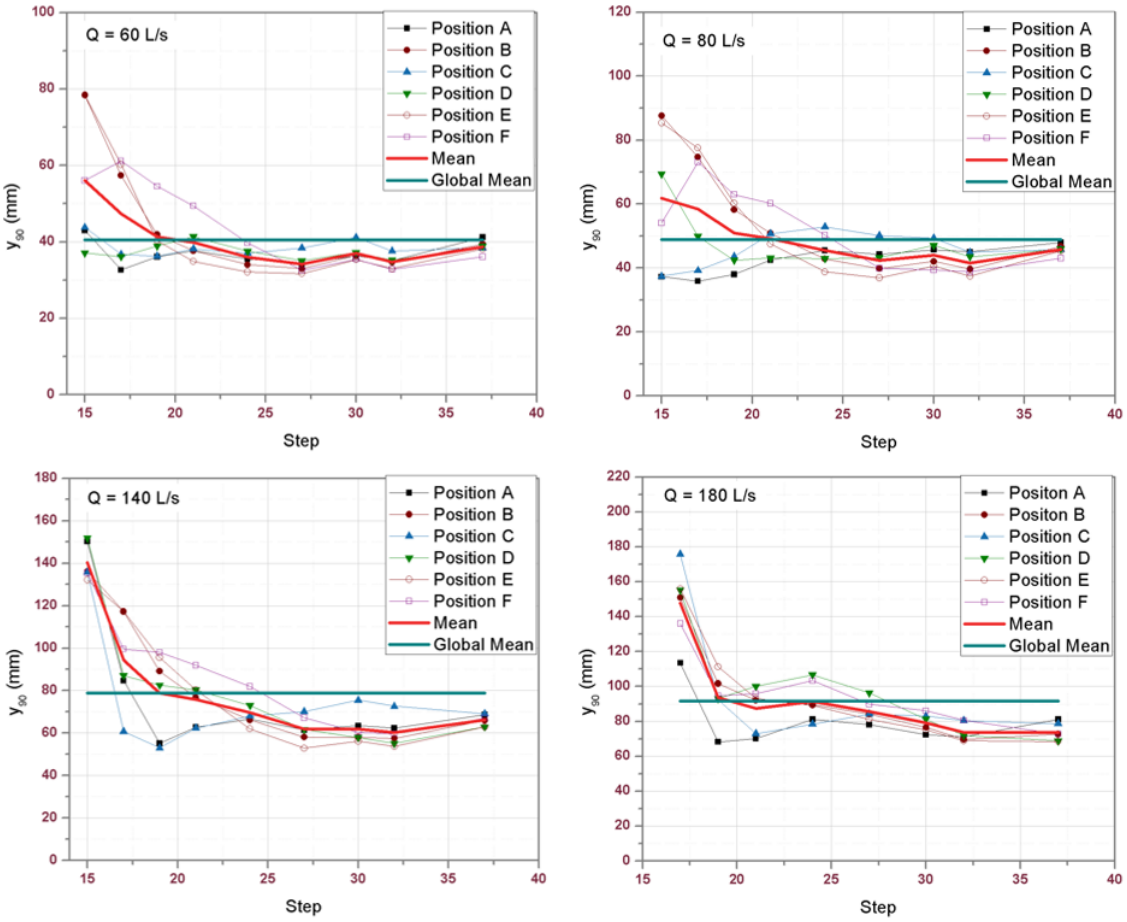

Figure 5.25: Characteristic depths along the stepped chute at 60 (Top left), 80 (Top right), 140 (Bottom left), and 180 L/s (Bottom right)

5.2.4. Mean Air Concentration

The variation in mean air concentration along the length of the flow channel at each discharge is presented in Figure 5.26. In all the graphs, the lines are more spaced-out in the beginning than at the end, thus indicating a decrease in the relative change in the parameter as water moves down the chute. The initial variation becomes stronger with an increase in flow rate, owing to the greater irregularity in the air concentration profiles and the higher flow depth near the crest.

The mean air concentration appears to vary within a very small range of values. This range also widens as the incoming flow rate increases. This phenomenon is particularly important in determining the point where water moves into the uniform flow regime. In this study, the flow did not reach this region for any of the tested flow rates, as can be observed in the graphs of Figures 5.25 – 5.27.

The graphs verify the trend seen earlier regarding the difference between the inlet and outlet keys. At all discharges, the mean air concentrations corresponding with the outlet keys are higher than the inlet keys, with the gap between the two becoming more pronounced as the flow rate increases. This occurs up to a given point, after which the trend reverses. The average value of mean air concentration also seems to lie in between the two keys.

The overall average value of the mean air concentrations decreases slightly as the flow rate increases. This may be justified by the fact that at higher discharges, due to a greater flow depth, air entrainment in the regions close to the pseudo-bottom is lower, which negatively affects the overall mean value.

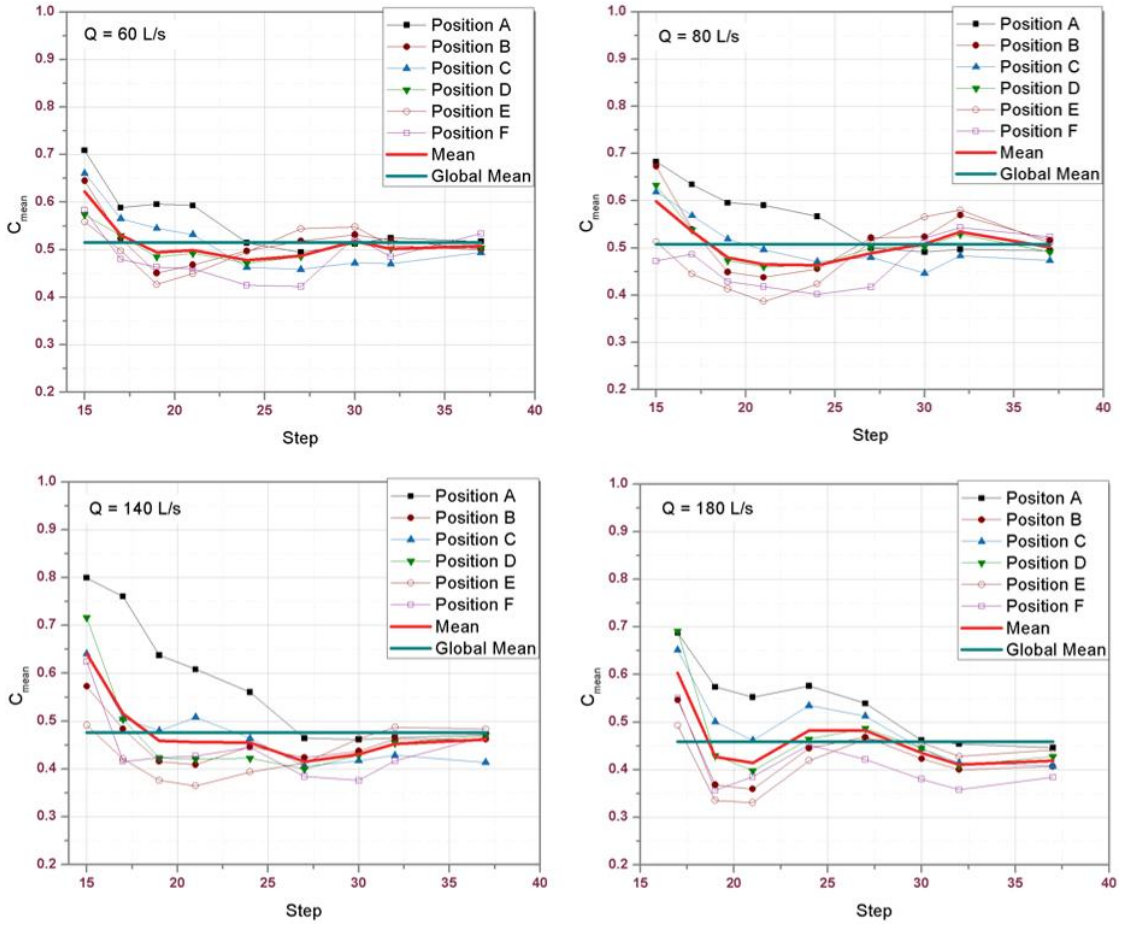

Figure 5.26: Mean air concentrations along the stepped chute at 60 (Top left), 80 (Top right), 140 (Bottom left), and 180 L/s (Bottom right)

5.2.5. Equivalent Clear-water Depth

The equivalent clear-water depths obtained at various steps along the channel's length for all four discharges are illustrated in Figure 5.27. These depths also present a trend similar to the previously discussed parameters, with a significant variation near the crest and an eventual smoothening as the flow moves towards the bottom. Similarly to the characteristic depth, the equivalent clear-water depth also

increases with an increase in the flow rate, as can be seen by the lines representing the global mean in all the graphs.

It may be observed in the graphs in Figure 5.27 that the depths corresponding with the inlet keys are initially high but decrease as the flow moves downstream and eventually become constant near the bottom. Depths corresponding with the outlet keys exhibit the opposite trend, with initially low values followed by an increase until they finally become constant as well. This may be justified by the fact that the inlet keys release more water directly to the higher steps, while the jets formed at the outlet keys reach the spillway at a step relatively downstream of the crest.

Since the equivalent clear-water depth represents the flow depth that would be achieved without air, it is always lower than the characteristic depth. This can be observed clearly upon comparing Figures 5.25 and 5.27. The relative difference between the two is a function of the air concentration profiles at each vertical, step, and discharge.

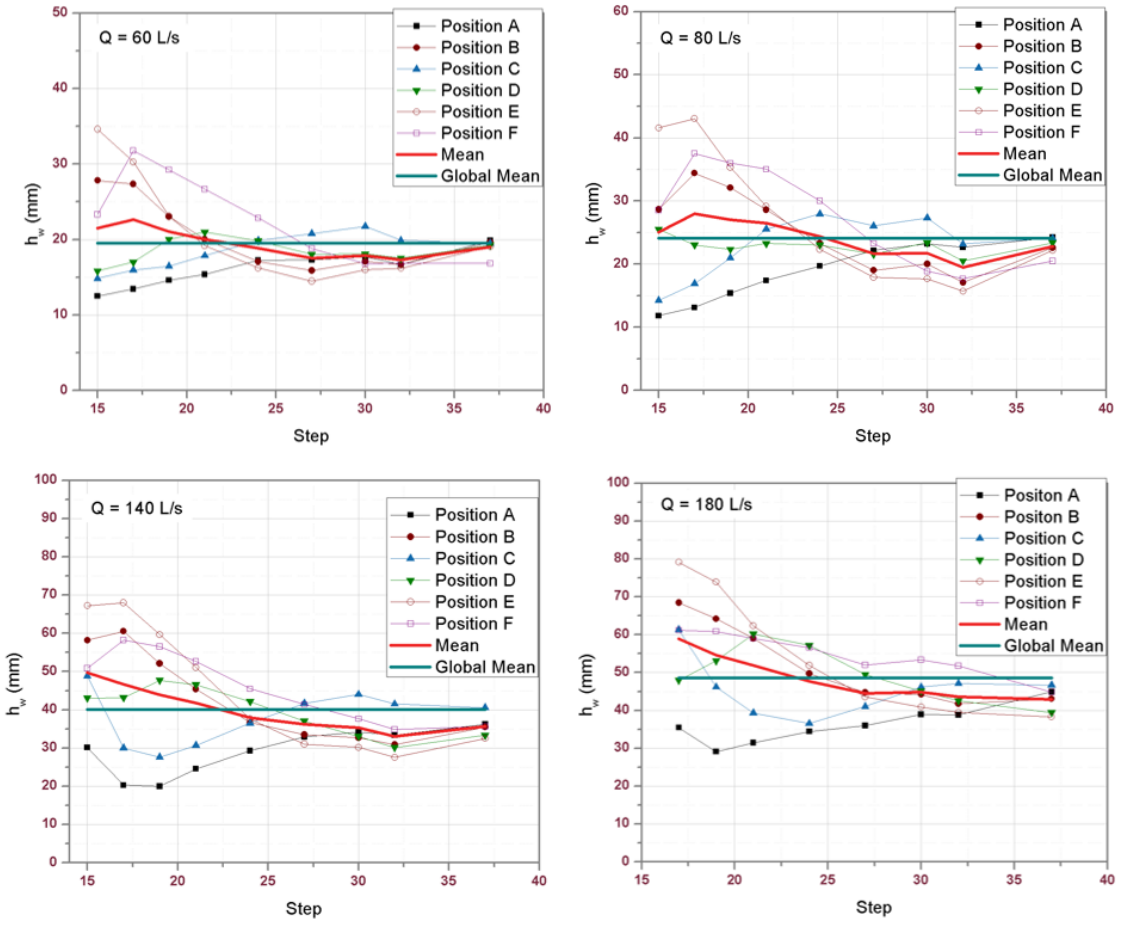

Figure 5.27: Equivalent clear-water depth along the stepped chute at 60 (Top left), 80 (Top right), 140 (Bottom left), and 180 L/s (Bottom right)

5.3. Energy Dissipation of the Flow

In order to study energy dissipation over the stepped chute, the amount of energy that reached the bottom was analyzed. This energy was derived by using a set of equations at steps close to the bottom, rather than analyzing the hydraulic jump in the stilling basin. Prior to making the desired calculations, the mean air concentrations and flow depths were analyzed for steps 32 and 37. This was done in order to study the cross-sectional uniformity of flow, since a greater number of points was analyzed along the cross-section.

The variation in characteristic depth at various positions across the channel's cross-section at each of the analyzed discharges is presented in Figure 5.28. The trends depicted by the characteristic depths are relatively smoother for step 37 than for step 32. The relative difference between their values remains within 5 mm, while the range within which the depths vary is around 1 cm for Q = 60 L/s and Q = 80 L/s, and 2 cm for Q = 140 L/s and Q = 180 L/s.

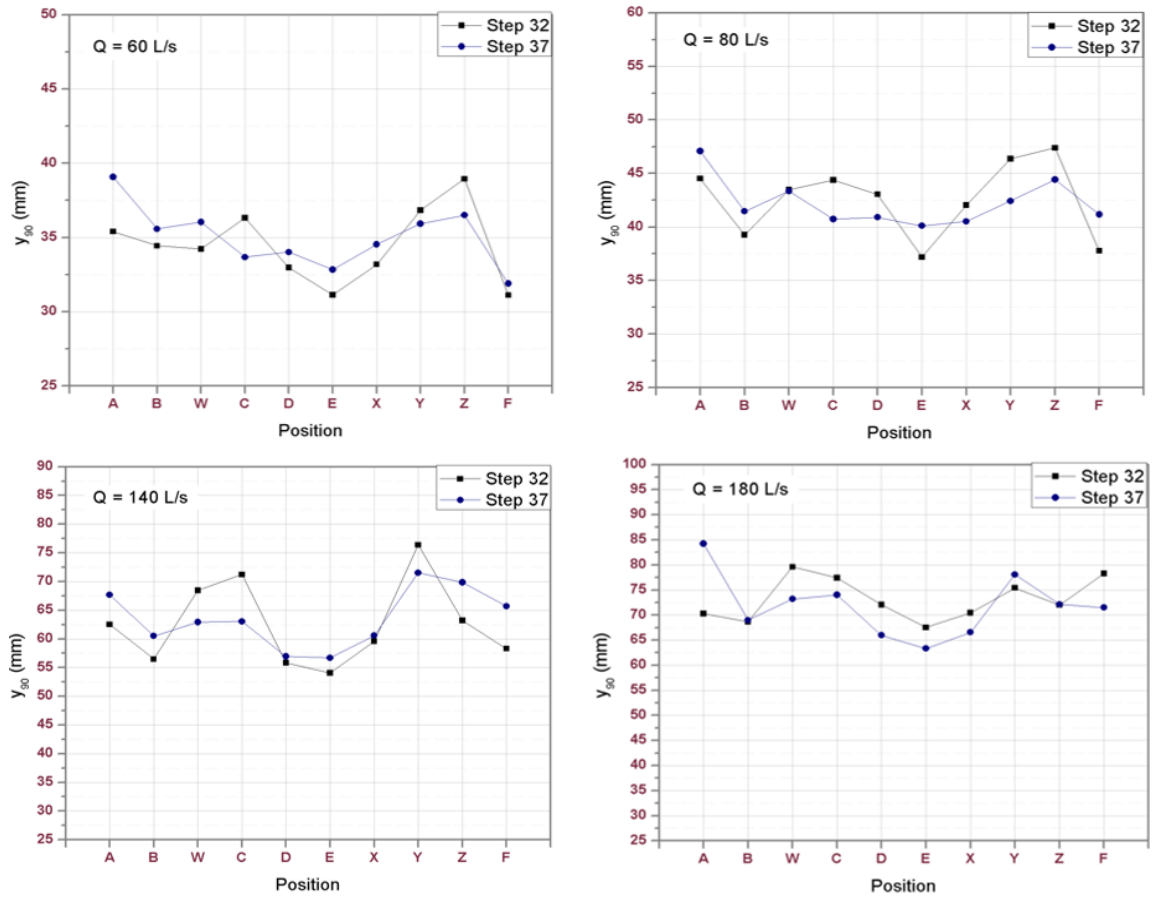

Figure 5.28: Comparison of characteristic depths, across the cross-section, close to the bottom at 60 (Top left), 80 (Top right), 140 (Bottom left), and 180 L/s (Bottom right)

A similar analysis was made for the mean air concentrations, which is presented in Figure 5.29. The graphs show that the relative change from one corner of the channel to the other is quite small for Q = 60L/s. For

the remaining three discharges, the variation is also well within 10%. This may be taken as an indicator that cross-sectional uniformity of flow may be achieved soon after step 37. Additionally, the overall mean values, included in Tables 5.1 and 5.2, decrease with an increase in the flow rate. This acts as a confirmation of the trends seen for the same analysis, with a fewer number of verticals, discussed in Subsection 5.2.4.

The trends exhibited by the mean air concentrations at Q = 60 L/s and Q = 80 L/s are nearly identical for both steps. The only difference that exists is in the amplitude of the fluctuations, which is higher at Q = 80 L/s. The trends at Q = 140 L/s are also fairly similar, with the exception of the verticals close to the walls. The lines at Q = 180 L/s are nearly horizontal, with peaks only at the verticals A and F, which are most likely caused by an influence of the side walls.

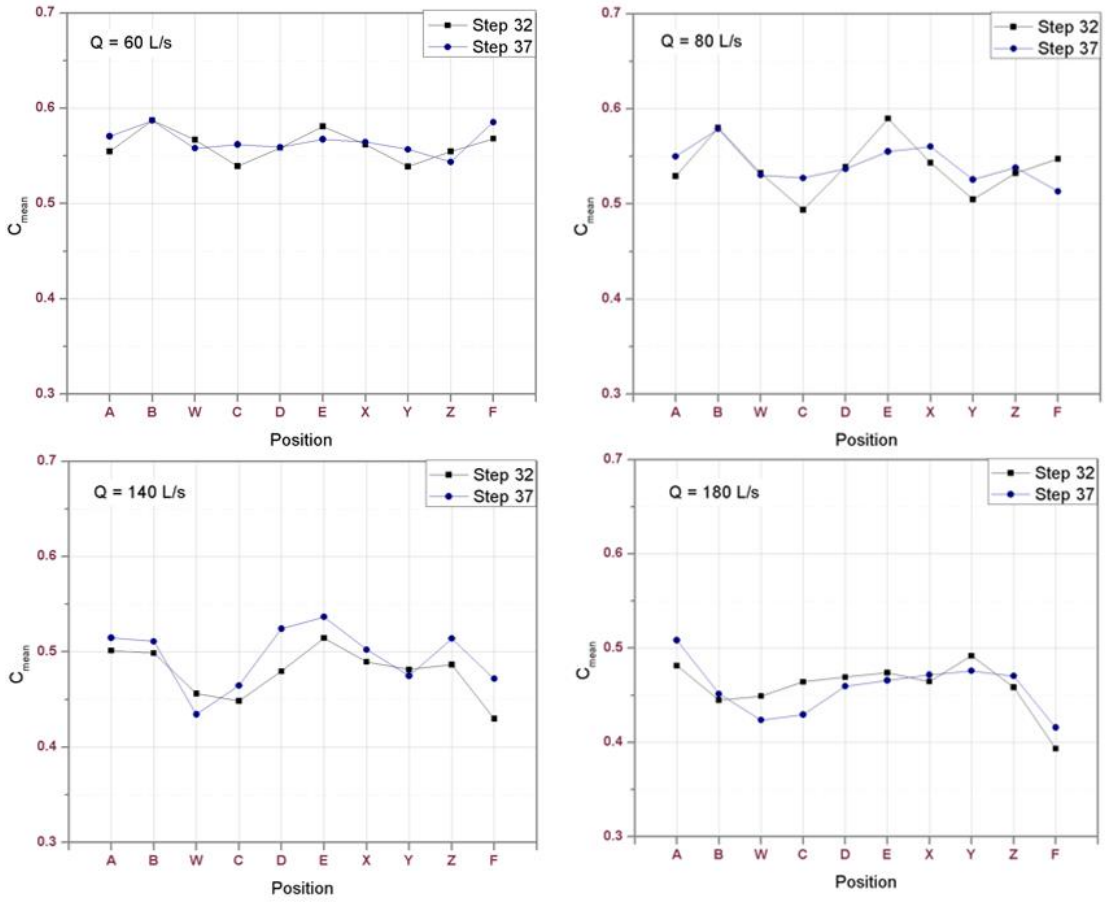

Figure 5.29: Comparison of the mean air concentrations, across the cross-section, close to the bottom at 60 (Top left), 80 (Top right), 140 (Bottom left), and 180 L/s (Bottom right)

An analysis of the equivalent clear-water depths led to a similar set of observations, as can be seen in Figure 5.30. The range of values varies within 5 mm for the two lower discharges and 1 cm for the two higher discharges. This is analogous with the range observed for the characteristic depths. Additionally, the trend of variations seen between each vertical is somewhat similar for Q = 60 L/s and Q = 80 L/s, and for Q = 140

L/s and Q = 180 L/s. The overall equivalent clear-water depth increases with an increase in the flow rate, which verifies the relation obtained earlier with the fewer number of verticals. However, it decreases slightly from step 32 to step 37, as can be seen in Tables 5.1 and 5.2.

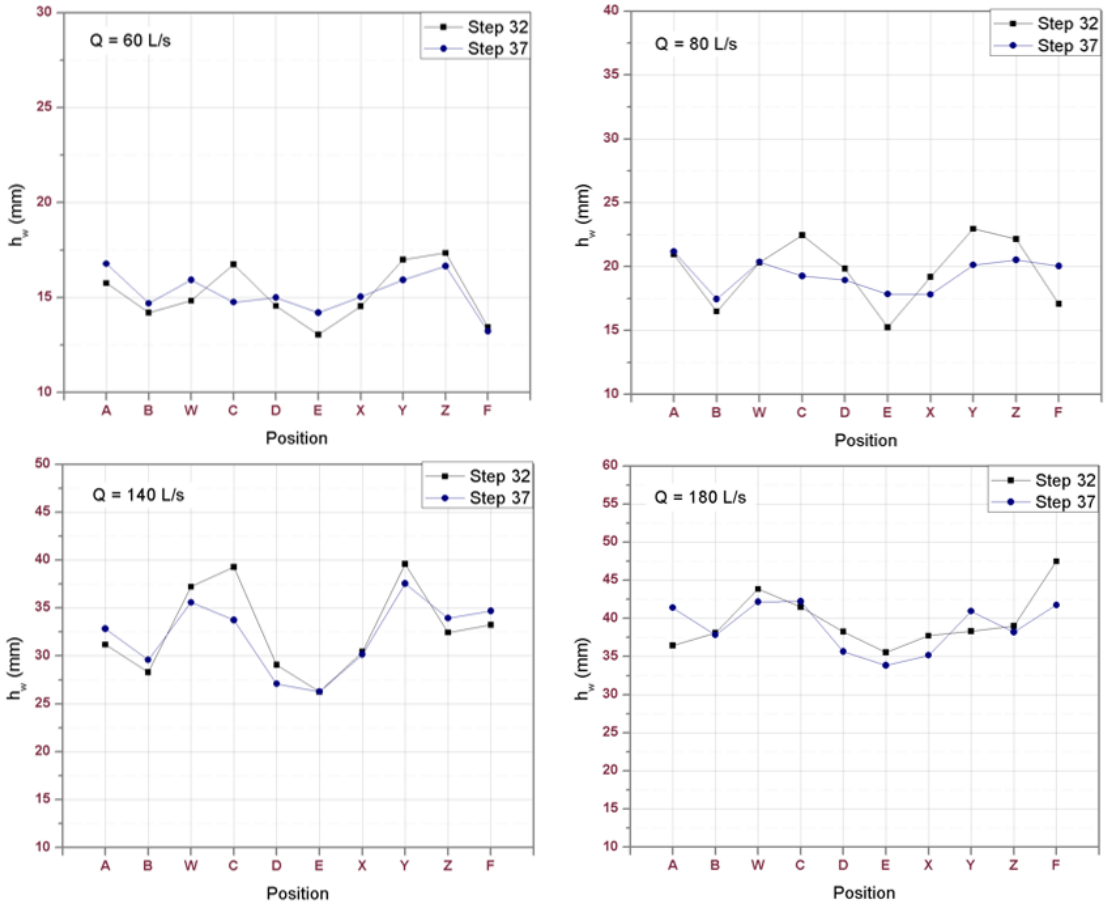

Figure 5.30: Comparison of the equivalent clear-water depths, across the cross-section, close to the bottom at 60 (Top left), 80 (Top right), 140 (Bottom left), and 180 L/s (Bottom right)

In addition to the mean air concentrations and equivalent clear-water depths at each flow rate, a summary of the parameters calculated to determine the energy dissipation along the stepped chute is presented in Tables 5.1 and 5.2, for steps 32 and 37, respectively. The values for mean air concentration and equivalent clear-water depth are calculated as a weighted average of the graphs in Figures 5.29 and 5.30, respectively and are included only to provide a clearer visualization of the pattern of variation with flow rate.

The velocity profiles obtained for this deeper analysis were also checked to see their adaptability to the Power law curve. This was done in order to obtain a value for the exponent ‘N”, which is particularly important here. Since this coefficient is an indicator of the channel bed’s resistance to flow, it has a significant impact on the energy lost by the water as it moves along the chute. The values calculated here were found to be consistent with the expected range for flows close to the bottom of a stepped spillway.

Table 5.1: Parameters involved in energy dissipation analysis at step 32 at each discharge

Parameter	Discharge (L/s)			
	60	**80**	**140**	**180**
C_{mean}	0.560	0.540	0.479	0.466
h_w (mm)	14.781	19.633	30.928	38.772
N	4.214	4.462	4.285	4.588
U_w (m/s)	4.059	4.075	4.527	4.643
α	1.061	1.154	1.109	1.166
E (m)	0.900	0.989	1.177	1.304
ΔE (m)	1.148	1.073	0.930	0.837
$\Delta E/E_{max}$	0.560	0.520	0.441	0.391

Table 5.2: Parameters involved in energy dissipation analysis at step 37 at each discharge

Parameter	Flow Rate (L/s)			
	60	**80**	**140**	**180**
C_{mean}	0.562	0.540	0.509	0.456
h_w (mm)	15.008	18.990	29.243	37.084
N	3.790	4.088	4.071	4.091
U_w (m/s)	3.998	4.213	4.787	4.854
α	1.187	1.188	1.134	1.210
E (m)	0.976	1.086	1.343	1.476
ΔE (m)	1.472	1.376	1.164	1.065
$\Delta E/E_{max}$	0.601	0.559	0.464	0.419

Another important parameter studied here was the mean water velocity, which increases with an increase in the flow rate, as expected. The difference between the values calculated at each discharge is synonymous with relative differences between the flow rates, i.e. the gap between the velocities is small if the difference between the flow rates is too.

The use of average velocity, or mean water velocity in this analysis, negates the effect of the non-uniform distribution of velocity across the flow depth. This yields a value of kinetic head which is lower than the actual value. In order to compensate for this underestimation, calculation of the kinetic energy coefficient carries immense importance. The results listed in Tables 5.1 and 5.2 clearly show that the values of 'α' are, in general, between 1.1 and 1.2 for all the analyzed discharges. These values are of the same order of magnitude as those reported by Matos [23], on a stepped spillway, with a step height of 8 cm, and an upstream WES crest.

All the parameters discussed above are used in the determination of the specific energy and consequently, the head loss as water reaches the bottom of the spillway. The obtained results indicate that a smaller amount of energy is lost at higher flow rates. The head loss, along with the change in energy relative to the maximum, increases as the distance from the crest increases, and water moves closer to the ground's surface.

Based on the results presented in Tables 5.1 and 5.2, the tested design is quite successful in breaking the strong force of water at all flow rates, particularly the higher ones. This is important in ensuring that the water causes minimal damage, to the base of the structure, as it falls from the upstream reservoir to the downstream stilling basin.

Chapter 6: Conclusions and Recommendations

This chapter discusses the conclusions driven from the results presented in Chapter 5. It also includes a number of suggestions for future areas of research that may be tapped to overcome the limitations involved in this study.

6.1. Conclusions

Based on the discussion of results presented in Chapter 5, followed by a comparison with literature on similar topics, the following conclusions may be drawn:

- Measurements made with the dual-tip probe were closely comparable with the single-tip probe at Q = 80 L/s and Q = 140 L/s. The relative differences observed between the two probes at both, the inlet and outlet keys, were relatively small and nearly identical at both discharges.
- Keeping in view the observation made above, use of the dual-tip probe may be preferred over the single-tip probe, as it provides more information on the flow characteristics. It allows the direct measurement of interfacial velocity, simultaneously with the void fractions at each point. Additionally, two separate sets of data are gathered at each point of measurement; one corresponding with the leading tip and the other with the trailing tip. This provides an estimate of the precision, along with the means to identify errors early on.
- By convention, the flow over a spillway shifts from the nappe to transitional to the skimming flow regime, with an increase in the incoming discharge. At all the tested discharges, the flow exhibited a skimming flow regime, which was achieved after the influence of the PKW's jets. In theory, at a steep slope of 53˚, the flow occurs as part of the skimming flow regime for fairly small flow rates, which was confirmed by the trends observed in this study.
- Based on a previous set of experiments conducted on the stepped chute at LNEC, the mean air concentration at the inception point was found to be around 0.2, regardless of the step height and unit discharge [14]. In the present study, the mean air concentrations along the analyzed verticals were, as expected, always greater than 0.2 at locations downstream of the impact of the PKW's jets.
- The overall thickness of the flow depth increased with an increase in discharge. The bottom layers were seen to be occupied more with water than the surface layers, and the relative thickness of each layer also increased with the flow rate. This pattern was confirmed by both, visual observation and data from the dual-tip probe. As a result, the air entrainment was higher near the surface than the pseudo-bottom at all four discharges, as expected based on similar studies on self-aerated skimming flows.
- Both, the characteristic and equivalent clear-water depths were higher near the crest, and showed a tendency to decrease as the water moved downstream. This further verified the occurrence of skimming flow at all discharges from Q = 60 L/s to Q = 180 L/s.

- The velocity profiles at each step and discharge were mostly found to fit well as a Power law curve, with the values of 'N' being within the expected range for skimming flows in open channels. However, there were a few points, close to the crest, before skimming flow was achieved, where this did not occur, and the values of 'N' were unrealistic.
- The interfacial velocities were found to increase as the flow moved from top to bottom, which is in accordance with the law of conservation of energy. Also, higher values were observed for higher discharges.
- The velocities generally increased very rapidly within the first few centimetres of the flow depth, which consisted mostly of water. After this, they became constant till the surface layer.
- Both, the air concentration and velocity profiles were more erratic near the crest and became smooth as water moved closer to the bottom of the stepped chute. The irregularity at each step also increased with an increase in the incoming discharge.
- The side walls of the flow channel had a considerable impact on the air entrainment behaviour of the water at all discharges. However, this influence was significant only till a certain step, which moved downstream with the increase in discharge, i.e. the effect lasted longer for higher flow rates.
- The use of a PKW, as the spillway's crest, had a significant impact on the flow characteristics in its vicinity. The trends of various parameters observed at the inlet and outlet keys were quite different. However, the values obtained were nearly identical for the same type of keys.
- The air concentration profiles corresponding with the inlet keys were lower than the outlet keys close to the crest. This trend reversed, generally around steps 19 and 21, as the water moved downstream.
- At Q = 60 L/s and Q = 80 L/s, the velocity profiles corresponding with the outlet keys were lower than the inlet keys near the top and began to merge as water moved towards the bottom. On the other hand, at Q = 140 L/s and Q = 180 L/s, the velocity profiles at the outlet keys were higher than the inlet keys near the crest, after which they began to merge similarly to the lower flow rates.
- The flow of water over the inlet keys of the PKW was quite smooth and entered the spillway as a steady stream. On the other hand, the flow over the outlet keys was more restricted and entered the stepped chute as a jet of water. This difference resulted in the formation of cross-waves, which was often observed in the flow profiles obtained at various locations along the cross-section.
- Flow in the stepped chute evolved from three-dimensional to two-dimensional flow, while moving closer to the uniform flow region of the skimming flow regime. The shift to two-dimensional flow was observed in the vicinity of step 24 at Q = 60 L/s, between steps 24 and 27 at Q = 80 L/s, and between steps 27 and 30 at the remaining two flow rates.
- Analysis of the channel's cross-section at steps 32 and 37 indicated that cross-sectional uniformity of flow was not achieved at any of the tested discharges. However, the flow moved quite close to it by step 37.

- The values of ‘N’ and ‘α’ calculated at steps 32 and 37 for use in the energy analysis were found within their expected applicable ranges. The kinetic energy coefficient increased from step 32 to step 37, whereas the adjustment coefficient decreased.
- As anticipated, the head loss, as well as the relative change in energy, increased as the flow moved from the crest to the bottom of the channel.
- The relative roughness of the surface exposed to water decreased as the discharge increased, due to higher equivalent clear-water depths. As a result, the head loss was lower at the higher discharges.

6.2. Recommendations

Based on the observations made during the experimental process and the subsequent analysis, a number of recommendations may be made for future studies.

- A machine operated mechanical arm may be used to move the probe while making measurements along the chute. This is likely to help ensure that the probe is placed precisely at the desired position for measurement. It will also improve the stability of the probe in high intensity flows, resulting in more accurate data. Additionally, it would speed up the data acquisition process, while reducing the amount of manual effort required and the susceptibility to human error.
- Similarly to the energy analysis, a greater number of verticals may be tested for the investigation of flow as well. This may help provide greater detail of the flow characteristics across the channel’s cross-section.
- The development of cross-waves may be characterized to properly identify their pattern and quantify the impact they have on the flow properties.
- Since air entrainment has a direct effect on aquatic life, the impact of a stepped chute, fitted with a PKW, may be investigated in this context in a real-life (or simulated) setting.
- Studies similar to the one presented in this dissertation may be conducted for the other three types of PKWs or different step heights of the stepped chute.

References

[1] Chanson, H., & Paintal, A. (2003). Hydraulics of stepped chutes and spillways. Appl. Mech. Rev., 56(1), B10-B11.

[2] Khanh, M. H. T. (2017). History and development of Piano Key Weirs in Vietnam from 2004 to 2016. In Labyrinth and Piano Key Weirs III: Proceedings of the 3rd International Workshop on Labyrinth and Piano Key Weirs (PKW 2017), February 22-24, 2017, Qui Nhon, Vietnam (p. 3). CRC Press.

[3] Erpicum, S., Archambeau, P., Dewals, B. J., & Pirotton, M. (2017). Hydraulics of piano key weirs: a review. In Proceedings of the 3rd International Workshop on Labyrinth and Piano Key Weirs (pp. 27-36). CRC Press.

[4] Felder, S., & Pfister, M. (2017). Comparative analyses of phase-detective intrusive probes in high-velocity air–water flows. International Journal of Multiphase Flow, 90, 88-101.

[5] Lempérière, F., & Ouamane, A. (2003). The Piano Keys weir: a new cost-effective solution for spillways. International Journal on Hydropower & Dams, 10(5), 144-149.

[6] Machiels, O., Erpicum, S., Dewals, B. J., Archambeau, P., & Pirotton, M. (2010). Piano Key Weirs: the experimental study of an efficient solution for rehabilitation. WIT Transactions on Ecology and the Environment, 133, 95-106.

[7] Pralong, J., Vermeulen, J., Blancher, B., Laugier, F., Erpicum, S., Machiels, O., Pirotton, M., Boillat, J.L., Ribeiro, M.L., & Schleiss, A. J. (2011). A naming convention for the Piano Key Weirs geometrical parameters. Labyrinth and piano key weirs, 271-278.

[8] Laugier, F., Vermeulen, J., & Blancher, B. (2017). Overview of design and construction of 11 piano key weirs spillways developed in France by EDF from 2003 to 2016. In Labyrinth and Piano Key Weirs III: Proceedings of the 3rd International Workshop on Labyrinth and Piano Key Weirs (PKW 2017), February 22-24, 2017, Qui Nhon, Vietnam (p. 37). CRC Press.

[9] Denys, F., & Basson, G. (2018) Transient hydrodynamics of Piano Key weirs. Proceedings of 7th IAHR international symposium on hydraulic structures, Aachen, Germany.

[10] Erpicum, S., Laugier, F., Pfister, M., Pirotton, M., Cicero, G. M., & Schleiss, A. J. (2013). Labyrinth and Piano Key Weirs II. CRC Press.

[11] Mehri, Y., Soltani, J., & Khashehchi, M. (2019). Predicting the coefficient of discharge for piano key side weirs using GMDH and DGMDH techniques. Flow Measurement and Instrumentation, 65, 1-6.

[12] Tiwari, H., & Sharma, N. (2015). Flow hydrodynamics near inlet key of Piano Key Weir (PKW). Sadhana, 40(7), 2253-2261.

[13] Chanson, H. (2000). Historical development of stepped cascades for the dissipation of hydraulic energy. Transactions of the Newcomen Society, 72(2), 295-318.

[14] Matos, J., & Meireles, I. (2014). Hydraulics of stepped weirs and dam spillways: engineering challenges, labyrinths of research. In 11th National Conference on Hydraulics in Civil Engineering & 5th International Symposium on Hydraulic Structures: Hydraulic Structures and Society-Engineering Challenges and Extremes (p. 330). Engineers Australia.

[15] "https://www.ajktours.com/waterfalls-in-neelum-valley/." [Online]. Available: https://www.ajktours.com/waterfalls-in-neelum-valley/. [Accessed: 05-Oct-2019].

[16] "http://www.jmwilkerson.com/." [Online]. Available: http://www.jmwilkerson.com/portfolio/stone-mountain-spillway/. [Accessed: 05-Oct-2019].

[17] Chanson, H. (1994). Hydraulics of nappe flow regime above stepped chutes and spillways. Australian Civil/Structural Engineering Transactions, (1), 69-76.

[18] Ward, J. P. (2002). Hydraulic design of stepped spillways. Ph.D. thesis, Colorado State University, US.

[19] Felder, S., & Chanson, H. (2015). Phase-detection probe measurements in high-velocity free-surface flows including a discussion of key sampling parameters. Experimental Thermal and Fluid Science, 61, 66-78.

[20] Gonzalez, C. A., & Chanson, H. (2004). Interactions between cavity flow and main stream skimming flows: an experimental study. Canadian Journal of Civil Engineering, 31(1), 33-44.

[21] Matos, J. (2000). Hydraulic design of stepped spillways over RCC dams. In Intl Workshop on Hydraulics of Stepped Spillways (pp. 187-194). Balkema Publ.

[22] Reis, M. (2015). Estudo experimental do escoamento em descarregadores de cheias em degraus com soleira em teclado de piano. M.Sc. thesis, Instituto Superior Técnico, Lisbon (in Portuguese).

[23] Matos, J. (1999). Emulsionamento de ar e dissipação de energia do escoamento em descarregadores em degraus. Ph.D. thesis, Instituto Superior Técnico De Lisboa, Portugal (in Portuguese).

[24] Meireles, I. (2004). Caracterizaçao do escoamento deslizante sobre turbilhoes e energia específica resiudal em descarregadores de Cheias em Degraus. M.Sc. thesis, Instituto Superior Técnico de Lisboa, Portugal (in Portuguese).

[25] Pinto, M. (2017). Dissipação de energia em descarregadores de cheias em degraus com soleira em teclado de piano: estudo experimental. M.Sc. thesis, Instituto Superior Técnico, Lisbon (in Portuguese).

[26] Gomes, R. (2018). Emulsionamento de ar e dissipação de energia do escoamento em descarregadores de cheias em degraus com soleira em teclado de piano. M.Sc. thesis, Instituto Superior Técnico, Lisbon (in Portuguese).

[27] Herringe, R. A., & Davis, M. R. (1974). Detection of instantaneous phase changes in gas-liquid mixtures. Journal of Physics E: Scientific Instruments, 7(10), 807.

[28] Neal, L. G., & Bankoff, S. G. (1963). A high resolution resistivity probe for determination of local void properties in gas-liquid flow. AIChE Journal, 9(4), 490-494.

[29] Chanson, H. (2002). Air-water flow measurements with intrusive, phase-detection probes: Can we improve their interpretation? Journal of Hydraulic Engineering, 128(3), 252-255.

[30] Felder, S., & Chanson, H. (2016). An experimental study of air-water flows in hydraulic jumps with channel bed roughness. Water Research Laboratory Research Report 259.

[31] Felder, S. (2013). Air-water flow properties on stepped spillways for embankment dams: Aeration, energy dissipation and turbulence on uniform, non-uniform and pooled stepped chutes. Ph.D. thesis, The University of Queensland, Australia.

[32] Lee, H. E., Lee, C., Kim, Y. J., Kim, J. S., & Kim, W. (2013). Power law exponents for vertical velocity distributions in natural rivers. Engineering, 5(12), 933.

[33] Matos, J., Gomes, R. & Felder, S. (2019). Sensitivity analysis of the dual-tip phase detection probe. Personal notes.

[34] Renna, F. (2004). Caratterizzazione fenomenologica del moto di un fluido bifasico lungo scaricatori a gradini. Phenomenological characterization of two-phase flow along stepped spillways. Ph.D. thesis, Politecnico di Bari, Cosenza, Italy (in Italian).

Appendix A: AutoCAD Drawings of the Experimental Facility

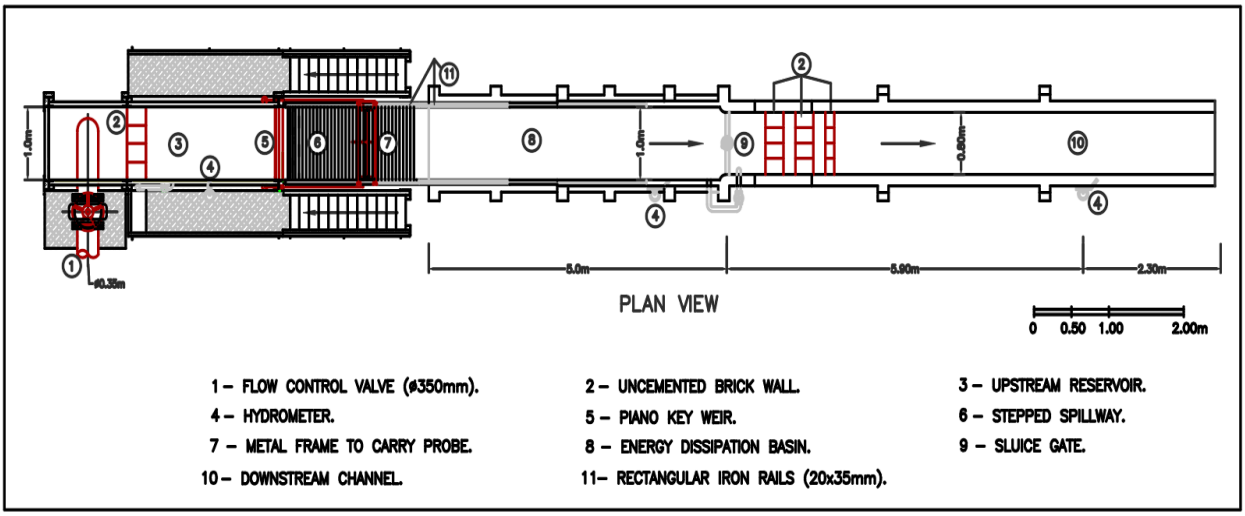

Figure A.1: Plan view of the experimental facility (adapted from [23])

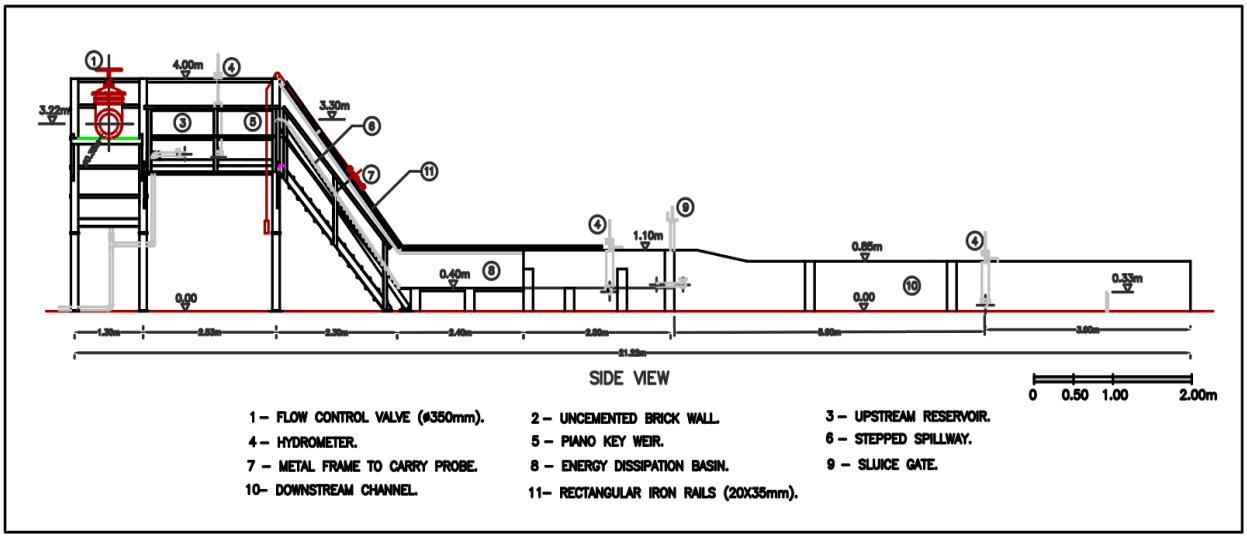

Figure A.2: Side view of the experimental facility (adapted from [23])

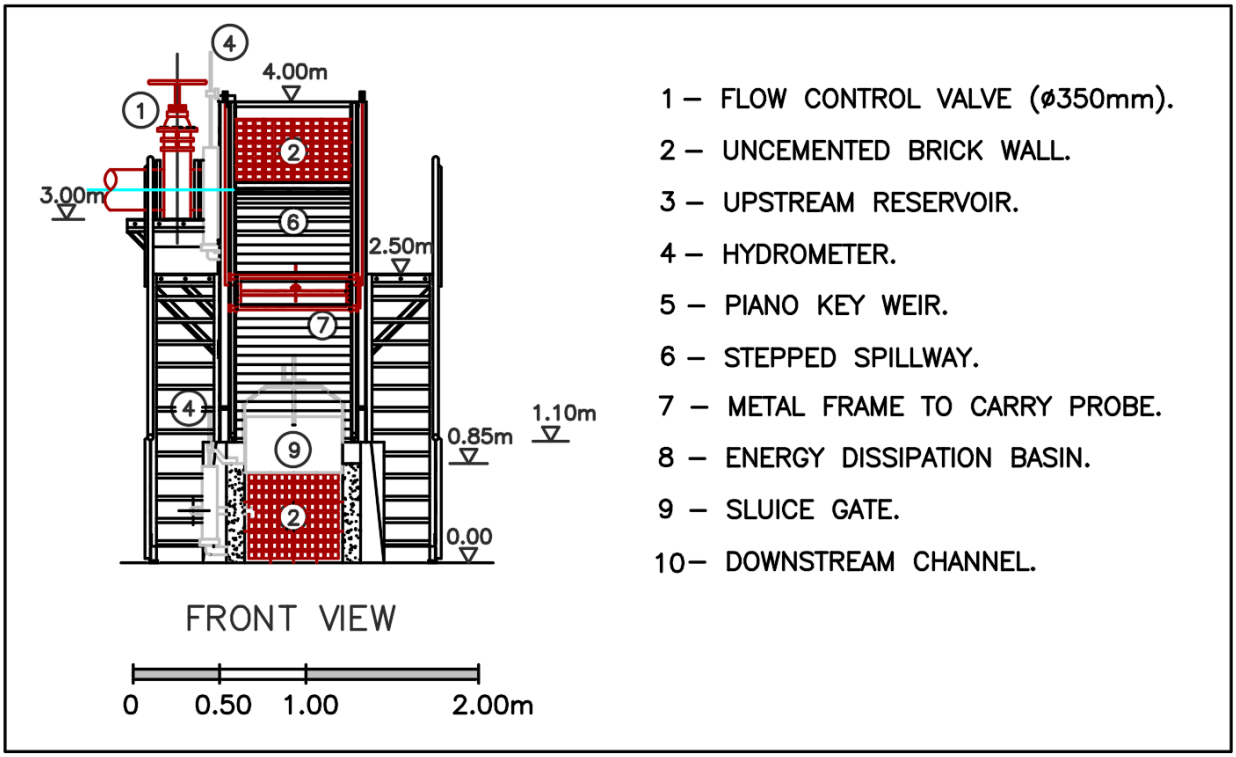

Figure A.3: Front view of the experimental facility (adapted from [23])

Appendix B: Normalized Air Concentration Profiles

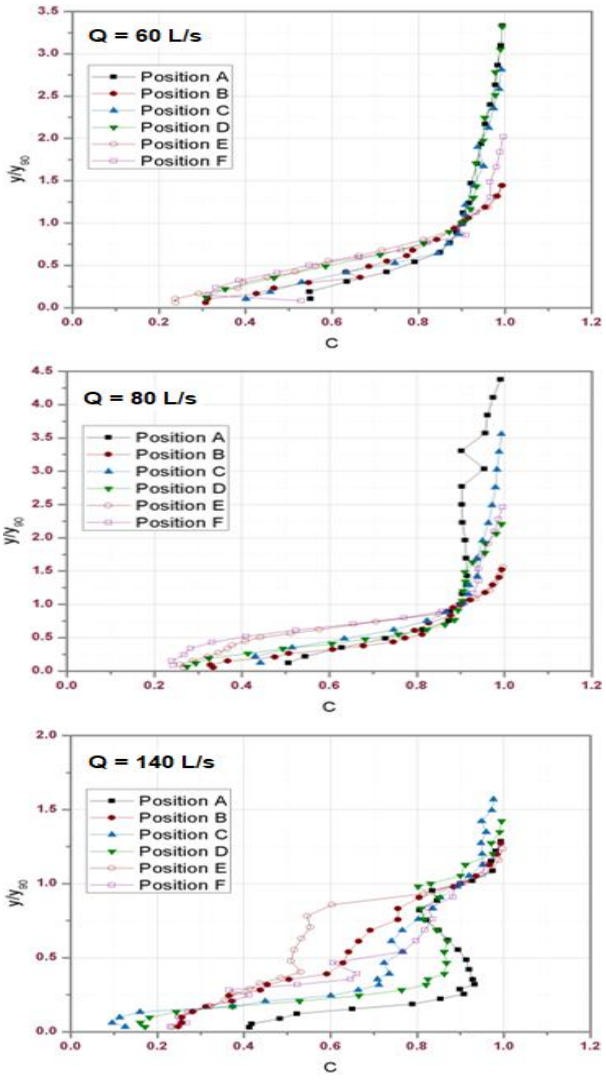

Figure B.1: Normalized air concentration profiles at step 15 for discharges of 60, 80, and 140 L/s (from top to bottom, respectively)

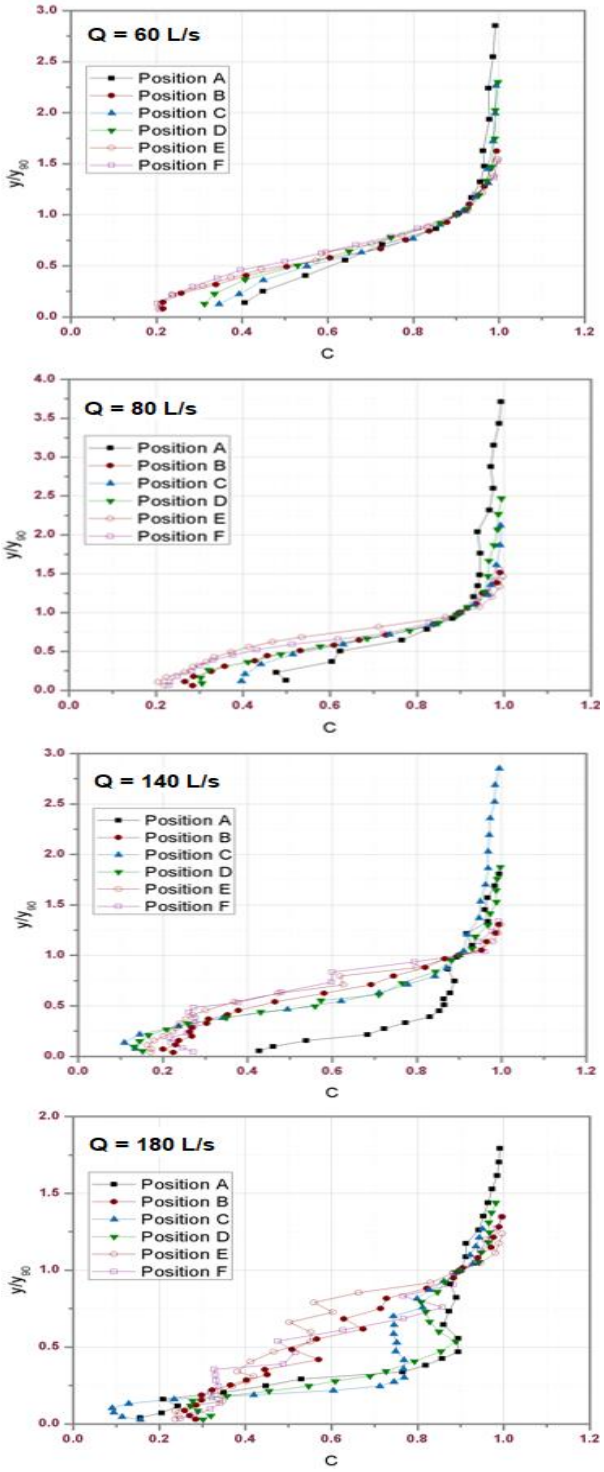

Figure B.2: Normalized air concentration profiles at step 17 for discharges of 60, 80, 140, and 180 L/s (from top to bottom, respectively)

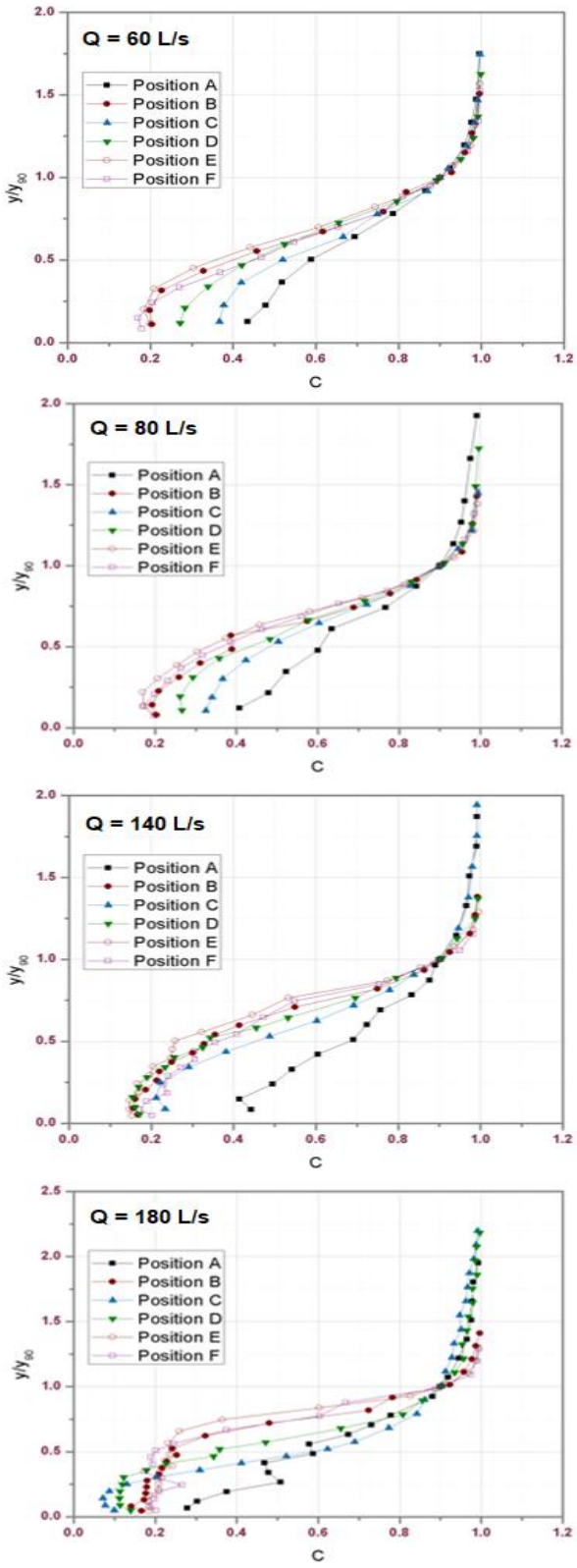

Figure B.3: Normalized air concentration profiles at step 19 for discharges of 60, 80, 140, and 180 L/s (from top to bottom, respectively)

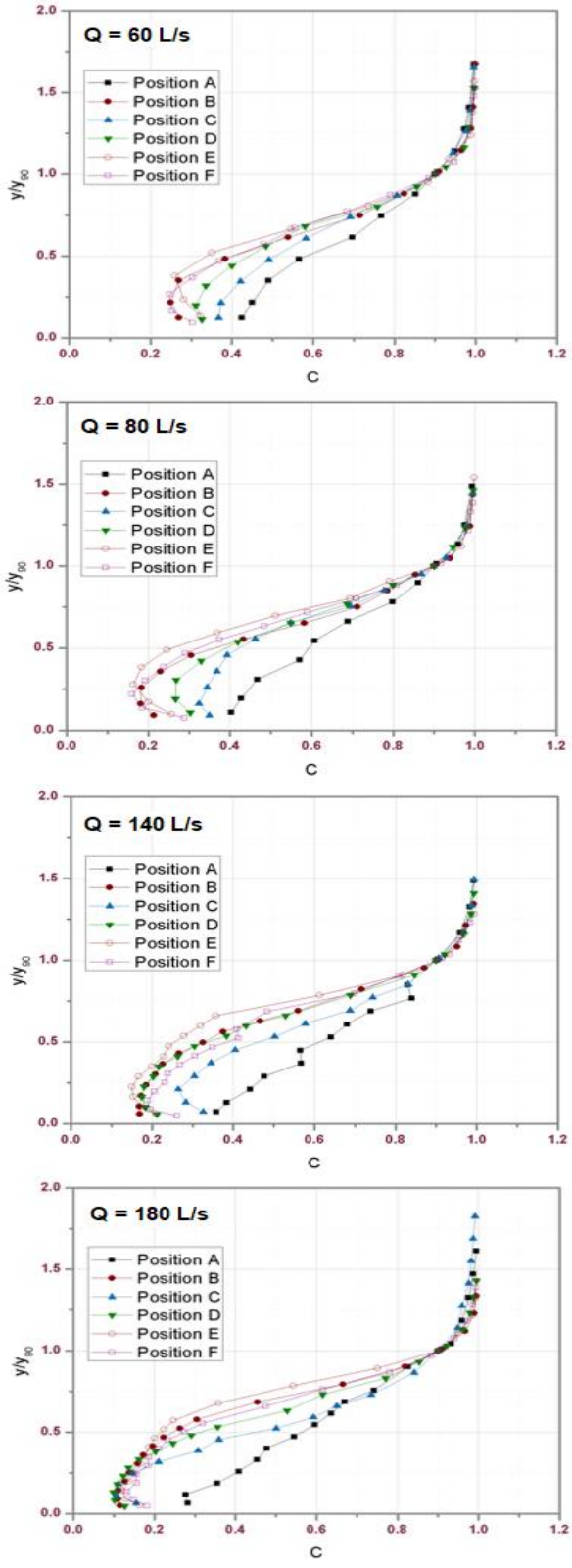

Figure B.4: Normalized air concentration profiles at step 21 for discharges of 60, 80, 140, and 180 L/s (from top to bottom, respectively)

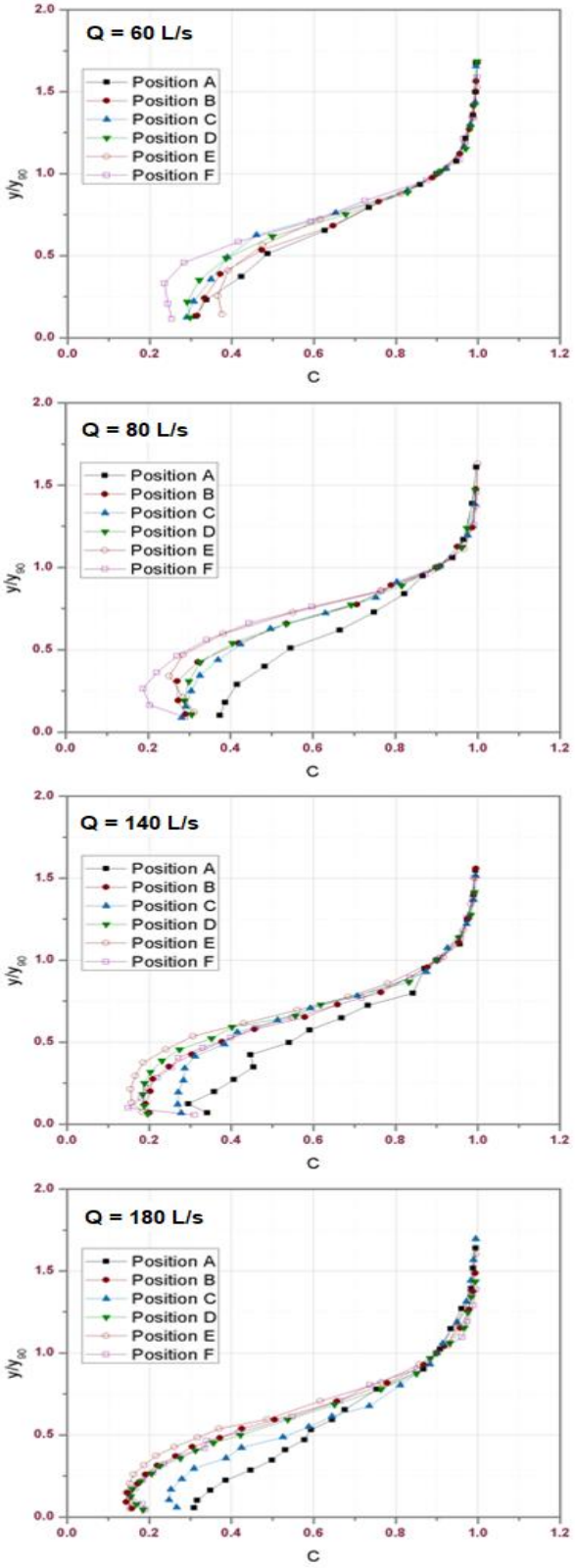

Figure B.5: Normalized air concentration profiles at step 24 for discharges of 60, 80, 140, and 180 L/s (from top to bottom, respectively)

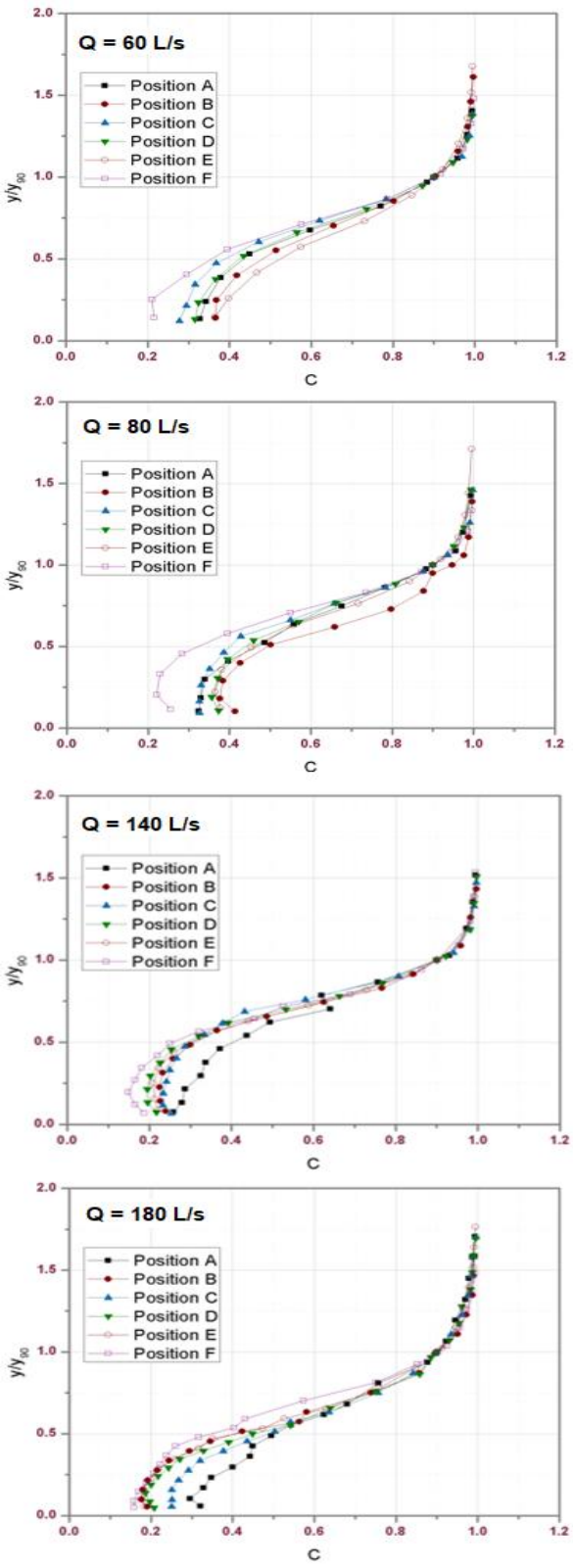

Figure B.6: Normalized air concentration profiles at step 27 for discharges of 60, 80, 140, and 180 L/s (from top to bottom, respectively)

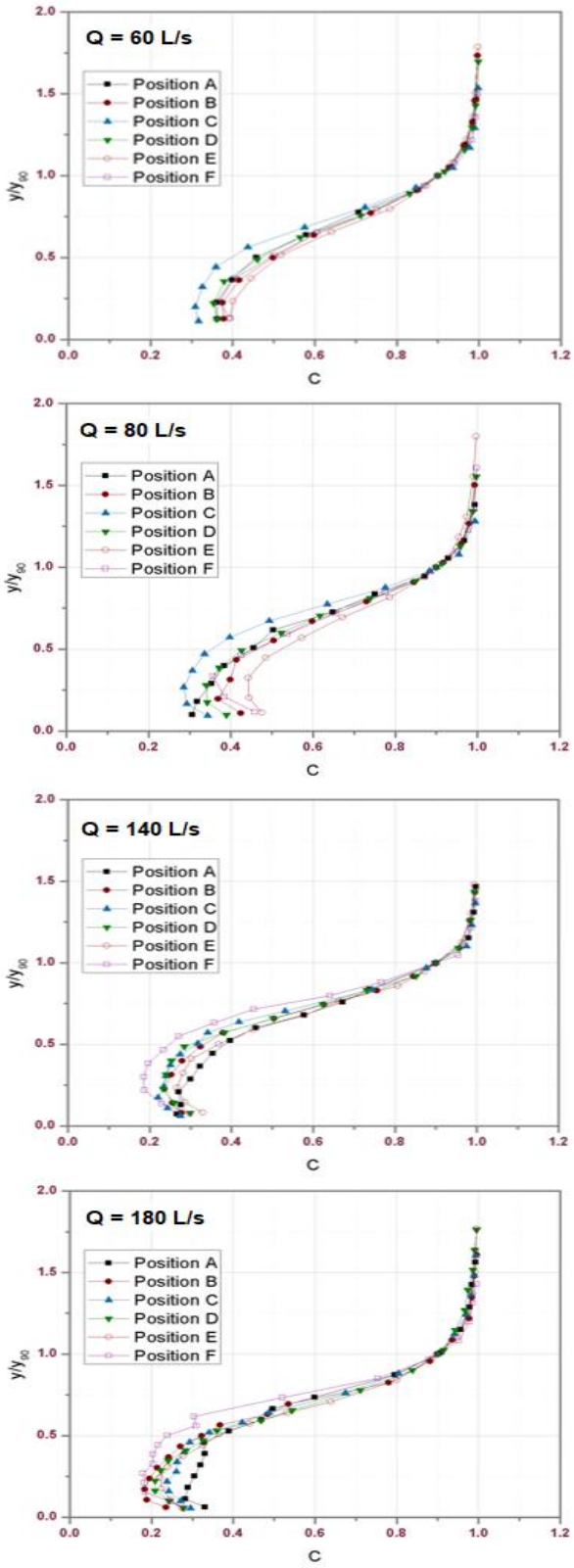

Figure B.7: Normalized air concentration profiles at step 30 for discharges of 60, 80, 140, and 180 L/s (from top to bottom, respectively)

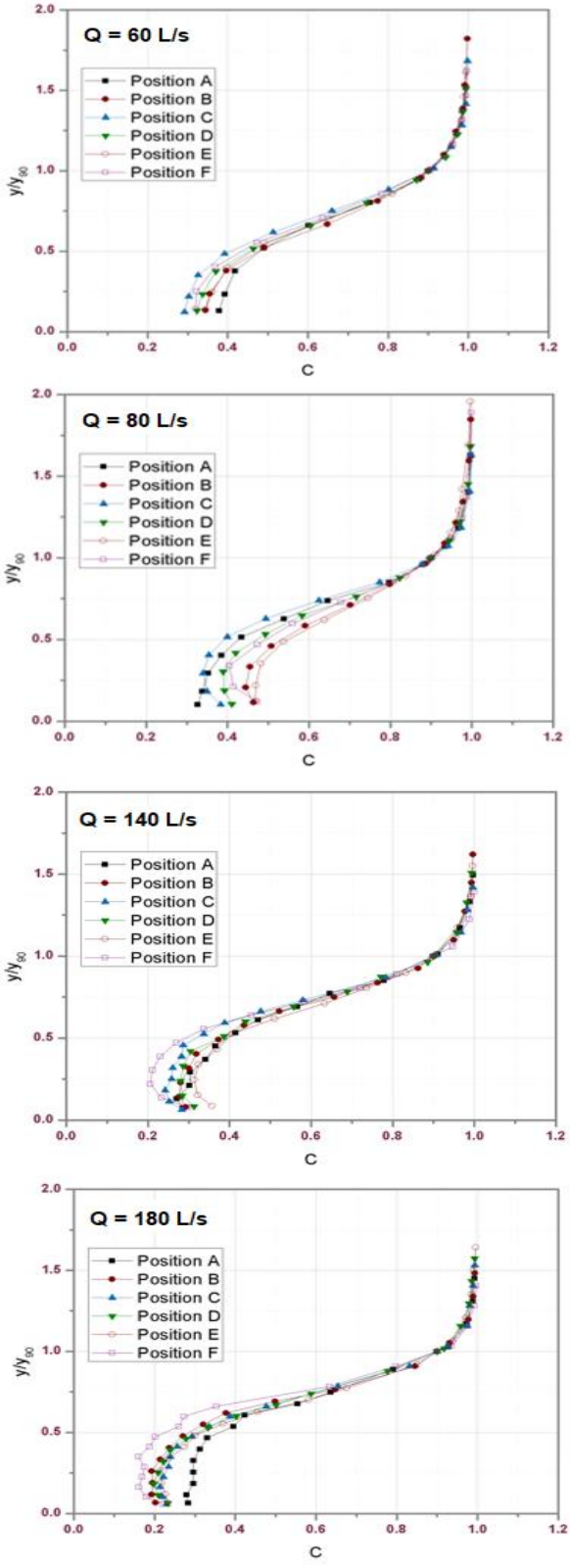

Figure B.8: Normalized air concentration profiles at step 32 for discharges of 60, 80, 140, and 180 L/s (from top to bottom, respectively)

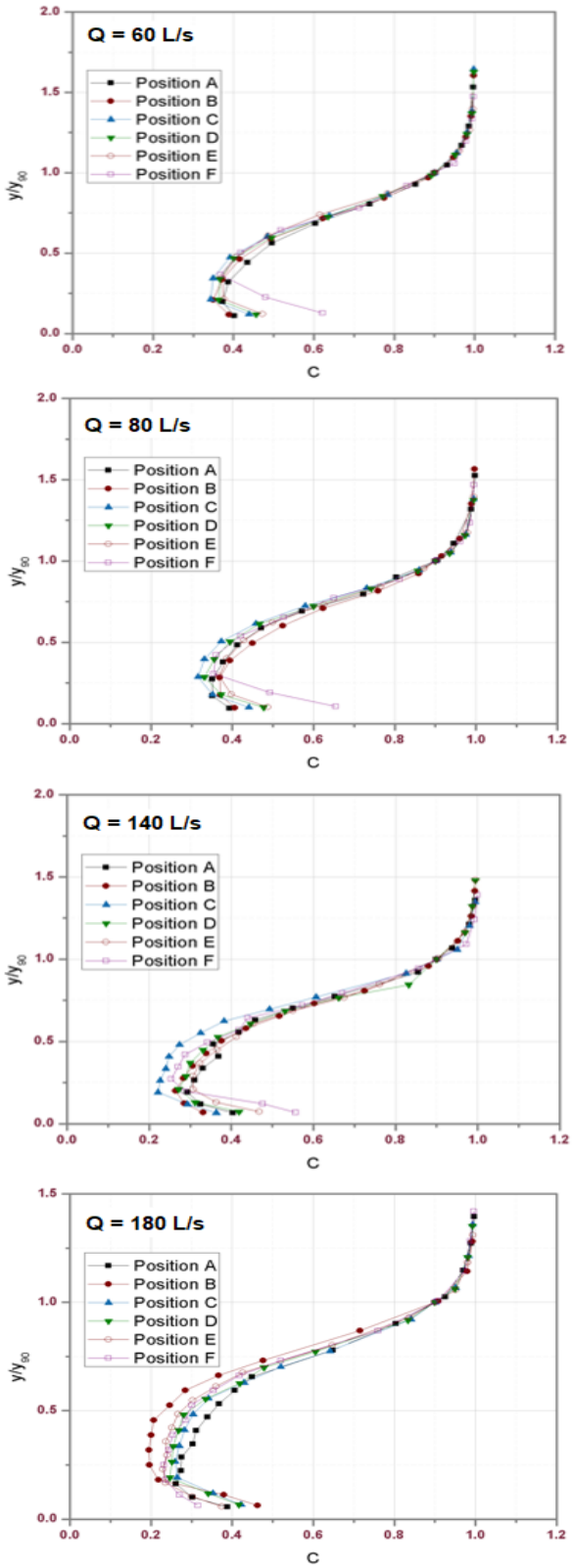

Figure B.9: Normalized air concentration profiles at step 37 for discharges of 60, 80, 140, and 180 L/s (from top to bottom, respectively)

Appendix C: Normalized Velocity Profiles

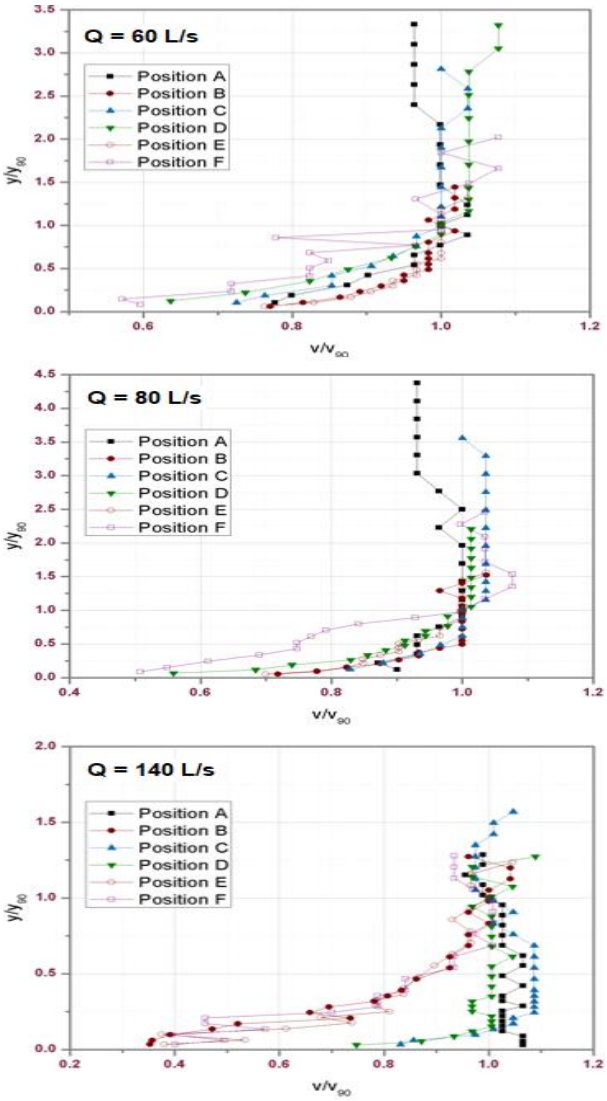

Figure C.1: Normalized velocity profiles at step 15 for discharges of 60, 80, and 140 L/s (from top to bottom, respectively)

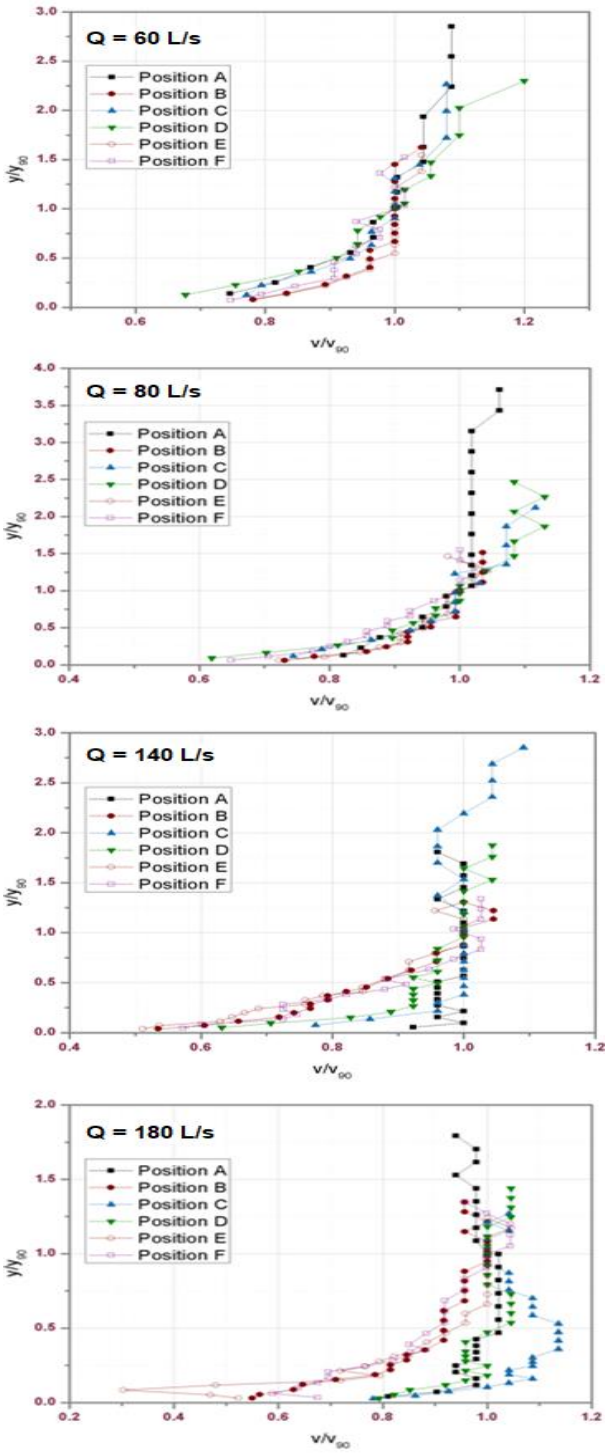

Figure C.2: Normalized velocity profiles at step 17 for discharges of 60, 80, 140, and 180 L/s (from top to bottom, respectively)

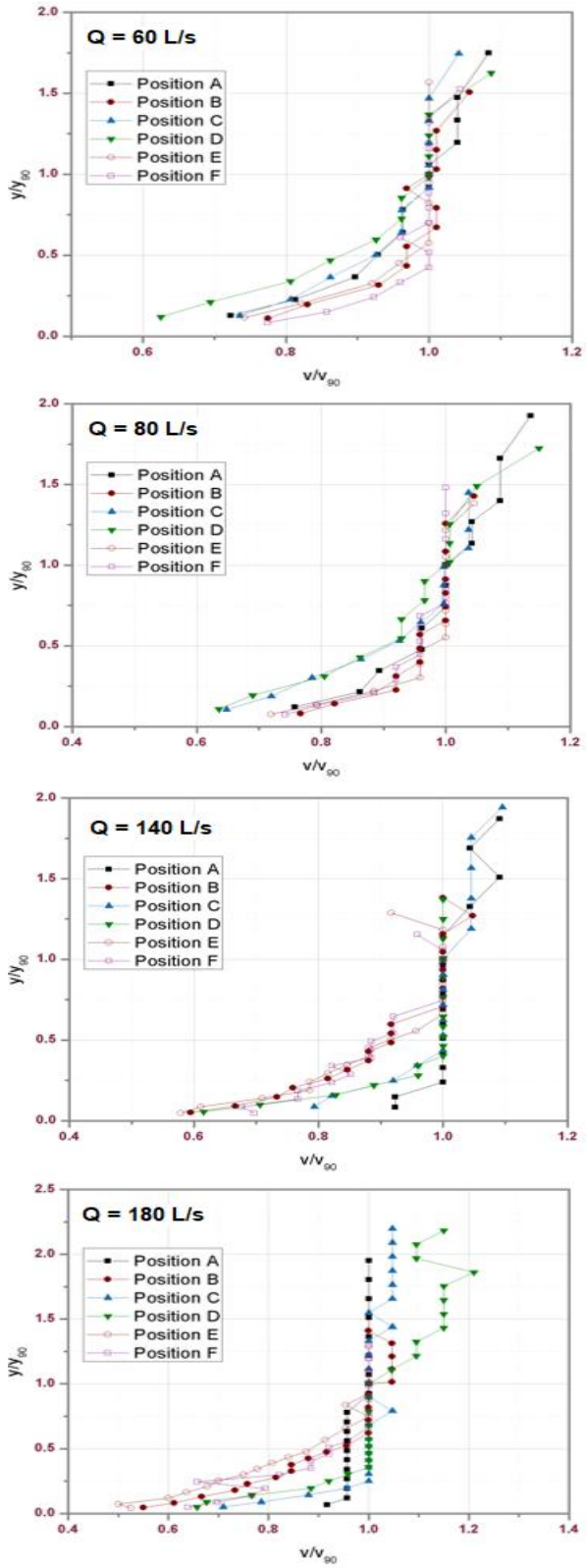

Figure C.3: Normalized velocity profiles at step 19 for discharges of 60, 80, 140, and 180 L/s (from top to bottom, respectively)

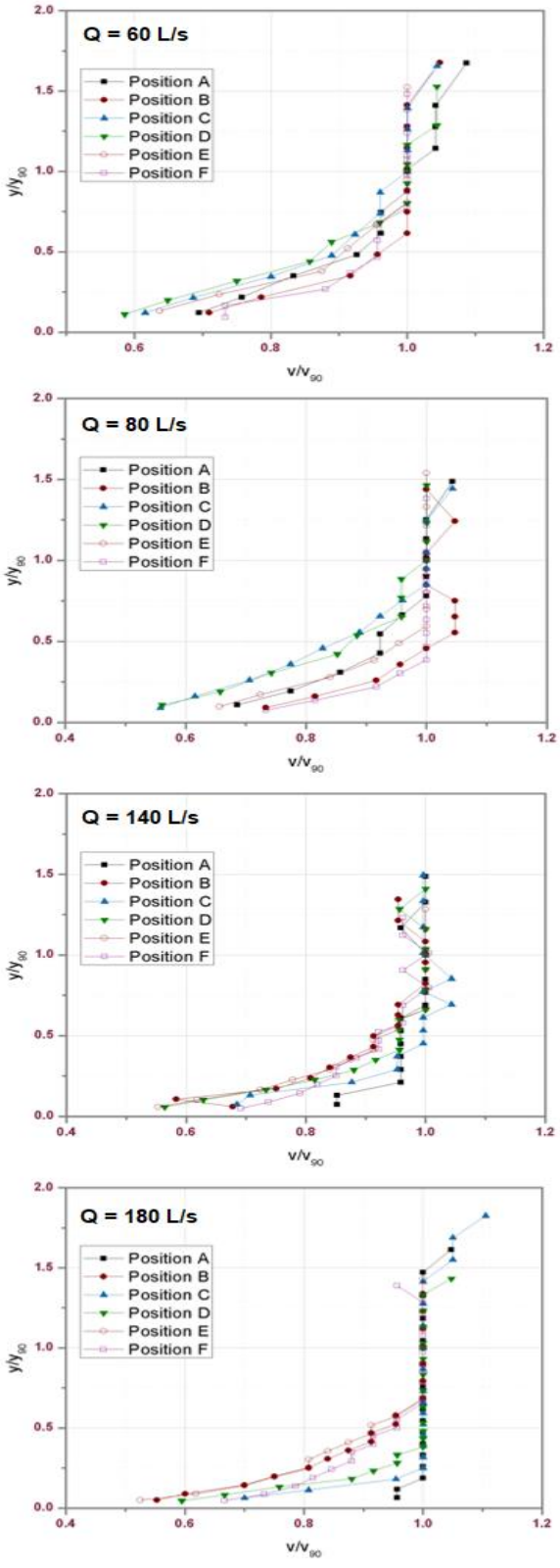

Figure C.4: Normalized velocity profiles at step 21 for discharges of 60, 80, 140, and 180 L/s (from top to bottom, respectively)

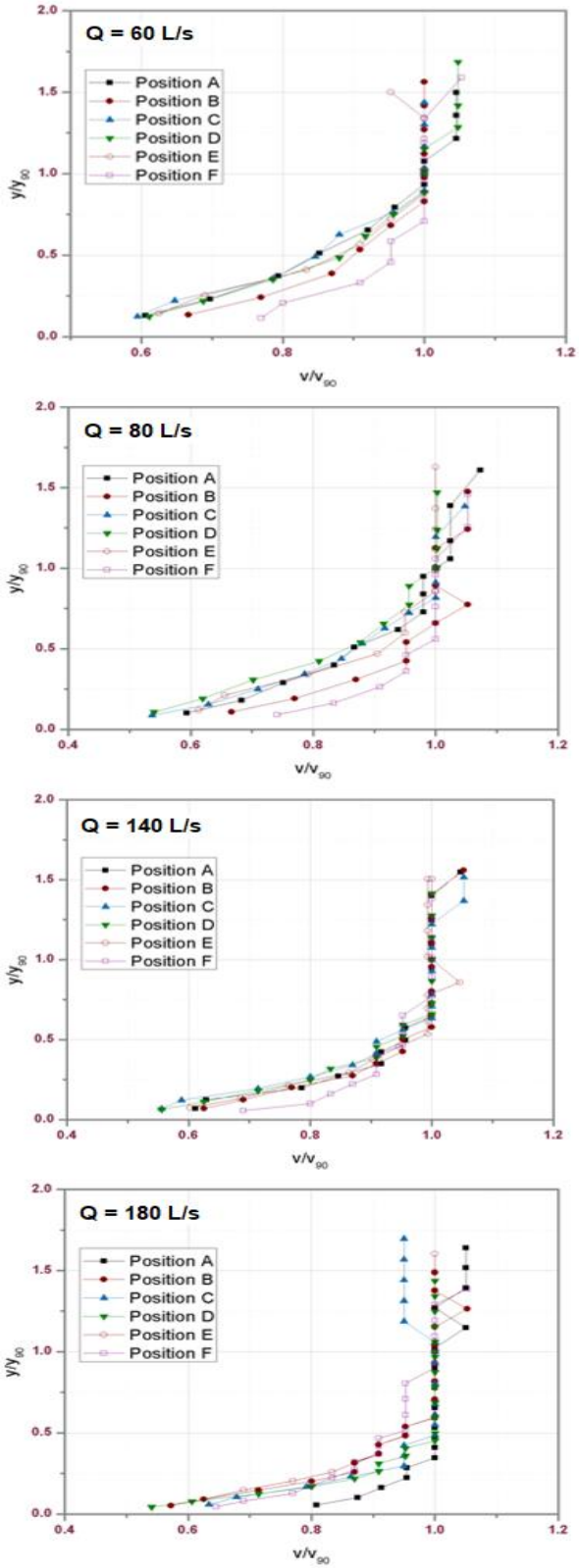

Figure C.5: Normalized velocity profiles at step 24 for discharges of 60, 80, 140, and 180 L/s (from top to bottom, respectively)

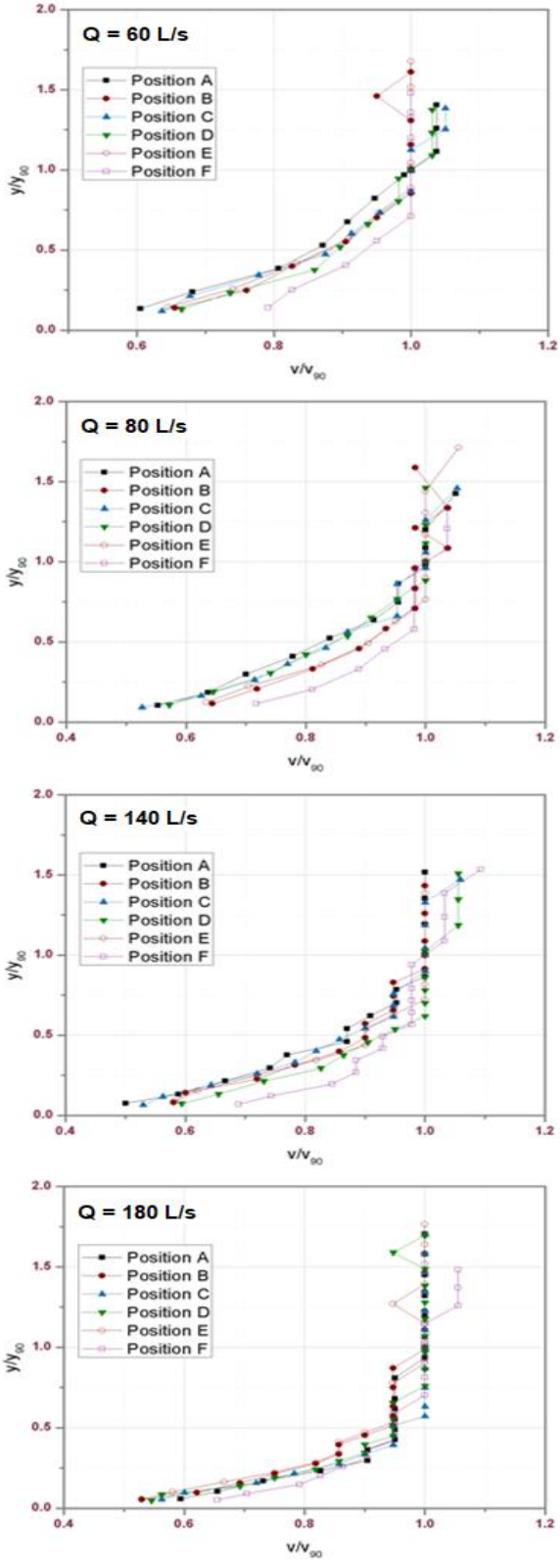

Figure C.6: Normalized velocity profiles at step 27 for discharges of 60, 80, 140, and 180 L/s (from top to bottom, respectively)

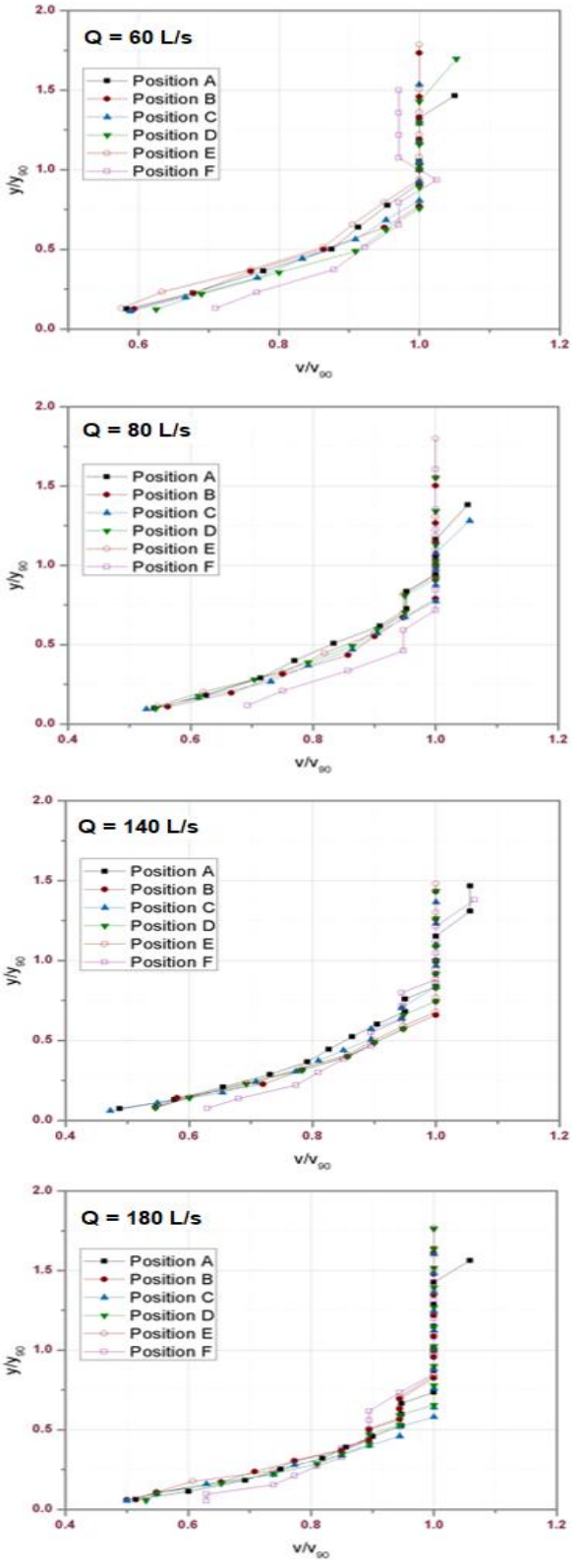

Figure C.7: Normalized velocity profiles at step 30 for discharges of 60, 80, 140, and 180 L/s (from top to bottom, respectively)

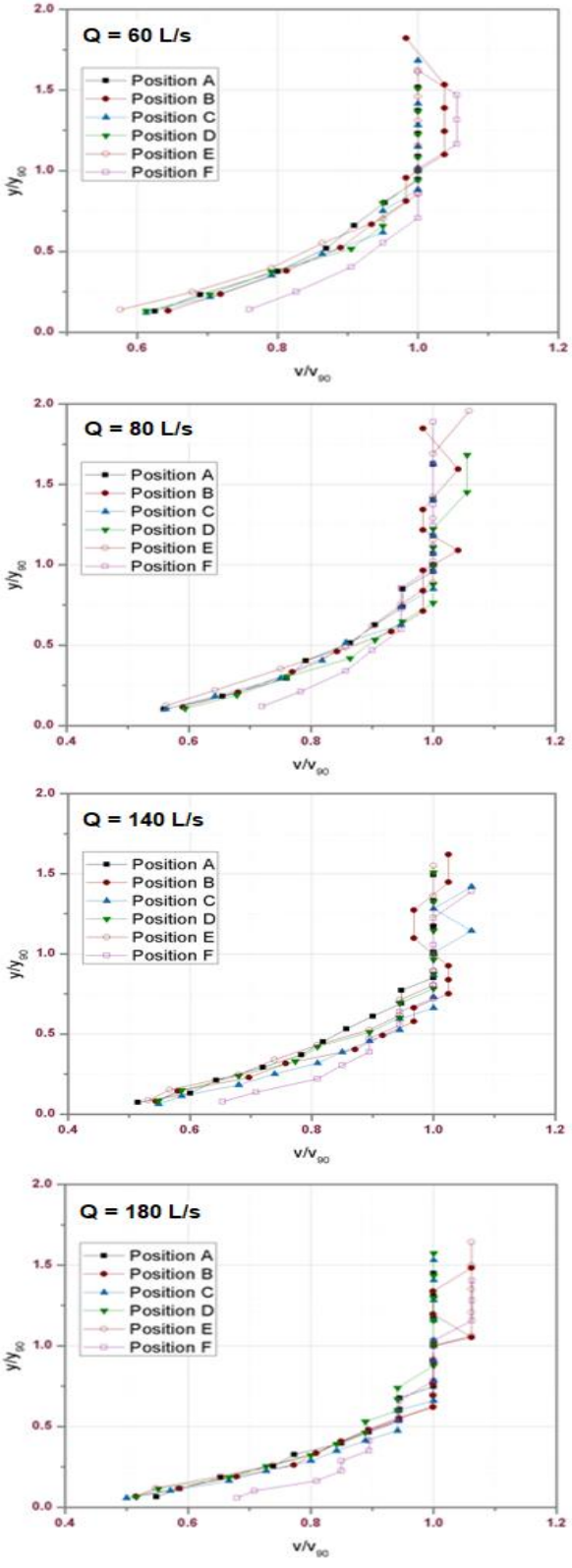

Figure C.8: Normalized velocity profiles at step 32 for discharges of 60, 80, 140, and 180 L/s (from top to bottom, respectively)

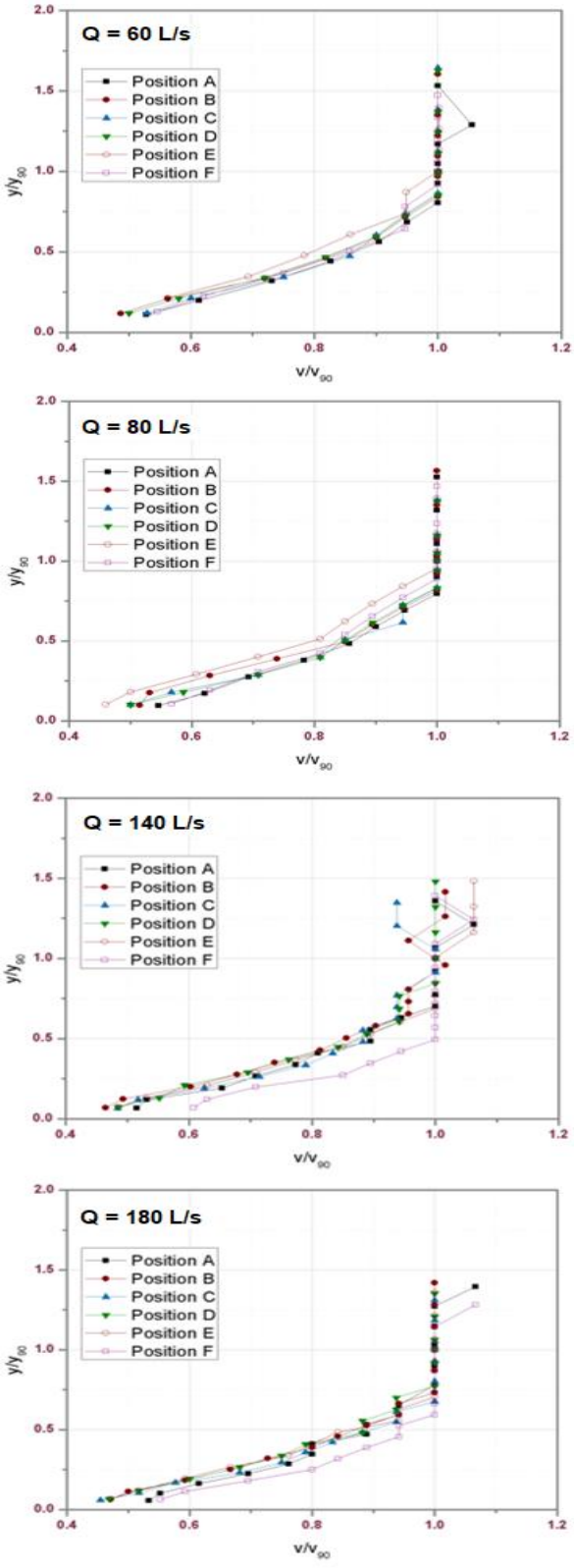

Figure C.9: Normalized velocity profiles at step 37 for discharges of 60, 80, 140, and 180 L/s (from top to bottom, respectively)

Appendix D: Power Law Exponents

Table D.1: Power law exponents 'N' obtained at Q = 60 L/s

Step	Vertical						Mean
	A	B	C	D	E	F	
15	8.613	12.330	6.684	4.890	12.870	4.034	8.237
17	6.784	11.792	7.610	5.498	12.453	9.099	8.873
19	7.032	10.225	6.944	4.619	8.826	13.158	8.467
21	5.942	7.184	4.466	4.122	4.892	7.837	5.740
24	4.124	5.373	3.897	4.323	4.165	8.650	5.089
27	3.987	4.883	4.502	5.141	4.560	8.347	5.237
30	3.948	4.029	4.232	4.585	3.584	6.196	4.429
32	4.232	4.619	4.442	4.297	3.679	7.669	4.823
37	3.560	3.057	3.408	3.137	2.828	3.428	3.236

Table D.2: Power law exponents 'N' obtained at Q = 80 L/s

Step	Vertical						Mean
	A	B	C	D	E	F	
15	14.327	10.695	12.610	5.501	8.718	3.130	9.164
17	9.542	9.971	7.364	5.568	9.747	6.234	8.071
19	8.985	11.521	5.333	4.955	10.204	10.131	8.522
21	6.579	10.834	4.023	4.078	6.373	11.890	7.296
24	4.531	6.693	4.112	3.613	4.386	10.309	5.607
27	3.734	5.112	3.864	3.965	4.776	7.519	4.828
30	3.723	4.105	3.935	3.812	3.655	6.266	4.249
32	4.057	4.239	4.078	4.533	3.666	6.579	4.525
37	3.864	3.193	3.423	3.467	2.720	3.775	3.407

Table D.3: Power law exponents 'N' obtained at Q = 140 L/s

Step	Vertical						Mean
	A	B	C	D	E	F	
15	-44.248	3.119	163.934	28.011	3.845	3.367	26.338
17	50.000	5.198	15.480	8.224	4.464	5.314	14.780
19	42.017	6.090	12.804	8.666	5.794	7.220	13.765
21	17.637	6.127	8.695	6.028	5.504	8.210	8.700
24	6.039	6.649	4.983	5.316	6.079	9.515	6.430
27	3.877	4.545	4.146	5.376	4.548	8.130	5.104
30	3.814	4.359	4.005	4.333	4.264	5.587	4.394
32	3.899	4.266	4.720	4.037	3.761	6.468	4.525
37	3.960	3.360	3.752	3.556	3.634	5.841	4.017

Table D.4: Power law exponents 'N' obtained at Q = 180 L/s

Step	Vertical						Mean
	A	B	C	D	E	F	
17	-44.248	5.777	181.818	22.075	4.153	5.942	29.253
19	29.762	5.479	14.535	9.099	4.305	6.592	11.629
21	92.593	5.556	13.774	8.446	5.342	8.224	22.323
24	19.802	6.161	7.788	6.766	5.896	7.593	9.001
27	6.270	5.165	5.845	5.543	4.833	7.949	5.934
30	4.632	4.259	4.572	4.708	4.221	5.949	4.724
32	4.507	4.482	4.619	4.241	4.196	7.663	4.951
37	4.294	3.564	3.741	3.540	3.536	5.118	3.965

Appendix E: Constants used in Energy Analysis

Table E.1: Depth of water above the PKW in the upstream reservoir at the analyzed discharges

Q [L/s]	**h_{PKW} [cm]**
60	4.69
80	5.99
140	10.12
180	13.28

Table E.2: Elevation of each analyzed step

Step	**Z [m]**
15	2.72
17	2.56
19	2.40
21	2.24
24	2.00
27	1.76
30	1.52
32	1.36
37	0.96